RESISTIVITY AND THERMOELECTRIC POWER STUDIES ON
$Bi_2Sr_2Ca_{1-x}M_xCu_2O_y$ (M=Pr, Ce & Tb) SYSTEMS

A thesis submitted for the award of
the degree of
Doctor of Philosophy

by
D. RAMA SITA

School of Physics
University of Hyderabad
Hyderabad-500 046
India
July 1997

Dedicated to...

my Parents

&

Sister

CERTIFICATE

Dated: 24 **JULY 1997.**

SCHOOL OF PHYSICS
UNIVERSITY OF HYDERABAD
HYDERABAD 500 046

This is to certify that **I, D. Rama Sita** have carried out the research embodied in the present thesis entitled **RESISTIVITY AND THERMO-ELECTRIC POWER STUDIES ON $Bi_2Sr_2Ca_{1\_x}M_xCu2O_y$ (M=Pr, Ce & Tb) SYSTEMS** for the full period prescribed under the Ph.D. ordinances of the University.

I declare to the best of my knowledge that no part of this thesis was earlier submitted for the award of research degree of any University.

D. Rama Sita
candidate

(D. Rama Sita)

Dean of the School

(Prof. K. N. SHRIVASTAVA)
DEAN,
SCHOOL OF PHYSICS,
UNIVERSITY OF HYDERABAD.

Supervisor

(Dr. RAJENDER SINGH)

Dr. R. SINGH
SCHOOL OF PHYSICS
UNIVERSITY OF HYDERABAD
HYDERABAD-500 046, INDIA

ACKNOWLEDGEMENTS

D. RAMA SITA

Table of Contents

Chapter 1

INTRODUCTION

During the ten years since the discovery of high temperature superconductivity in La-Ba-Cu-0 system with critical transition temperature of 30 K by Bednorz and Miiller in 1986; an enormous amount of experimental and theoretical effort has been expended leading to a considerable advancement in our understanding of these materials. However, a clear understanding of the mechanism of high temperature superconductivity remains elusive. This chapter is intended to provide a short discussion on the historical background and basic properties of superconductors followed by a brief review of various developments in the field of high T_c superconductivity. Finally, the motivation for the studies presented in this thesis is discussed.

1.1 Historical background on superconductors

Helium was discovered on earth in 1895 by William Ramsay. Kammerling Onnes succeeded in liquifying helium gas at 4 K in 1908. Using liquid helium, he proceeded to investigate the electrical resistivity in various metals as a function of temperature. In 1911, he discovered that the electrical resistance of mercury suddenly dropped to zero whenever the sample was cooled below 4.2 K [1]. He called this new phenomenon *i.e.,* the absence of resistance below a critical temperature, as superconductivity; and that temperature the critical temperature, T_c. A year later, Onnes reported that an applied

magnetic field (H_c) as well as a sufficiently strong electric current can destroy the super-conductivity.

Meissner and Ochenfield [2] in 1933, discovered another distinct property of the superconducting state called the perfect diamagnetism. They found that the magnetic flux is expelled from the interior of the sample if a superconductor is cooled in a weak magnetic field to below superconducting transition temperature. This phenomenon is called the Meissner effect.

In an effort to find superconductors with higher critical temperatures, early researchers investigated many other metals and metallic alloys. Several metals like Nb and alloys like Nb_3Ge were found to be superconducting. In 1986, the highest critical temperature superconductor was Nb_3Ge with T_c 23 K.

Several experimental studies have been carried out to study various properties of the superconductors. Alexei Abrikosov studied the behavior of superconductors in an external magnetic field and discovered that one can distinguish two types of materials: type-I and type-II superconductors. Superconducting materials that completely expel the magnetic flux until they become completely normal are called type-I superconductors. Above the critical field (H_c), the superconductor is normal and magnetization M = 0. For a type-II superconductor, there are two critical fields; the lower H_{c1} and the upper H_{c2}. The flux-is completely expelled only up to the field H_{c1}. Above H_{c1}, the flux partially penetrates into the material until upper critical field H_{c2} is reached. Above H_{c2}, the material returns to the normal state. Between H_{c1} and H_{c2}, the material is said to be in mixed state.

From the specific heat measurements as a function of temperature. it was found that

specific heat shows a jump at T_c together with the more rapid decrease with decreasing temperature. This decrease is proportional to exp(-A/T) in the superconducting state and suggestive of excitation of carriers across an energy gap, A [3].

In 1962, Brian Josephson postulated a quantum tunnelling effect that should occur when a supercurrent tunnels through an extremely thin layer (as $10\AA$) of an insulator. His predictions were confirmed in a year and the effects are known as the Josephson effects [4].

Many phenomenological theories have been proposed to explain the experimental results. Taking the transition between the normal and superconducting states as reversible and by applying the general principles of thermodynamics to the transition, the expressions for Gibb's free energy, entropy and specific heat in the normal state and superconducting state in terms of field and temperature were derived. The entropy in the normal state is greater than the entropy of the superconducting state, which shows that the superconducting state is a more ordered state. Entropy change is continuous and specific heat shows a discontinuity at the transition, which implies that superconducting to normal state transition is a second order transition in the absence of the magnetic field, while it is first order in the presence of the field.

In 1935, London proposed a classical model of superconductivity. This theory essentially incorporates the fundamental superconducting properties of zero resistance and perfect diamagnetism into electromagnetic constitutive relations known as London equations [5]. This model explained the Meissner effect and predicted the penetration depth A: this is a characteristic length of penetration of the static magnetic flux into a superconductor. While the interior of a pure superconductor expels the magnetic flux and is, therefore, flux free (perfect diamagnetism), the static flux persists within a sheath of

depth A at the surface of the sample and its magnitude decreases towards the core of the superconductor.

In 1950, Ginzburg and Landau developed a remarkable phenomenological theory of superconductivity that integrates electrodynamic, quantum mechanical and thermodynamic properties of superconductors. They have taken the complex wave function of superelectrons as the order parameter and introduced a new parameter called the 'coherence length' [3]. Coherence length is defined as the characteristic length scale over which the order parameter changes to produce the condensation energy.

Despite their utility, the models discussed above are phenomenological in nature. In other words, these models do not give any explanation as to how superconductivity occurs.

In 1957, Bardeen, Cooper and Schrieffer developed the theory that provides microscopic explanation for superconductivity [6]. The basis of this theory is that the electrons that carried lossy currents in the normal state pair together in the superconducting state. These pairs which carry lossless supercurrents arc called Cooper pairs. The effective unit of charge of a cooper pair is 2e rather than e. Like in conventional superconductors, it has been established by Gough *et al* [7] that the effective unit of charge in high T_c superconductors is *2c*.

1.2 High Temperature superconductors

In 1973, Johnson by discovering superconductivity in $Li\text{-}Ti\text{-}O_3$ at temperatures as high as 13 K, removed the belief that superconductivity in the oxide materials was limited to very low temperatures [S]. In 1975, superconductivity was discovered in $BaPb_{1-x}Bi_xO_3$

at around 14 K to report another member to the growing class of superconducting oxides [9]. In 1986, the first high temperature superconductor La-Ba-Cu-O with T_c of 30 K was discovered by Bednorz and Müller [10]. Takagi *et al* [11] confirmed that La-Ba-Cu-0 had the tetragonal K_2NiF_4 structure. Uchida *et al* [12] found the exact composition of the superconducting phase. Jorgenson *et al* [13] reported the crystal structure from neutron diffraction study of these samples. They reported that this structure had copper ions coordinated to four oxygen in a square plane and two 0 atoms along c-axis to form an octahedral coordination. The parent compound La_2CuO_4 is an antiferromagnetic insulator with orthorhombic structure. Superconductivity can be achieved by replacing La in this parent compound with alkaline earth metal (example Sr) [14] or by forcing excess oxygen into the compound [15]. For $La_{2-x}Sr_xCuO_{4-y}$ system, the T_c is optimal ($\approx$ 36 K) for x = 0.15 [16]. Several substitution effects have been studied in $La_{2-x}Sr_xCuO_4$ system. The 3d transition metal ions at Cu site depresses the T_c very rapidly [17, 18]. This suggests the importance of Cu-0 planes in superconductivity.

Superconductivity in Y-Ba-Cu-0 (Y-123) superconductors was discovered by Wu, Chu and coworkers in 1987 with T_c about 92 K [19]. The composition of the phase was found to be $YBa_2Cu_3O_{(7-\delta)}$ [20-21]. The crystal structure has been reported by many groups [22-24]. The structure of the superconducting material is orthorhombic. There are two sites in the unit cell; the copper in the Cu-0 oxide plane and the copper in the Cu-0 chain. The parent compound $YBa_2Cu_3O_6$ is antiferromagnetic insulator with tetragonal structure [25].

The properties of this system are very sensitive to oxygen content [26,27]. The compound undergoes an orthorhombic-tetragonal transition at elevated temperature [28]. The substitution of Yttrium by other rare-earth elements (except for Pr, Ce and Tb) do

not affect superconductivity [29-35]. Substitution of 3d transition metal ions at Cu-site suppresses the T_c rapidly [36-41].

Two other superconducting phases in the homologous series of compounds having formula $Y_2Ba_4Cu_{6+n}O_{14+n}$ namely $YBa_2Cu_4O_y$ ((124) with n = 2) [42-44] and $Y_2Ba_4Cu_7O_y$ ((247) with n = 0) [44] were identified with T_c of 80 K and 40 K respectively. Their crystal structures are also reported [45]. Migataka *et al* reported T_c of 90 K in $Y_{0.9}Ca_{0.1}Ba_2Cu_4O_y$ system [46].

Superconductivity in Bi-Sr-Cu-0 system was discovered in 1988 by Michel *et al* [47] with T_c around 20 K. Superconductivity was subsequently discovered in the related Bi-Sr-Ca-Cu-0 systems by Macda *et al* [48]. Three superconducting phases have been identified with the general formula $Bi_2Sr_2Ca_{n-1}Cu_nO_y$ with n = 1, 2, 3 and having T_cs 10, 85 and 110 K respectively [49-53].

Superconductivity in Tl-based compounds was discovered by Sheng and Herman [54]. Two homologous series of superconducting compounds have been reported in the Tl-Ba-Cu-0 system [55-63], the compositions of which may be noted as $Tl_mBa_2Ca_{n-1}Cu_nO_{2(n+1)+m}$, where m = 1 or 2 and n, the number of CuO_2 planes upon which superconductivity occurs ranging over n = 1 to 4 for m = 1; and 1 to 3 for m = 2. These two scries of cuprates contain the compounds with highest known T_c of 125 K for m = 2, n = 3 [58] and 122 K for m = 1, n = 4 [63]. The structures of Tl-compounds are similar to that of Bi-compounds except for c-axis lengths.

Cava *et al* [64] reported a new family of superconductors with the general formula $Pb_2Sr_2ACu_3O_{8+\delta}$ (A = Y, rare-earths, Ca, Sr) with T_c = 70 K.

The electron doped superconductors with formula $La_{2-x}M_xCuO_{4-y}$ (Ln = Nd, Ce, Pr, Sm, Eu; M = Ce, Th) were discovered with critical temperatures as high as ss 25 K for $x \approx 0.15$ and $y \approx 0.02$ [65-67]. In this family of superconductors, electrons are the charge carriers unlike other Cu-oxide based superconductors in which holes are the charge

The discovery of conductivity in A_xC_{60} (where A represents an alkali metal) [68] and superconductivity in K_xC_{60} [69] has been followed by reports of superconductivity in other alkali-metal doped fullerides with transition temperatures as high as 33 K [70].

Superconductivity at about 94 K has been discovered in $HgBa_2CuO_4$ (Hg-1201) by Putillian *et al* [71]. Schilling *et al* reported a $T_{c(onset)}$ of 133 K in Hg-Ba-Ca-Cu-O system [72].

Recently, Nagarajan *et al* reported superconductivity in borocarbide system Y-Ni-B-C with T_c around 12 K [73].

1.3 Bi-Sr-Ca-Cu-O superconductors

The superconductor $Bi_2Sr_2CuO_y$ (2201) is the first of a series $Bi_2Sr_2Ca_{n-1}Cu_nO_y$ of modular layered structures in which copper and oxygen in sheets, typical of all high T_c materials, are spaced by alkaline earth cations, and interlayered with Bi_2O_2 layers. In $Bi_2Sr_2CaCu_2O_y$ (2212) the Cu-0 sheet in Bi-2201 is replaced by $CuO_2/Ca/CuO_2$ sandwiches and in the case of $Bi_2Sr_2Ca_2Cu_3O_y$ (2223) the additional CuO_2 and Ca layers are inserted within the $CuO_2/Ca/CuO_2$ sandwich of Bi-2212, yielding a $CuO_2/Ca/CuO_2/Ca/CuO_2$ sandwich.

Though the basic topology is simple, these structures are always complicated by stacking faults, modulations and oxygen and cationic disorder. Different types of unit cells with different unit cell parameters have been reported in the literature [74-79]. The crystal structures reported by Tarascon *et al* [52] are shown in **Fig**. 1.1. They assumed **pseudo** tetragonal symmetry and reported the unit cell parameters (a, *b* and c) for the three crystal structures; a $\sim$ b $\approx$ 5.4 $\mathring{A}$ and the c values are 24.6, 30.6 and 37.1 A respectively for the three systems.

The 2201 structure consists of a corner linked plane of Cu square coordinated by 01 (Cu-$O1$ = 1.9 A), sandwiched between two Sr-02 layers. The 02 oxygens lie immediately above and below each oxygen (Cu-02 = 2.6 A), thus forming an extremely elongated CuO_6 octahedron. Strontium has nine nearest oxygens with an average Sr-0 distance of $\sim 2.7\mathring{A}$. The $SrO/CuO_2/SrO$ module is sandwiched between BiO_2 bilayers in which bismuth adopts a very distorted octahedral coordination. Four Bi-03 bonds near the (001) plane range from 2.2 to 2.8 $\mathring{A}$, while the Bi-02 bond linking Bi to the Sr-02 layer is much shorter (about $2.0\mathring{A}$). In contrast, the sixth Bi-03 bond which joins the adjacent sheets in Bi_2O_2 bilayers is longer than 3.0A. This long and weak Bi-03 bond parallel to the c-axis results in very much weak interlayer bonding and mica like behavior in all the Bi-superconductors.

In 2212 structure, Ca adopts eight coordination similar to Y environment in **Y-123**. There are no oxygen atoms at this level, so copper atoms have only five nearest neighbors in square pyramidal coordination rather than the elongated octahedral coordination of 2201. The structure slab containing $SrO/CuO_2/Ca/CuO_2/SrO$ is topologically identical to $YBa_2Cu_2O_6$ (122) module portion of the **Y-123** structure.
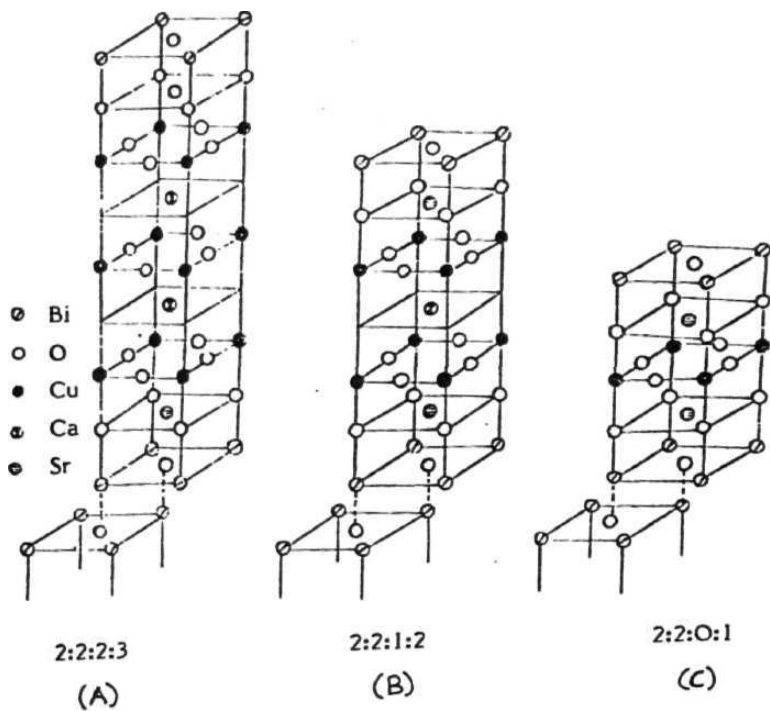
Fig.1.1 Crystal structure of the three superconducting phases of Bi-Sr-Ca-Cn-O superconductors

In 2223 the outer Cu2 **atoms** are in square pyramid coordination as found in **Y-123** and 2212, while the **Cu1** atoms are in square planar coordination.

Substitutional studies at Cu site [80-84] have been reported in this system. The substitution at Cu site is found to suppress the superconductivity very fast. This indicates the importance of Cu-0 planes for superconductivity in these systems.

1.4   Motivation for the present work

It is generally realized that the physical properties of the CuO_2-based superconducting systems are strongly related to **the** carrier concentration [85]. **Fig.** 1.2 shows the model phase diagram for high T_c superconductors. The parent materials *i.e.,* the systems corresponding to left end of the phase diagram are charge-transfer insulators with long range antiferromagnetic ordering. Charge carriers are introduced into the parent material by doping, while hole carriers can be introduced by either cationic doping or oxygen intercalation. Upon doping, the **antiferromagnetic** ordering collapses dramatically and gives **way** to superconductivity. The effectiveness of holes in destroying the magnetic order is interpreted as follows. The holes, which mainly enter into the oxygen $2p$ orbital, are quite effective in frustrating the antiferromagnetic (AF) coupling between the Cu spins. For a certain range of hole concentration, this leads to the formation of spin-glass state at low temperatures. Neutron-scattering experiments indicate **that** AF correlations does persist in the superconducting **state**, but the AF correlation length is much shorter. At a certain critical doping concentration, the system undergoes an **Insulator-Metal (M-I)** transition and superconductivity emerges.

With increase in the hole **concentration,** the superconducting transition temperature
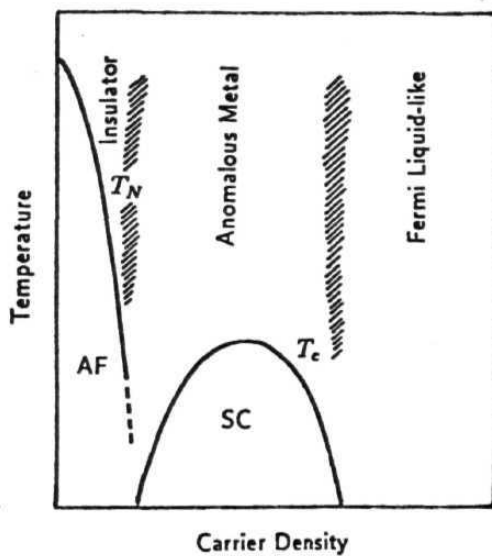
Fig.1.2 Model phase diagram of the high T_c cuprate system

(T_c) increases and reaches a maximum, and further increase in hole concentration leads to a decrease in T_c and the sample becomes a **non-superconducting** metal. The composition which gives the maximum T_c for a given system is called 'optimally doped'. The lower carrier density side of the T_c maximum is called 'underdoped' and the higher carrier **density** side of the T_c **maximum** is called **'overdoped'** regions.

Briefly, one can say that the fully metallic overdoped **region** is Fermi liquid like, while the undoped material is insulator. The questions of fundamental importance are, how to explain the nature of the intermediate phase (superconducting phase), the change in electronic structure of CuO_2 planes as the carrier (hole) density increases and the observed **MI** transition. To get the answers to these questions, various physical properties have been studied theoretically and experimentally. Among these, the transport property experiments are very sensitive probes to get useful information about the electronic structure and serve as a test for theories.

In this process, many studies on transport coefficient measurements like resistivity and thermoelectric power (TEP) have been made in various systems [85, 86]. TEP measurements provide not only the information complementary to resistivity, but they are also more direct probes to the intrinsic properties of polycrvstalline materials because TEP is less sensitive to the grain boundary effects than the electrical resistivity. It is an interesting transport coefficient which can provide information about the concentration and sign of the carriers and the band structure of the material.

$YBa_2Cu_3O_y$ exhibits a larger **nonstoichiometry** for y = 6 to 7 and its physical properties are strongly dependent on the oxygen content (y) [26,27]. It undergoes a transition from superconductor to semiconductor with decreasing oxygen content [28]. Whereas in

Bi-based cuprates, the oxygen content is relatively stable with respect to substitutions under the same conditions of sample preparation and the fundamental crystal structure remains unchanged during the Superconductor-Insulator transition. All the Cu sites in these cuprates are equivalent and its modulation structure is not influencing the super-conductivity of the system [87]. So, the observed changes in the physical parameters can be explained by taking dopant concentration as the monitoring parameter.

In $YBa_2Cu_3O_7$ except Pr, Ce and Tb, all other rare-earth substitutions at Y-site hardly affect the superconductivity [29-35]. These three elements have the common feature that they can exist both in +3 and +4 valence states. The Ce and Tb substi-tutions lead to the formation of multiphases in $YBa_2Cu_3O_y$ (Y-123) system, while in $Y_{1-x}Pr_xBa_2Cu_3O_7$ system, T_c decreases and vanishes at around x = 0.5 [88].

In $Bi_2Sr_2CaCu_2O_y$ (Bi-2212) system also, several reports have described the effects of rare-earth replacing Ca or Sr ion [89-95,96-99]. However, only a few studies on Pr [100-103] and Ce [99, 103-105] substitution effects and none on Tb doped Bi-2212 system have been reported to our knowledge. Moreover, no TEP studies have been reported on Pr, Ce and Tb doped Bi-2212 system. Therefore, a systematic study on the effect of sub-stitution of these elements in Bi-2212 system has been undertaken, which might give an information about the valence state of these ions, the crystal structure and the relation between the normal state properties and T_c. The present studies were undertaken with the following objectives.

(1) To synthesize samples of $Bi_2Sr_2Ca_{1-x}M_xCu_2O_y$ (M = Pr, Ce and Tb) systems and find out the solid solubility limit of each dopant.

(2) To characterize the synthesized materials for phase purity and estimate the lattice

parameters from the X-ray diffraction (XRD) studies. To study the effect of dopant ion on the crystal structure of Bi-2212 system.

(3) To measure AC susceptibility of the samples in order to find out bulk T_c and its variation with dopant nature and content.

(4) To undertake detailed resistivity measurements on the Pr, Ce and Tb doped Bi-2212 system to understand the effect of rare-earth substitution on T_c and normal state properties. To understand the nature of conduction in the semiconducting samples of the present systems.

(5) To undertake the study of temperature variation of TEP of the Pr, Ce and Tb doped Bi-2212 system so as to obtain information about the band structure of these materials and ascertain the validity of various theoretical models to the TEP experimental data.

Second chapter contains the details about the experimental techniques employed in the present studies.

Third chapter describes the sample preparation and their characterization by X-ray diffraction and AC susceptibility.

Fourth chapter contains the detailed resistivity studies and the analysis.

Fifth chapter contains the TEP studies and the analysis.

Sixth chapter describes the summary of the results and conclusions arrived at from the present studies.

1.5 References

1. H. Kammerlingh Onnes, *Leiden Commun.* **1206,** 1226 (1911).

2. W. Meissner and R. Ochenfeld, *Naturwiss* **21,** 787 (1933).

3. A. C. Rose-Innes and E. H. Rhoderick, *Introduction to Superconductivity,* p. 61, (Pergamon Press, UK) (1978).

4. J. Clarke, *Amer. J. Phys.* **38,** 1070 (1970).

5. F. London and H. London, *Physica* 2, 341 (1935).

6. J. Bardeen, L. N. Cooper and R. J. Schrieffer, *Phys. Rev.* **106,** 162 (1957); **108,** 1175 (1957); C. G. Kuper, *An Introduction to the theory of Superconductivity,* p.101, 105 & 184, (Clarendon Press, Oxford) (1968).

7. C. E. Gough, M. S. Colclough, E. M. Forgan, R. G. Jordan, M. Keene, C. M. Muirhead, A. I. M. Rea, N. S. Thomas, J. S. Abell and S. Sutton, *Nature* **326,** 855 (1988).

8. J. R. Galaver, *Appl. Phys. Lett* 23, 480 (1973).

9. A. W. Sleight, J. L. Gillson and P. E. Bierstedt, Solid State Commun.17, 27 "(1975).

10. J. G. Bednorz and K. A. Miiller, *Z. Phys. B Conden. Matter* **64,** 189 (1986).

11. H. Takagi, S. Uchida, K. Kitazawa and S. Tanaka, *Jpn. J. Appl. Phys.* **26,** L123 (1987).

12. S. Uchida, H. Takagi, K. Kitagawa and S. Tanaka, *Jpn. J. Appl. Phys.* **26,** L1 (1987).

13. J. D. Jorgenson, H. B. Schüttler, D. G. Hinks, D. W. Capone II, K. Zhang, M. B. Brodsky and D. J. Scalapino. *Phys. Rev. Lett.* 58, 1024 (1987).

14. J. M. Tarascon, L. H. Greene, W. R. McKinnon, G. W. Hull and T. M. Geballe, *Science* 235, 1371 (1987).

15. J. D. Jorgenson, B. Dabrowski, S. Pei, D. G. Hinks, L. Soderholm, B. Morosin, J. E. Schirber, E. L. Venturini and S. Ginley, *Phys. Rev.* **B38,** 11337 (1988).

16. J. B. Torrance, A. Bezinge, A. I. Nazzal, T. C. Huang, S. S. P. Parkin, D. T. Keane, S. L. Laplaca, P. M. Horn and G. A. Held, *Phys. Rev.* **B40,** 8872 (1989).

17. J. M. Tarascon, L. H. Greene. P. Barboux, W. R. McKinnon, G. W. Hull, T. P. Orlando, K. A. Delin, S. Foner and E. J. McNiff, *Phys. Rev.* **B36,** 8393 (1987).

18. G. Xiao, A. Bakhshai, M. Z. Cieplak, Z. Tesanovic and C. L. Chien, *Phys. Rev.* **B39,** 315 (1989).

19. M.X. Wu, J.R. Ashburn, C.J. Torng, P.H. Hor, R.I.Meng, L. Gao, Z.J. Huang, Y.Q. Wang and C.W. Chu, *Phys. Rev. Lett.* 58, 908 (1987).

20. R.M. Hazen, L.W. Finger, R.J. Angel, C.T. Prewitt, N.L. Ross, H.K. Mao, C.G. Hadichiacos, P.H. Hor, R.L. Meng and C.W. Chu, *Phys. Rev.* B35, 7238 (1987).

21. T. Siegrist, S. Sunshine, D.W. Murphy, R.J. Cava and S.M. Zahurak, *Phys. Rev.* B 35, 7137 (1987).

22. R.J. Cava, B. Batlogg, R.B. VanDover, D.W. Murphy, S. Sunshine, T. Siegrist, J.P. Remeika, E.A. Rietman, S. Zahurak and G.P. Espinosa, *Phys. Rev. Lett.* 58, 1676 (1987).

23. P.M. Grant, R.B. Beyers, E.M. Engler, G. Lim, S.S.P. Parkin, M.L. Ramirez, V.X. Lee, A. Nazzal, J.E. Vazquez and R.J. Savoy, *Phys. Rev.* B 35, 7242 (1987).

24. J. D. Jorgensen, *Jpn. J. Appl. Phys.* 26, 2017 (1987).

25. M. Sato, S. Shamato, J. M. Tranquada, G. Shirane and B. Keimer, *Phy. Rev. Lett* 61, 1377 (1988).

26. R.J. Cava, B. Batlogg, C.H. Chen, E.A. Rietman, S.M. Zahurak and D. Werder, *Phys. Rev.* B 36, 5719 (1987).

27. P.K. Gallagher, H.M. O'Bryan, S.A. Sunshine, D.W. Murphy, *Mat. Res. Bull.* 22, 995 (1987).

28. J. D. Jorgenson, B. W. Veal, W. K. Kwok, G. W. Crabtree, A. Umezawa, L. J. Nowicki and A. P. Paulikas, *Phys. Rev B36*, 5731 (1987).

29. P.H. Hor, R.L. Meng, Y.Q. Wang, L. Gao, Z.J. Huang, J. Bechtold, K. Foster and C.W. Chu, Phys. Rev. Lett. 58, 1891 (1987).

30. J.M. Tarascon, W.R. McKinnon, L.H. Greene, G.W. Hull and E.M. Vogel, Phys. Rev. B 36, 226 (1987).

31. Z. Fisk, J.D. Thompson, E. Zirngiebel, J.L. Smith and S.W. Cheong, Solid State Commun. 62, 743 (1987).

32. S. Hasoya, S.I. Shamoto, M.K. Onoda and M. Sato, *Jpn. J. Appl. Phys.* 26, L325 (1987)/

33. D.W. Murphy, S. Sunshine, R.B. VanDover, R.J. Cava, B. Batlogg, S.M. Zahurak and L.F. Schneemeyer, *Phys. Rev. Lett.* 58, 1888 (1987).

34. J.R. Thompson, S.T. Sekula, D.K. Christen, B.C. Sales, L.A. Boatner and Y.C. Kim, *Phys. Rev.* B 36, 718 (1987).

35. A.R. Modenbaugh, M. Suenaga, T. Asano, R.N. Shelton, H.C. Ku, R.W. McCallum and P. Klavin, *Phys. Rev. Lett.* 58, 1885 (1987).

36. J.M. Tarascon, P. Barboux, P.F. Miceli, L.H. Greene and G.W. Hull, *Phys. Rev.* B **37,** 7458 (1988).

37. G. Xiao, F.H. Streitz, A. Gavrin, Y.W. Du and C.L. Chien, *Phys. Rev.* B **35,** 8782 (1987).

38. Y. Maeno, T. Tomita, M. Kyogoku, S. Awaji, Y.A. Oki, K. Hoshino, A.A. Minami and T. Fujita, *Nature* **328,** 512 (1987).

39. Y.K. Tao, J.S. Swinnea, A. Manthiram, J.S. Kim, J.B. Goodenough and H. Stein-fink, *J. Mater. Res.* 3, 248 (1988).

40. S. Mazumder, H. Rajagopal, A. Sequeira, J. Singh, A.K. Rajarajan, L.C. Gupta, and R. Vijaya Raghavan, *Phase Trans.* 19, 97 (1989).

41. H. Maeda, A. Koizumi, N. Bamba, E. Takayama- Muromachi, F. Izumi, H. Asano, K. Shimizu, H. Moriwaki, H. Maruyama, Y. Kuroda and H. Yamakazi, *Physica* C **157,** 483 (1989).

42. A. F. Marshall, R. W. Barton, K. Char, A. Kapitulnik, B. Oh, R. H. Hammond and S. S. Laderman, *Phys. Rev.* **B37,** 9353 (1988).

43. J. Karpinski, E. Kaldis, E. Jilek, S. Rusieeki and B. Bucher, Nature **336,** 660 (1988); R. J. Cava, J. J. Karajewski, W. F. Peck Jr., B. Batlogg, L. W. Pupp Jr., R. M. Fleming, A. C. W. P. James and P. Marsh, *Nature* **338,** 328 (1989).

44. P. Bordet, C. Chaillout, J. Chenavas, J. L. Hodeau, M. Marezio, J. Karpinski and E. Kaldis, *Nature* **334,** 596 (1988).

45. P. Marsh, R. M. Fleming, M. L. Mandich, A. M. De Santolo, J. Kwo, M. Hong and L. J. Martinez- Miranda, *Nature* **334,** 141 (1988).

46. Migataka, S. Gotoh, N. Koshizuka and S. Tanaka, *Nature* **341,** 41 (1989).

47. C. Michel, H. Hervieu, M.M. Borel, A. Gradin, F.Deslandes, J. Provst and B. Raveau, *Z. Für. Phys. Cond. Matt.* 68, 421 (1987).

48. H. Maeda, Y. Tanaka, M. Fukutomoi and T. Asano, *Jpn. J. Appl. Phys.* **27,** L209 (1988).

49. H.W. Zanbergen, Y.K. Huang, M.J.V. Menken, Li, K. Kadouaki, A.A. Menovsky, G. Van Tendelooz and S. Amelinckx, *Nature* **332,** 620 (1988).

50. R. Ramesh. C.J.D. Hetheringcon, G. Thomas. S.M. Green, C. Jiang, M.L. Pudee and H.L. Luo, *Appl. Phys. Lett.* **53,** 615 (1988).

51. J.L. Taloon. R.G. Buckley, P.W. Gilberd, M.R. Presland, I.M. Brown, M.E. Bowden, L.A. Christian and E. Goguel, *Nature* **333,** 153 (1988).

52. J.M. Tarascon, W.R. McKinnon, P. Barboux. D.M. Huang, B.G. Badley, L.H. Green, G.W. Hull, Y. LePage, N. Stoffel and M. Giroud, *Phys. Rev.* **B38,** 8885 (1988).

53. S.A. Sunshine, T. Siegrist, L.F. Schneemeyer, D.W. Murphy, R.J. Cava, R.B. Van Dover, R.M. Fleming, S.H. Glarum, S. Nakahara, R. Farrow, J.J. Krajewski, S.M. Zahurak, J.V. Wasczak, J.H. Marshall, P. Marsh, L.H. Rupp Jr., and W.F. Peck, *Phys. Rev.* B **38,** 893 (1988).

54. Z.Z. Sheng and A.M. Herman, *Nature* **332,** 55 (1988).

55. R.M. Hazen, L.W. Finger, R.J. Angel, C.T. Prewitt, N.L. Ross, C.G. Hadidiacos, P.J. Heaney, D.R. Veblen, Z.Z. Sheng, A. El Ali and A.M. Hermann, *Phys. Rev. Lett.* **60,** 1657 (1988).

56. M.A. Subramanian, J.C. Calabrese, C.C. Torardi, J. Gopalakrishnan, T.R. Askew, R.B. Flippen, K.J. Morrisscy, V. Chowdhry and A.W. Sleight, *Nature* **332,** 420 (1988).

57. C.C. Torardi, M.A. Subramanian, J.C. Calabrese, J. Gopalakrishnan, K.J. Morrissey, T.R. Askew, R.B. Flippen, U. Chowdhry and A.W. Sleight, *Science* **240,** 631 (1988).

58. S.S.P. Parkin, V.Y. Lee, E.M. Engler, A.I. Nazzal, T.C. Huang, G. Gorman, R. Savoy and R. Beyers, *Phys. Rev. Lett.* **60,** 2539 (1988).

59. S.S.P. Parkin, V.Y. Lee, A.I. Nazzal, R. Savoy, R. Beyers and S. La Placa, *Phys. Rev. Lett.* 61, 750 (1988).

60. S.S.P. Parkin, V.Y. Lee, A.I. Nazzal, R. Savoy, T.C. Huang, G. Gorman and R. Beyers, *Phys. Rev.* **B38,** 6531 (1988).

61. M.A. Subramanian, J.B. Parise, J.C. Calabrese, C.C. Torardi, J. Gopalakrishnan and A.W. Sleight, *J. Solid State Chem.* **77,** 192 (1988).

62. M.A. Subramanian, C.C. Torardi, J. Gopalakrishnan, P.L. Gai, J.C. Calabrese, T.R. Askew, R.B. Flippen and A.W. Sleight, *Science* **242,** 249 (1988).

63. R. Sugise and H. Ihara, *JPn. J. Appl. Phys.* 28, 334 (1989).

64. R.J. Cava, B. Batlogg, J.J. Krajewski, L.W. Rupp, L.F. Schneemeyer, T. Siegrist, R.B. Van Dover, P. Marsh, W.F. Peck Jr., P.K. Gallagher, S.H. Glarum, J.H. Marshall, R.C. Farrow, J.V. Waszczak, R. Hull and P. Trevor, *Nature* **336,** 211 (1988).

65. Y. Tokura. H. Takagi and S. Uchida, *Nature* **337,** 345 (1989).

66. H. Takagi, S. Uchida and Y. Tokura, *Phys. Rev. Lett.* **62,** 1197 (1989).

67. J.T. Markert and M.B. Maple, *Solid State Commun.* **70,** 145 (1989); J. T. Markett, E. A. early. T. Bjornholm, S. Ghamati, B. W. Lee, J. J. Neumeier, R. D. Price, C. L. Seaman and M. B. Maple, *Physica* **C158,** 178 (1989).

68. R. C. Haddon *et al*, *Nature* **350,** 320 (1991).

69. A.F. Herbard et al., Nature 350, 600 (1991).

70. K. Tanigaki, T.W. Ebbesen, S. Saito, J. Mizuki, J.S. Tsai, Y. Kulo and S. Kuroshima, Nature **352,** 223 (1991).

71. S.N. Putillin, E.V. Antipov, 0. Chmaissem and M. Marezio, Nature **362,** 226 (1993).

72. A. Schilling, M. Cantoni, J.D Guo and H.R. Ott, Nature **363,** 56 (1993).

73. R. Nagarajan, Chandan Mazumdar, Zakir Hossain, S. K. Dhar, K. V. Gopalkrishnan, L. C. Gupta, C. Godart, B. D. Padalia and R. Vijayaraghavan, *Phys. Rev. Lett.* **72,** 274 (1994).

74. C.C. Torardi, M.A. Subramanian, J.C. Calabrese, J. Gopalakrishnan, E.M. McCarron, K.J. Morrissey, T.R. Askew, R.B. Flippen, V. Chowdhry and A.W. Sleight, *Phys. Rev.* **B38,** 225 (1988).

75. K. Imai, I. Nakai, T. Kawashima, S. Sueno and A. Ono, *Jpn. J. Appl. Phys.* **27,** L1661 (1988).

76. M. Onoda and M. Sato, *Solid State Commun.* **67,** 799 (1988).

77. R.M. Hazen, C.T. Prcwitt, R.J. Angel, N.L. Ross, L.W. Finger, C.G. Hadidiacos, D.R. Veblon, P.J. Heaney, P.H. Hor, Z.J. Huang, L. Gao, J. Bechtold and C.W. Chu, *Phys. Rev. Lett.* 60, 1174 (1988).

78. J.M. Tarascon, Y. Le Page. P. Barboux, B.G. Bagley, L.H. Greene. W.R. McKinnon, G.W. Hull, M. Giroud and D.M. Hwang, *Phys. Rev.* **B37, 9382** (1988).

79. J.K. Liang, S.S. Xie, G.C. Che, J.Q. Huang, Y.L. Zhang and Z.X. Zhao, *Mod. Phys. Lett.* B 2, 483 (1988).

80. K. Uchinokura, T. Yabe, S. Takebayashi, M. Hase and A. Maeda. *Physica* **C162-164,** 981 **(1989);** T. E. Jones, P. M. Thibado, W. C. Mcginnis, R. D. Boss, J. W. Schindler and S. Oseroff, *Physica* C **162-164,** 25 (1989).

81. A. Maeda, T. Yabe, S. Takebayashi, M. Hase and K. Uchinokura. *Phys. Rev.* **B41,** 4112 (1990).

82. S. K. Agarwal, V. N. Moorlhy, G. L. Bhalla. V. P. S. Awana and A. V. Narlikar, *Ind. J. Pure and Appl. Phys.* 30, 586 (1992).

83. P. S. Prabhu, M. S. R. Rao and G. V. S. Rao, *Physica* **C211,** 279 (1993).

84. E. Zacharias and R. Singh. *Int. J. Mod. Phys.* B 9, 549 (1995).

85. Y. Iye in *Physical properties of high temperature superconductors* ///edited by D. M. Ginsberg (World scientific, Singapore) (1992) and references therein.

86. C. Uher and A. B. Kaiser. *Studies on high temperature superconductors,* edited by A. V. Narlikar 7. 352 (Nova Science, New York, 1992) and references therein

87. J.M Tarascon, P. Barboux, G.W. Hull, R. Ramesh, L. H. Greene, M. Giroud, M. S. Hedge and W. R. McKinnon, *Phys. Rev.* 39, 4316 (1989).

88. L. Soderhelm, K. Zhang, D. G. Hinks, M. A. Beno, J. D. Jorgensen, C. U. Segre and I. K. Schuller, *Nature* 328, 604 (1987).

89. T. Tamegai, K. Koga, K. Suzuki, M. chihara, F. Sakai and Y. Iye, *Jpn. J. Appl. Phys.* 28, L1 12 (1989).

90. Y. Ando, K. Fukuda, S. Kondoh, M. Sera, M. Onoda and M. Sato, *Solid State Commun.* 67, 815 (1988).

91. B. Jayaram, P.C. Lanchester and M. T. Weller, *Phys. Rev.* **B43,** 5444 (1991).

92. V. P. S. Awana, S. K. Agarwal, R. Ray, S. Gupta and A. V. Narlikar, *Physica* **C191,** 43 (1992).

93. M. Presland, J. L. Tallon, *Physica* **C177,** 1 (1991)

94. M. A. Subramanian, A. R. Strzelecki, J. Gopalakrishnan and A.W. Sleight *J. Sol. Stat. Chem.* 77, 196 (1988).

95. C. Paracchini, G. Calestani and M. G. Francesconi, *Physica C* **167** 247 (1990).

96. D. Mandrus, L. Forro, C. Kendziora and L. Mihaly, *Phys. Rev.* B **44,** 2418 (1991).

97. J. B. Mandal. S. Keshri, P. Mandal, A. Poddar, A. N. Das and B. Ghosh, *Phys. Rev.* **B46,** 11840 (1992).

98. V. E. Gasumyants, N. V. Ageev, E. V. Vladimirskaya, V. I. Smirnov, A. V. Kazanskiy and V. I. Kaydanov, Phys. Rev. B53, 905 (1996).

99. Ruiping Wang, Hisashi Sekine and Hua Jin, *Supercond. Sci. Technol.* 9, 529 (1996).

100. Y. Gao, N. Spencer, H. Chen and R. E. Salamon, *Phys. Rev.* **B45,** 13 (1992).

101. P. Sumana Prabhu, M. S. Ramachandra RAO, U. V. Varadaraju and G. V. Subba Rao, *Phys. fler.*B50, 6929 (1994).

102. Xiaolong Chen. Jingkui Liang, Jinrong Min, Jianqi Li, Guanghui Rao, *Phys. Rev.*B50, 3431 (1994).

103. V. P. S. Awana. S. K. Agarwal and A. V. Narlikar and M. P. Das *Phys. Rev.* **B48,** 1211 (1993).

104. Frederic Jordan and Octavio Pena, *PhysicaC231,* 311 (1994).

105. Akihito Sawa. Tae-Su Han, Takayuki Iwamatsu, Hiromoto UWE, Tunetaro Sakudo, *Physica* **B165&166**, 1553 (1990).

Chapter 2

EXPERIMENTAL TECHNIQUES

In this chapter, various experimental techniques employed in the course of this study have been described. These include X-ray diffraction (XRD), AC susceptibility, DC four probe resistivity and thermoelectric power (TEP).

2.1 X-ray Diffraction studies

The diffraction data which depends on the lattice parameters is unique for a particular material and can be employed in the identification of a material, just as fingerprints are used to identify a human being. X-ray is that part of the **electromagnetic** spectrum which covers the wavelength range $0.1\text{-}200\text{\AA}$. Only a relatively small part of the total X-ray region is covered by the conventional X-ray spectrometer. The X-rays used for the material characterization is CuK_α, whose wavelength is $1.5418A$. The basic principle involved in the X-ray studies is the **Bragg's** law *i.e.,* $n\lambda = 2d\sin\theta$, where θ is the glancing angle at which the X-ray strikes the surface of the crystal, A is the wavelength of the X-ray used, n (an integer) is the order of diffraction and d_{hkl} is the distance between the parallel planes having miller indices h, k, l. The lattice parameters a, 6 and c can be calculated by indexing the sharp peaks (assigning h, k, l values) and using the equation

$$\left(\frac{h^2}{a^2} + \frac{k^2}{b^2} + \frac{l^2}{c^2}\right) d_{hkl}^2 = 1 \qquad (2.1.1)$$

In polycrystalline samples or powder of a crystalline material, the crystals are randomly oriented. If such a sample is struck by an X-ray beam, there may be many planes which

are oriented in such a way that **Bragg's** law is satisfied and we obtain a resultant diffraction pattern with **peaks** corresponding to all such planes. In order that more number of planes are exposed, the sample is rotated by an angle *0* on its own axis during exposure. The **diffracted** beams are collected by scintillating counter, which acts as a detector, at an angle *28*. This output is fed to a recorder which records the output (which is proportional to the intensity of the diffracted beam) versus **2θ.** From the positions, relative intensities of the peaks and from the area under its profile, the position of the atoms in a unit cell can be determined. The orientation of the crystallites can also be determined from the relative intensities. The shape of the peak provides information regarding the crystallite size and lattice imperfections including strains.

The XRD studies at room temperature were carried out using a SIEFERT X-RAY **diffractometer,** the schematic diagram of which is given in **Fig.2.1.** The fine powder of the material under study was mounted on a perspex plate using vacuum grease as a binder. **CuK$_\alpha$** radiation (A = 1.5418 $\overset{\circ}{A}$) was used. The machine was operated with a beam current of 30 raA and power of 40 kV. For phase identification, the patterns were compared against standard patterns reported in the literature. The cell parameters were calculated by using the least square refinements with an accuracy of 2 decimal places. The error in estimation of cell parameters could be due to small error in reading the **2θ** values which is ± 0.1°.

2.2   AC susceptibility

The ac susceptibility measurements were carried out using a mutual inductance method. Schematic diagram of the set-up is shown in Fig.2.2. It consists of a primary coil and two **co-axially** wound secondary coils. Current was driven through the primary coil using an oscillator. In the absence of any sample, the mutual inductance of the combined coils
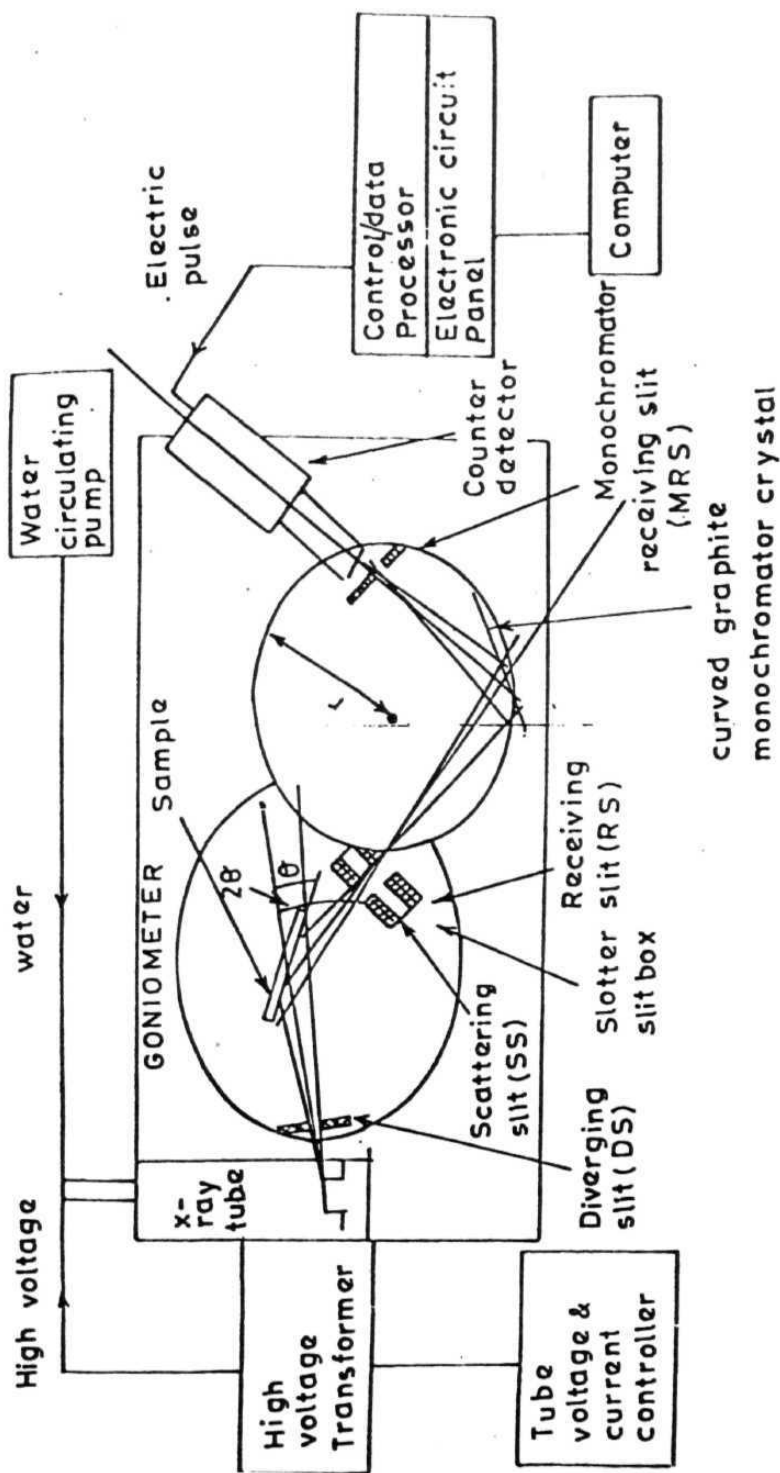
Fig.2.1 Schematic diagram of an X-ray Diffractometer
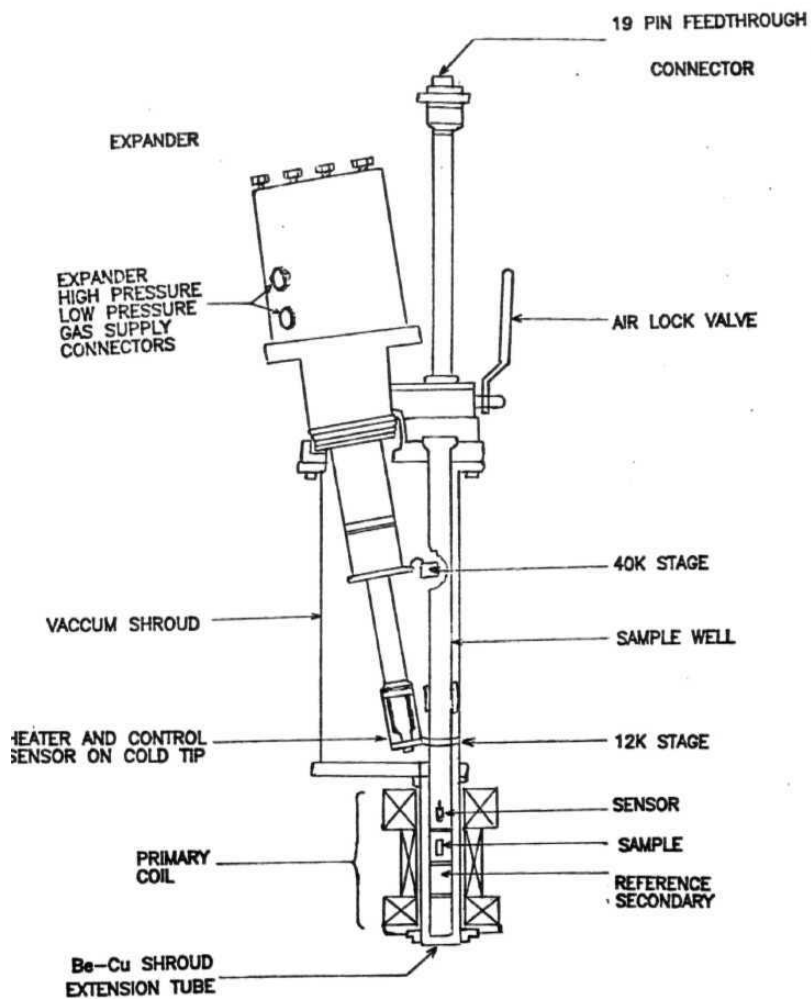
Fig.2.2 Schematic diagram of AC susceptibility set-up

should be zero. When the sample is kept at the center of one of the secondary coils, voltage is induced across the secondaries depending on the magnetization and hence upon susceptibility of the sample. In practice, it is **difficult** to make the two secondary coils exactly identical in all respects. Hence, even when there is no sample, a small voltage is observed across the secondaries. This is nullified by subtracting the background voltage (voltage appearing **when** sample is not present) from the voltage obtained with sample present.

The primary coil was wound on a bakelite former of length **11.0** cm and inner diameter 3.0 cm. The primary coil assembly is fixed on the outside of the $Be - Cu$ extension tube as shown in Fig.2.2. The primary coil resistance is 35 fi and it could produce a field of 0.036 **Tesla** for the applied current of 1 Amp. Additional number of turns were wound at both the edges of the primary coil for field uniformity throughout its length. Both the secondaries are kept inside the cryostat and length of each secondary is 2.54 cm. Each secondary coil has 3250 turns of 38 gauge standard insulated copper wire. The sample to be measured was kept at the center of the upper secondary coil. Temperature of the sample was measured using a calibrated Si-diode sensor which is placed close to the sample.

The primary coil was energized by sending an ac current at a frequency of 33 Hz and an amplitude of 1.999 V using the internal oscillator of the dual phase EG **&** G **PAR-5210** lock-in amplifier whose output impedance is 600 Ω. The induced voltage at the secondaries was measured using the same lock in amplifier in differential mode to get better signal to noise ratio. The field generated by the primary is calculated by measuring the current flowing through it. This current is estimated by measuring the voltage drop across a standard 1 K fi resistor connected in series with the primary coil.

The temperature of the sample was measured using a Si-diode sensor and was controlled using a **temperature** controller (Scientific Instruments **Inc,** series 5500). The accuracy of the temperature measurement was better than 0.5 K. The **in-phase** (inductive) component (x') and out of phase (resistive) component (x") of the complex susceptibility were measured simultaneously as a function of temperature.

2.3   Resistivity measurements

The resistivity measurements were carried out using the standard four probe method. The measurements were performed from 8 K to room temperature using a closed cycle refrigerator (APD make). The temperature of **the** specimen was monitored and controlled by using Lakeshore 330 auto tuning temperature controller. The electrical contacts were made on the sample by the application of silver paint (Elteks). The sample was mounted directly on the cold head of the closed cycle system using General Electric adhesive and the leads were taken out through a 10 pin connector. Temperature of the specimen is monitored and controlled by using a calibrated Si-diode (DT-470-SD-12) sensor mounted on the cold head. The accuracy of temperature measurement was better than ± 0.1 K. A heater wire of $100\,\Omega$ was wound on the cold head. The diode sensor and the heater are connected to the Lakeshore temperature controller, which supplies controlled amount of power to the heater.

Schematic diagram of the resistivity measurement setup is given in Fig.2.3. A constant current (I) was passed through the sample using a constant current source (Keitheley model 224) and the voltage drop (V) across the sample was measured with a resolution of 10 nV by using Keitheley model 181 nanovoltmeter. Care was taken to eliminate the **thermo-e.m.f.** developed across the voltage leads.
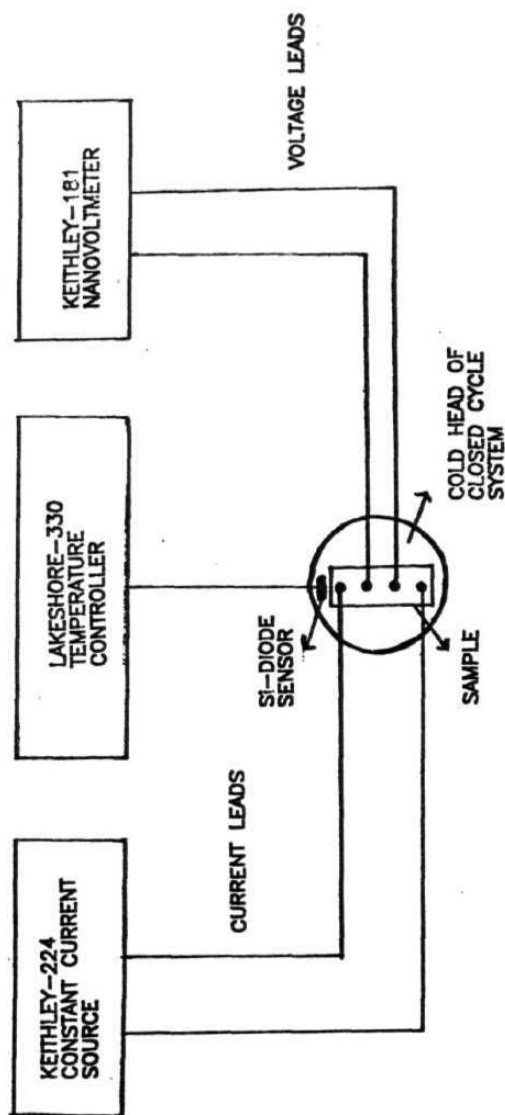
Fig.2.3 Schematic diagram of Resistivity set-up

The resistivity at a given temperature is calculated by using the relationship

$$\rho(T) = R(T)A/l \qquad (2.3.1)$$

where $R(T) = V/I$, is the resistance at temperature T, A is the area of cross section of the sample and l is the distance between the voltage leads. The accuracy of the absolute value of resistivity is $\pm$ $10\,\mu\Omega$ cm.

2.4   Thermoelectric Power

Seeback coefficient is the e.m.f., ΔV, developed when two conductors A and B are joined together with their two junctions at different temperatures T_1 and T_2 under the condition that no current flows in the circuit. It is the thermal e.m.f. which is measured in an ordinary thermocouple arrangement. The TEP is the e.m.f. produced per unit temperature difference between the two junctions i.e. AV/dT.

A thermal gradient AT is created between the two junctions $(\mathrm{AT} = T_2 - T_1)$, where T_1 and T_2 are the temperatures of the two ends. The voltage developed between the two junctions is AV, then TEP is defined as

$$S = \frac{\Delta V}{\Delta T} \quad for \quad \Delta T \to 0 \qquad (2.4.1)$$

i.e., S is the voltage produced per unit temperature difference between the two junctions.

There are two methods of measuring TEP of a sample. One is the integral method and another the differential method. In the integral method, one end of the sample is kept at a fixed temperature (in liquid nitrogen or liquid helium) and the temperature of the other end is changed continuously. This method can be used for long specimens like wires. In the second method a small temperature gradient AT is maintained across the

sample and the **seeback** voltage (AV) developed across the sample is measured. Owing to the size of our samples, the differential method was adopted to obtain the TEP data.

The schematic diagram of the experimental set-up is shown in Fig.2.4. TEP measurements were carried out on well characterized samples using dc differential technique in a closed cycle refrigerator system (APD make) in vacuum in the temperature range 40-300 K. The sample is held between the two copper electrodes. The sample and electrode assembly is mounted on the cold head of the closed cycle refrigerator. The temperature of the assembly is controlled and measured by the Si-diode sensor (DT-470) which is mounted on the cold head. One of the electrodes is mounted on the cold head itself, the second copper electrode is placed at the other end of the sample. The heater mounted on the second electrode is used to create a small temperature gradient of 1-3 K across the sample. The **temperature** gradient is measured by using calibrated coppcr-constantan thermocouple. The junctions of the thermocouples were fused on thin copper foils which were attached to the **electrodes** by using GE Varnish and Cigarette paper in between, which ensured good thermal contact as well as electrical isolation. Thin copper wires were attached to copper foils, which in turn were attached to the sample faces with silver paint. The voltage developed across the sample due to the temperature gradient is fed to a **Nanovoltmeter** (Keithley 181 model) through these copper leads. The entire sample assembly was covered by mylar foils to minimize the radiation losses.

The TEP measurements were carried out in the temperature range 40-300 K because of the poor sensitivity of the differential thermocouple below 40 K. At a fixed sample mean temperature, the voltage (ΔV) across the **sample** was measured for different values of AT between 1-3 K. TEP was calculated from the slope of AV vs AT curve. The measured TEP is the difference between the TEP of copper and the sample . So, the
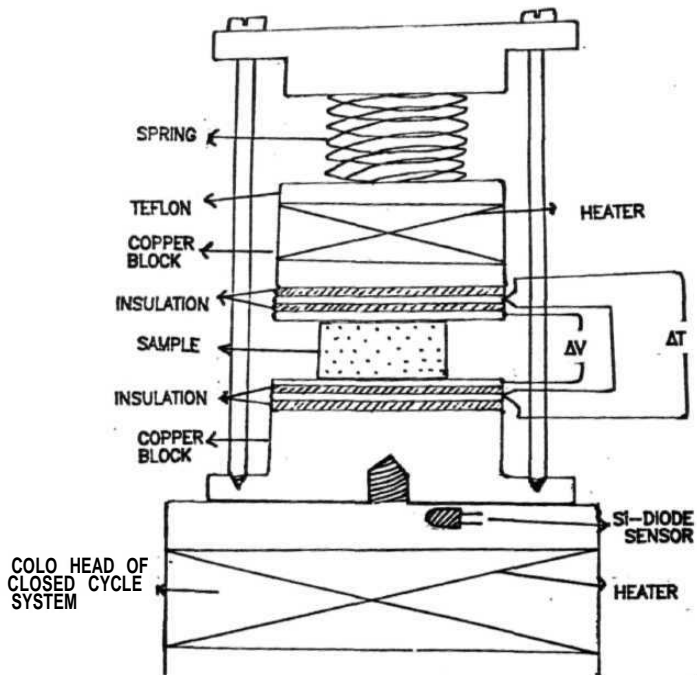
Fig.2.4 Schematic diagram of Thermoelectric power set-up

absolute TEP of the sample was obtained by correcting it for the thermoelectric power of the copper leads.

Chapter 3

SAMPLE PREPARATION AND CHARACTERIZATION

This chapter deals with the preparation and characterization of $Bi_2Sr_2Ca_{1-x}M_xCu_2O_y$ compounds, where M = Pr, Ce & Tb.

The synthesized samples were characterized by X-ray diffraction (XRD) for phase purity and solubility limits of various dopants. The lattice parameters were estimated and their dependence on the nature and the content of the dopant is discussed. The superconducting transitions were measured by AC susceptibility and the results are presented in this chapter.

3.1 Sample Preparation

All the samples were prepared by solid state reaction met hod. Samples of nominal composition $Bi_2Sr_2Ca_{1-x}M_xCu_2O_y$ (M = Pr, Ce & Tb and 0<x<1) were synthesized using the oxides; Bi_2O_3 (99.99 %), CuO (99.99 %), Pr_6O_{11} (99.9 %), CeO_2 (99.9 %) and Tb_4O_7 (99.9 %) and carbonates; $SrCO_3$ (99.9 %) and $CaCO_3$ (99.9 %) [1-3]. The chemicals were weighed out in the appropriate ratio and mixed thoroughly. The mixture was calcinated at $800\,^\circ C$ for 24 hours in a muffle furnace in air with several intermediate grindings. The reacted black powder was pressed into pellets of 13mm diameter and heat treated at $830\,^\circ C$ for 24 hours and quenched to room temperature. The pellets were again heat treated at $880\,^\circ C$ for 20-30 minutes (samples with higher dopant content required longer

heat treatment) and then **quenched** to room temperature. The pellets were given a final heat treatment at **830°C** for 24 hours and then quenched to room temperature. The room temperature quenching is found to be useful in raising the T_c values.

3.2 Structural studies

The samples were characterized by X-ray diffraction (XRD) in order to ascertain the phase purity and to estimate the lattice parameters from the observed reflections. The sample was taken in the form of powder and the X-ray diffractogram was recorded at room temperature using SIEFERT X-ray diffractometer with CuK_α radiation, whose characteristic wavelength is 1.5418 A . For phase identification, the patterns were compared against standard patterns reported in the literature and indexed (assigning h, k, l values). The lattice parameters were calculated by least square fitting assuming pseudo tetragonal symmetry.

3.2.1 Pr doped Series

Fig.3.1 shows the X-ray diffraction pattern obtained for Pr-doped series. The X-ray diffraction patterns reveal predominantly single phase formation in the substitution range 0<x<0.6 [1]. **Sumana** Prabhu *et al* also reported solid solutions upto 60% replacement of Ca by Pr in $Bi_2Sr_2CaCu_2O_y$ (Bi-2212) system [4]. Whereas, Gao *et al* [5] and **Xiaolong** Chen *et al* [6] have obtained complete solid solubility of Pr in the same system. Awana *et al* could obtain solid solutions only upto 50% of the doping level [7]. The plots of a and c lattice parameter vs. Pr-concentration (x) are shown in Fig.3.4. The **a-lattice** parameter increases slightly with increasing Pr-content. Whereas, the **c-lattice** parameter decreases significantly with increasing x.

3.2.2 Ce-doped series

Fig.3.2 shows the X-ray diffraction patterns obtained for Ce-doped series. The X-ray diffraction patterns reveal predominantly single phase formation in the substitution range $0<x<0.4$ [2]. Awana *et al* [7], Jordan *et al* [8] and Wang *et al* [9] have also reported solid solution formation only upto 40% replacement of Ca by Ce in **Bi-2212** system. Sawa *et al* [10], however could prepare solid solutions upto 50% dopant content in Ce-doped Bi-2212 system. The impurity phase started emerging for higher dopant concentration. The a **&** c lattice parameters are plotted against Ce-concentration (x) (Fig.3.4). As observed in the case of Pr-doped series, the a-lattice parameter increases marginally with increasing **Ce-content.** The *c*-**lattice parameter** shows a marked decrease with increasing x. The decrease in c-lattice parameter is faster compared to Pr-doped series.

3.2.3 Tb-doped series

Fig.3.3. shows the X-ray diffraction patterns obtained for Tb-doped series. The X-ray diffraction patterns reveal predominantly single phase formation in the substitution range $0<x<0.6$ [3]. The impurity phase started emerging above this dopant concentration. The plots of a and c lattice parameters vs. Tb-concentration (x) are shown in Fig.3.4. As observed in the case of Pr and Ce doped series, the increase in a-lattice parameter is marginal with increasing Tb-content (x). The c-lattice parameter, however, decreases significantly with increasing x. The decrease in c-lattice parameter is comparable with the depression rate observed for Pr-doped series.

Small increase in a-lattice parameter with increase in x is observed in all the three series of samples [1-3]. Similar changes in a-lattice parameter value have been reported in other rare-earth substituted Bi-2212 systems and **Tl-based** systems [4-13]. The elongation of the a-axis is attributed to the decrease in **Cu-valence.** The dopant ion introduces
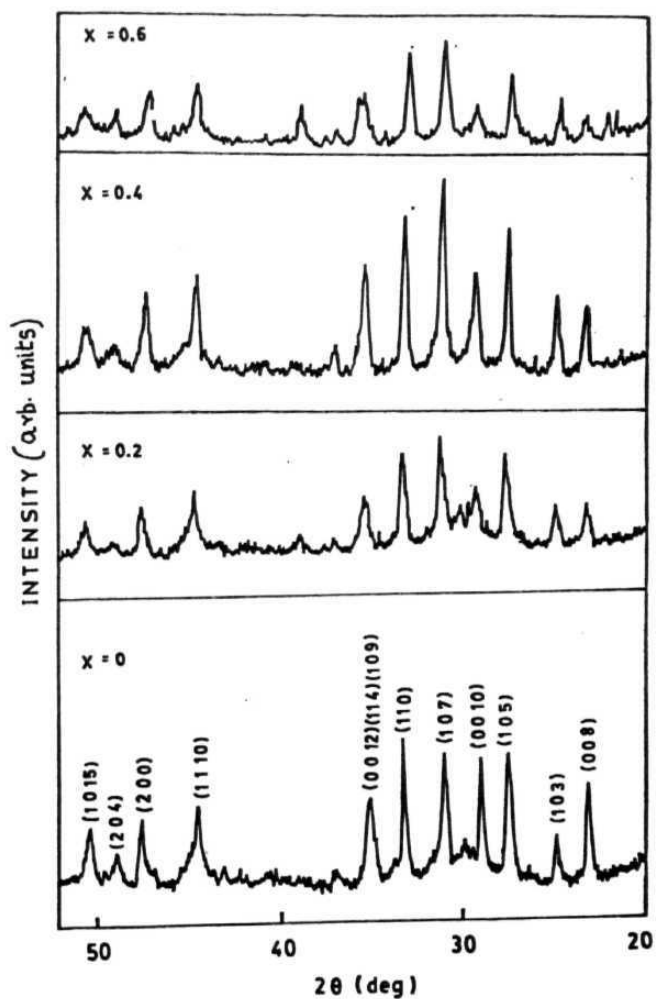
Fig.3.1 XRD patterns for the samples $Bi_2Sr_2Ca_{1-x}Pr_xCu_2O_y$ where x = 0, **0.2,** 0.4 and 0.6
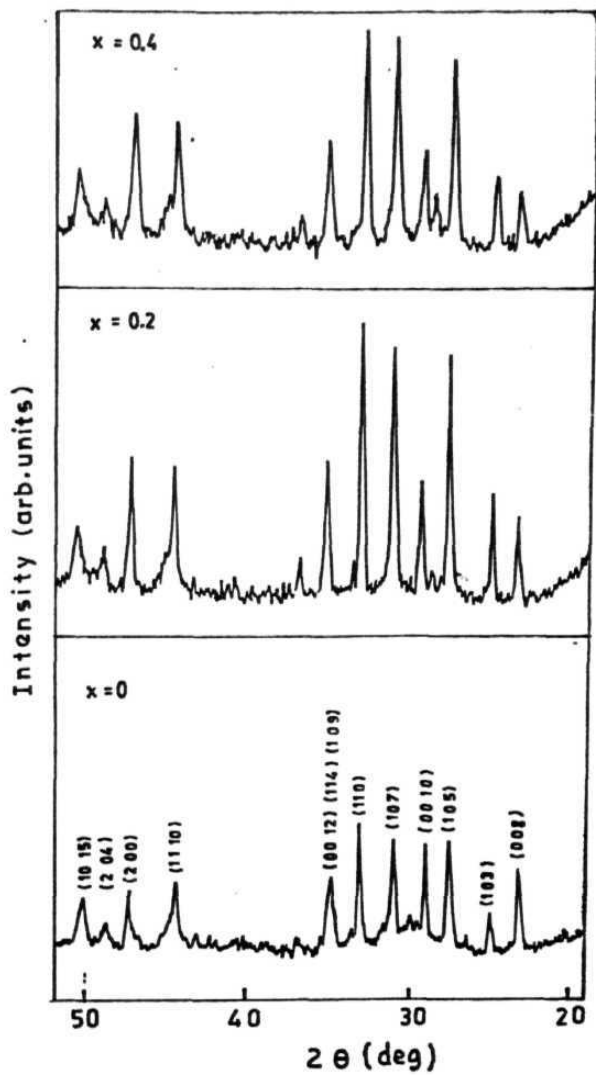
Fig.3.2 XRD patterns for the samples $Bi_2Sr_2Ca_{1-x}Ce_xCu_2O_y$ where x = 0, 0.2 and 0.4
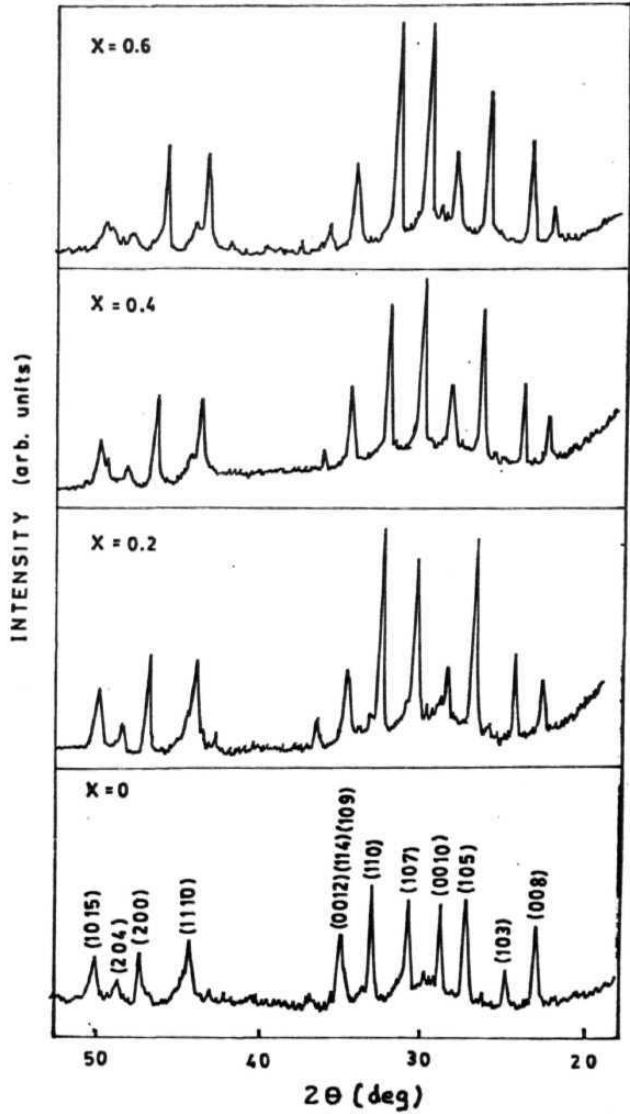
Fig.3.3 XRD patterns for the samples $Bi_2Sr_2Ca_{1-x}Tb_xCu_2O_y$ where x = 0 0 2 0.4 and 0.6
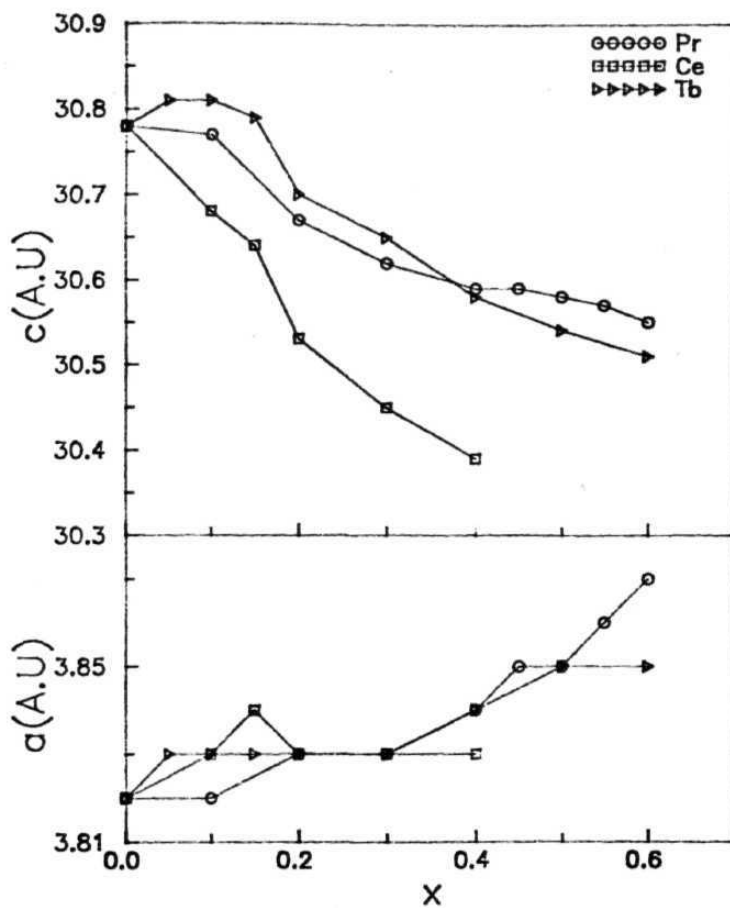
Fig.3.4 Vanation of a and c lattice **parameters** as function **ot** dopant **concen-**
tration (x)

extra electrons in the lattice. The extra **electrons** reduce the Cu valence and thus lead to an increase in Cu-0 bond length, reflected as an increase in the **a-lattice** parameter.

The **c-lattice** parameter, however, decreases with increase in x. Among the three series of samples studied, the c-lattice parameter falls sharply for Ce-doped samples in comparison to **the** other two series. Decrease in c-lattice parameter is also reported in other rare-earth doped **Bi-2212** systems [4-13]. In the case of other rare-earth substitutions like Y [5] and Gd [13], this change can be attributed to the smaller radius of the substituent ion. In the case of present samples also, one can attribute the same reason to the present systems, provided the substituent ion exists either in +4 state or between +3 and +4 states. It is likely that the rare earth ions may be distributed between the Ca and Sr sites, as in the case of Y-doped Bi-2212 system reported by Almeras *et al* [14] from photocmission spectroscopy studies. From the comparison of ionic radii of Sr^{+2} (1.13), Ca^{+2} (0.99), Ce^{+3} (1.11), Ce^{+4} (1.01), Pr^{+3} (1.09), Pr^{+4} (0.92), Tb^{+3} (1.0), Tb^{+4} (0.90), it is likely that larger trivalent rare-earth ion may substitute Sr site in preference to Ca site, and thus lead to the decrease in c-lattice parameter. However, detailed analysis is necessary to resolve this issue.

There can be, however, another explanation for the decrease in c-lattice parameter. The substitution of rare-earth ion at Ca site introduces excess oxygen in between the Bi-0 double layers [11. 12, 15-17], which consequently decreases the **metallicity** and the superconducting transition temperature [18]. This excess oxygen reduces the net positive charge and thus repulsion between the Bi-0 double layers leading to a decrease in c-lattice parameter [2.15]. The observed decrease in c-lattice parameter, therefore, can be ascribed to the excess oxygen between the Bi-0 double layers. This effect is likely to be more pronounced, if Ce exists as Ce^{+4} ion and thus the faster decrease in c-lattice

parameter of Ce-doped Bi-2212 system in comparison to other rare-earth dopants can be explained [2]. This is consistent with the faster depression rate in superconducting transition temperature in the case of Ce-doped Bi-2212 system [2].

3.3 AC susceptibility

AC susceptibility study gives information about the superconducting transition temperature, volume fraction of the superconducting phase, **microstructure** etc [19,20]. The complex AC susceptibility (x) is defined as $\chi = \chi' + i\chi''$, where χ', the in-phase (inductive) component describes the dispersive response to the diamagnetic transition and x" the out-of-phase (resistive) component describes energy dissipation. AC susceptibility measurements were carried out on these series of samples at a field of 0.3 Oe and a frequency of 33 Hz. The samples were cooled in zero field. The χ' and x" as a function of temperature for Pr, Ce and Tb doped Bi-2212 samples are shown in **Fig.** 3.5, 3.6 and 3.7 respectively.

The sintered high T_c materials exhibit double drop behavior in x'-T curve. The drop at high temperatures is intrinsic to the grains of the superconductor $(T_c(\text{gran}))$ and the other drop at low temperatures is characterstic of the coupling between grains, which determines the bulk superconducting properties of the compound $(T_c(\text{bulk}))$ [21-24]. Both these critical temperatures are field **dependent** [22, 25]. Multiphase compounds also exhibit this type of double drop behavior of χ'-T plots. Measurements were carried out on powders of these samples which contained only isolated grains. A single drop in x'-T plot was observed, which is due to the grains. This observation and the fact that the XRD studies indicate no impurity phases, confirm that the double drop behavior observed in X'-T plot is characteristic of the granular nature of the present samples. With increasing x, decrease in the diamagnetic onset temperatures $(T_c(\text{bulk})$ and $T_c(\text{gran}))$ is observed
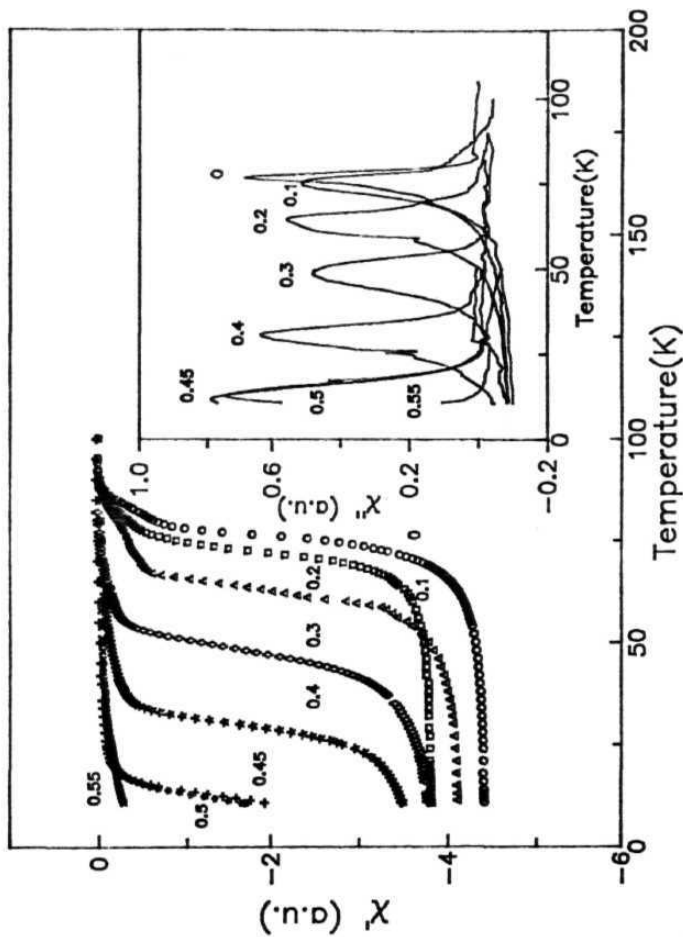
Fig.3.5 Plot of χ' vs. T for $Bi_2Sr_2Ca_{1-x}Pr_xCu_2O_y$ samples (χ''-T plot shown as an inset)
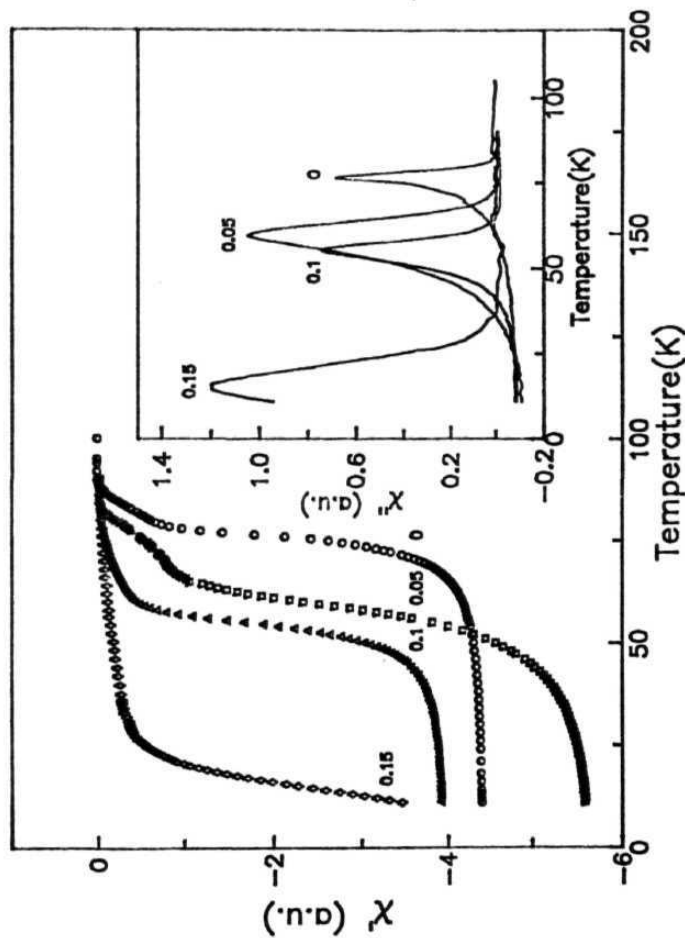
Fig.3.6 Plot of χ' vs. T for $Bi_2Sr_2Ca_{1-x}Ce_xCu_2O_y$ samples (χ''-T plot shown as an inset)
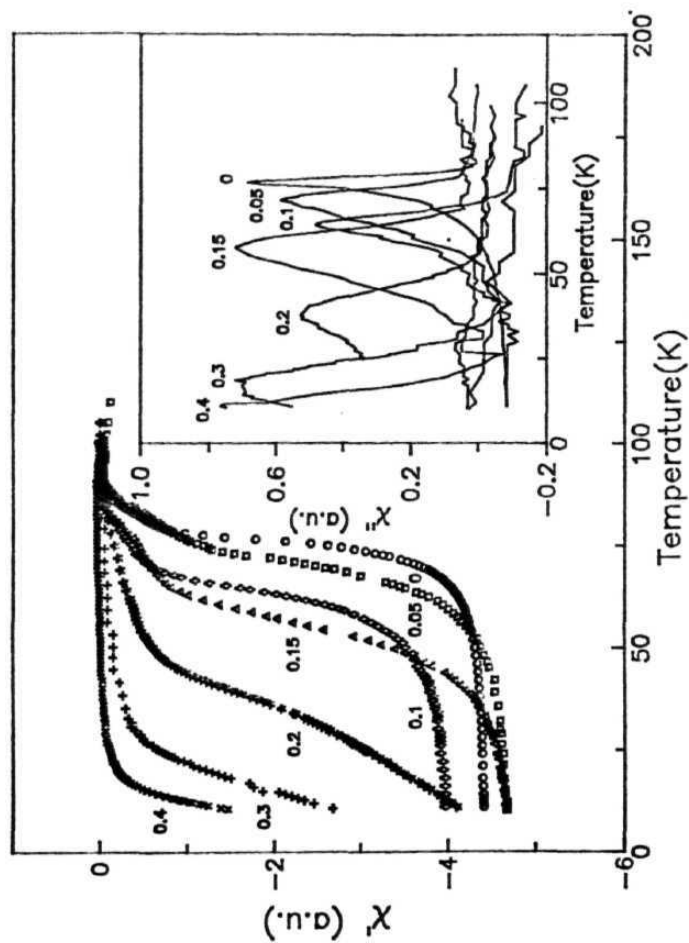
Fig. 3.7 Plot of χ' vs. T for $Bi_2Sr_2Ca_{1-x}Tb_xCu_2O_y$ samples (χ''-T plot shown as an inset).

for all the three series of samples.

$\chi"$-$\mathbf{T}$ plots show a peak, whose width depends on the connectivity between the grains [19]. The broadening of this peak is seen with increase in x and its absence for higher dopant concentrations may be due to the reduction in volume fraction of superconducting phase with increase in x. The parameters $(\mathbf{T_c(gran)},$ $\mathbf{T_c(bulk)}$ and $\chi"(T)$ peak temperature) obtained from the measurements are listed in **Table-3.1** for all the three series of samples.

Table-3.1

peak temperature, T_c(gran) and T_c(bulk) for various superconducting samples

x	χ'' peak temperature (K)	T_c(gran) (K)	T_c(bulk) (K)
Pr-doped			
0	77	90	79
0.1	72	88	75
0.2	65	84	68
0.3	49	71	55
0.4	**31**	70	35
0.45	13	70	28
0.5	-	42	21
0.55	-	40	18
Ce-doped			
0.05	60	82	64
0.1	**51**	**84**	54
0.15	-	78	19
Tb-doped			
0.05	72	90	74
0.1	64	87	69
0.15	**58**	87	**65**
0.2	38	87	**54**
0.3	**16**	85	**29**
0.4	-	82	20

3.4 References

1. D. Rama Sita and R. Singh, *Int. J. Mod. Phys.* B 8, 2283 (1994).

2. D. Rama Sita and R. Singh, *Solid State Commun.* 94, 969 (1995)

3. D. Rama Sita and R. Singh, *Proceedings of DAE Solid State Physics Symp. (India)* **38C**, 283 (1995).

4. P. Sumana Prabhu, M. S. Ramachandra Rao, U. V. Varadaraju and G. V. Subba Rao, *Phys. Rev.* **B50,** 6929 (1994).

5. Y. Gao, N. Spencer, H. Chen and R. E. Salamon, *Phys. Rev.* **B45,** 13 (1992).

6. Xiaolong Chen, Jingkui Liang, Jinrong Min, Jianqi Li, Guanghui Rao, *Phys. Rev.* **B50,** 3431 (1994).

7. V. P. S. Awana, S. K. Agarwal and A. V. Narlikar and M. P. Das *Phys. Rev.* **B48,** 1211 (1993).

8. Frederic Jordan and Octavio Pena, *Physica* C231, 311 (1994).

9. Ruiping Wang, Hisashi Sekine and Hua Jin, *Supercond. Sci. Technol.* 9, 529 (1996).

10. Akihito Sawa, Tae-Su Han, Takayuki Iwamatsu, Hiromoto UWE, Tunetaro Sakudo, *Physica* B165&166 553 (1990)

11. A. Manthiram and J. B. Goodenough, *Appl. Phys. Lett.* 53, 420 (1988).

12. B. Jayaram, P. C. Lanchester and M. T. Weller, *Physica* C160, 17 (1989).

13. B. Jayaram, P. C. Lanchester and M. T. Weller, *Phy. Rev.B* 43, 5444 (1989).

14. P. Almeras, H. Berger and G. Margaritondo, *Solid State Commun.* **87,** 425 (1993).

15. Y. Y. Xue, P. H. Hor, Y. Y. Sun, Z. J. Huang, L. Gao, R. L. Meng, C. W. Chu, J. C. Ho and C. W. Wu, *Physica* C158, 211 (1989).

16. S. Olivier, W. A. Groen, C. Van der Beek and H. W. Zandbergen, *Physica* **C157,** 531 (1989).

17. J.M Tarascon, P. Barboux, G.W. Hull, R. Ramesh, L. H. Greene, M. Giroud, M. S. Hedge and W. R. McKinnon, *Phys. Rev.* 39, 4316 (1989).

18. S. B. Samanta. P. K. Dutta, V. P. S. Awana, E. Gmelin and A. V. Narlikar, *Physica* **C178,** 171 (1991).

19. R. B. Goldfarb. M. Lelental and C. A. Thompson, *Magnetic susceptibility of superconductors and other spin systems* edited by R. A. Hein, T. L. Francavilla & D. H. Liebenberg (Plenum press. New York & London).

20. M. Couach and A. F. **Khoder,** *Magnetic Susceptibility of Superconductors and Other Spin Systems* edited by **R.** A. Hein, T. L. Francavilla and D. H. Lienbenberg, Plenum Press, New York (1992).

21. M. B. Elzinga and C. **Uher,** *Phys.* ***Rev.*B32,**88 (1985).

22. R. B. Goldfarb, A. F. Clark, A. I. Branginski and A. J. Panson, *Cryogenics* 27 457 (1988).

23. D. X. Chen, R. B. Goldfarb, J. Nogues and K. V. Rao, *J.* ***Appl.*** *Phys.* 63 980 (1988).

24. H. Kupfer, I. Apfelstedt, W. Schauer, R. Flukiger, R. **Meier-Hirmer** and H. **Wühl,** *Z. Phys.* B69 159 (1987).

25. J. Garcia, C. **Rillo,** F. Lera, J. **Bartolome,** R. Navarro, D. H. A. Blank and J. Flokstra, *J. Magn. Magn. Mater.* 69, L225 (1987).

Chapter 4

RESISTIVITY STUDIES

This chapter deals with the resistivity studies on $Bi_2Sr_2Ca_{1-x}M_xCu_2O_y$ (M = Pr, Ce & Tb) samples as a function of temperature. The systematic resistivity measurements on these samples were carried out by the standard four probe method as a function of temperature in the temperature range 8-300 K using a closed cycle He-refrigerator. The results obtained are presented below.

4.1 Results

Fig.4.1 shows the temperature dependence of resistivity for various members of the Pr-doped $Bi_2Sr_2CaCu_2O_y$ (Bi-2212) system. In the normal state, the samples for $0<x<0.55$ are characterized by linear temperature dependence of resistivity of the form

$$\rho = \rho_o + \alpha T \qquad (4.1.1)$$

where ρ_o and a = $(d\rho/dT)$ are the residual resistivity and the **metallicity** of the material respectively. In the normal **state,** the temperature derivative of resistivity is positive. The sample with x = 0.6 shows semiconducting behavior throughout the temperature range of measurement. The room temperature resistivity (ρ_{300}), residual resistivity (ρ_o), metallicity (a), superconducting onset temperature $T_c(onset)$, the zero resistivity temperature $T_c(zero)$ and the temperature at which $d\rho/dT$ is maximum T_c, are given in **Table-4.1.** A linear increase in ρ_{300} and ρ_o is observed with increasing Pr-content (x)
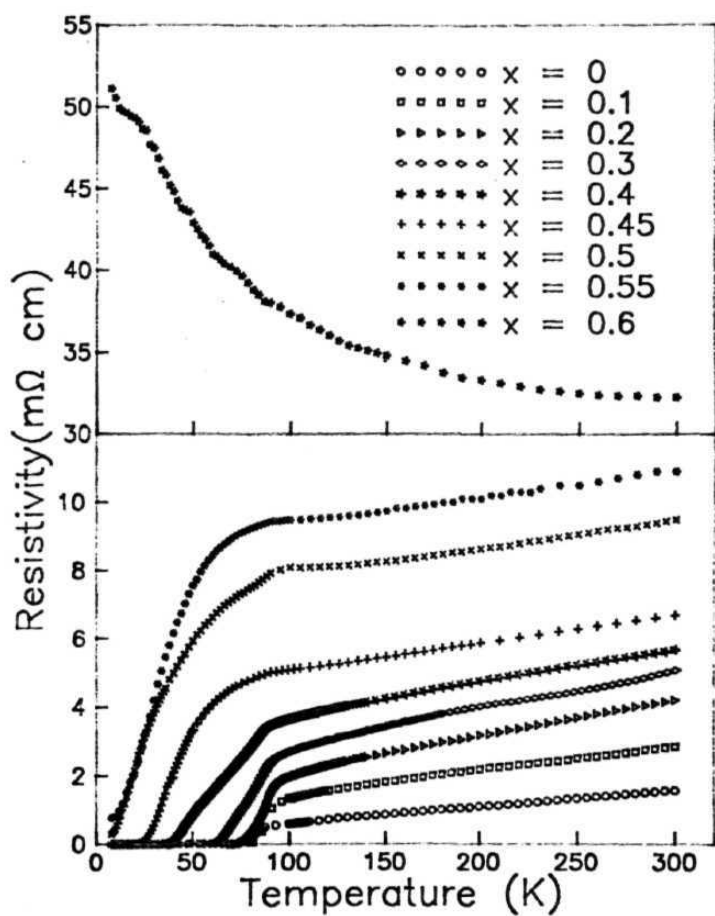
Fig.4.1 Plot of resistivity vs. temperature for $Bi_2Sr_2Ca_{1-x}Pr_xCu_2O_y$ samples

Table-4.1

Various physical parameters obtained for $Bi_2Sr_2Ca_{1-x}M_xCu_2O_y$ (M = Pr, Ce and Tb) systems

sample x	ρ_{300} (*mil* cm)	P_O (mΩ cm)	a ($\mu\Omega$ cm K^{-1})	T_c(zero) (K)	T_c(onset) (K)	T_c (K)	P
Pr-doped							
0	1.56	0.14	4.7	78	86	82	0.20
0.1	2.84	0.81	6.7	77	93	89	0.18
0.2	4.20	1.09	10.3	75	93	87	0.13
0.3	5.08	1.94	10.3	61	92	80	0.12
0.4	5.68	2.87	9.4	37	87	64	0.10
0.45	6.62	4.23	8.2	20	58	42	0.08
0.5	9.49	7.00	8.3	-	52	29	0.07
0.55	10.90	8.56	7.9	-	54	**31**	0.07
0.6	32.3	-	-	-	-	-	-
Ce-doped							
0.05	3.01	1.25	**5.9**	69	**87**	78	0.12
0.1	3.89	1.48	**8.0**	67	85	77	0.12
0.15	16.6	14.39	7.4	20	88	65	0.10
0.2	19.3	-	-	-	54	30	0.07
0.3	72.2	-	-	-	-	-	-
0.4	75.2	-	-	-	-	-	-
Tb-doped							
0.05	3.16	1.14	6.8	**63**	**98**	92	0.16
0.1	3.22	0.96	7.6	60	**98**	92	0.16
0.15	5.87	3.13	9.3	54	98	89	0.14
0.2	9.27	6.13	10.7	30	98	83	0.13
0.3	16.85	12.56	14.6	-	86	61	0.10
0.4	11.25	5.37	19.8	-	84	33	0.07
0.5	160.6	-	-	-	-	-	-
0.6	271.3	-	-	-	-	-	-

upto x = 0.55. With increase in Pr-content (x), the superconducting transition width is found to increase. The Metal-Insulator (MI) transition *i.e.,* the change in the sign of the temperature coefficient of resistivity is observed for room temperature resistivity value $\approx 2 \times 10^{-2} \Omega$ cm. With increasing Pr-content, there is no significant change in T_c(zero) for $x \leq 0.2$; while for 0.3<x<0.55 the decrease is rather fast. The T_c(onset) increases with increasing x upto x<0.2 and for x>0.3 it decreases. T_c(zero) is observed for samples with x<0.45 whereas only T_c(onset) is seen for x<0.55. The sample with x = 0.6 shows semiconducting behavior.

Fig.4.2 shows the temperature dependence of resistivity for various members of the Ce-doped series. The superconducting samples with 0<x<0.15 are characterized by linear temperature dependence of resistivity in the normal state with positive temperature derivative of resistivity (α). The sample with x = 0.2 shows weak semiconducting behavior and superconducting onset temperature around 54 K. Samples with x = 0.3 and x $\leq$ 0.4 show semiconducting behavior throughout the temperature range. The values of ρ_{300}, ρ_o, a, T_c(onset), T_c and T_c(zero) are listed in Table-4.1. Slow increase in ρ_{300} and ρ_o with increasing Ce concentration (x) upto x = 0.1 is observed. The increase is sharp as we go towards the higher dopant concentrations. T_c(onset) is more or less constant and T_c(zero) decreases with increase in x. The pronounced change in the normal state resistivity and its temperature dependence is accompanied by the drastic decrease in T_c as x increases from 0.1 to 0.2, This means that upto 10% of Ce substitution, the dopant can be accommodated without seriously affecting the superconducting matrix. With increase in x, the transition width is also found to increase. For Ce-substitution between 10-20% of Ca, the T_c depression rate is very fast in comparison to other rare-earth substitutions. In this system also MI transition is observed around the normal state resistivity value of $2 \times 10^{-2} \Omega$ cm.
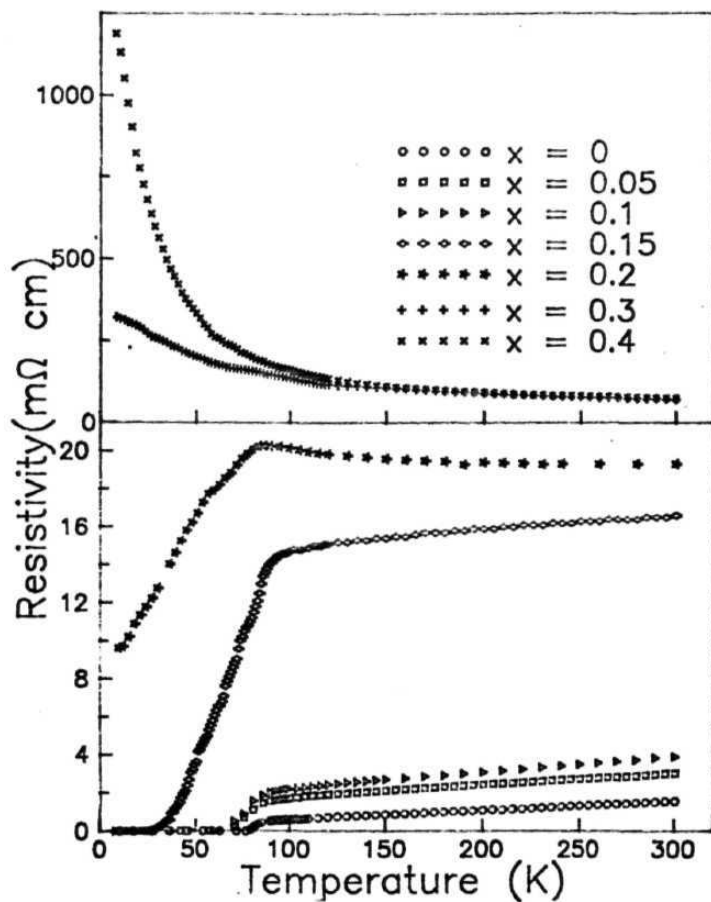
Fig.4.2 Plot of resistivity vs. temperature for $Bi_2Sr_2Ca_{1-x}Ce_xCu_2O_y$ samples

Fig.4.3 shows the resistivity variation as a function of temperature for various samples of **Tb-doped** series with 0<x<0.6. Samples with x<0.4 are superconducting and charac- terized by linear temperature dependence of resistivity in the normal state **[Eqn.(4.1.1)]**. Samples with x = 0.5 and 0.6 are semiconducting. The room temperature resistivity ρ_{300}, ρ_o, a, T_c(onset), T_c(zero) and T_c are given in **Table-4.1.** The ρ_{300} and ρ_o values are found to increase with increase in dopant concentration except for the sample with x = 0.4. The increase in ρ_{300} is sharp for x > 0.4. The α value increases with **increasing** x value. The **MI** transition is observed when ρ_{300} ≈ $2 \times 10^{-2} \Omega$ cm. T_c(zero) decreases with the increase in dopant concentration. Initially T_c(onset) increases when x is increased from 0 to 0.05 and then it attains a constant value for 0.05<x<0.2. Only T_c(onset) could be observed for sample with x = 0.4. From the T_c vs x plot, it can be seen that T_c initially increases marginally with x, reaching a **maximum** value at around x = 0.1 and then it decreases rapidly for higher dopant content [Fig.4.4]. The transition broadening takes place with increase in x value. The **MI** transition is observed at around x = 0.5.

4.2 Analysis of the resistivity data of the superconducting samples

The observed increase in ρ_{300} and ρ_o can be attributed to the impurity scattering due to the introduction of dopant ion into the lattice. Similar kind of changes are reported in other rare-earth doped systems [1].

The transition broadening is observed in all the three series of samples with increase in x value. The transition broadening may indicate the presence of secondary phases, but XRD patterns do not indicate the presence of any secondary phases. Rare-earth substitution in **Bi-2212** system is expected to reduce the hole concentration and raise
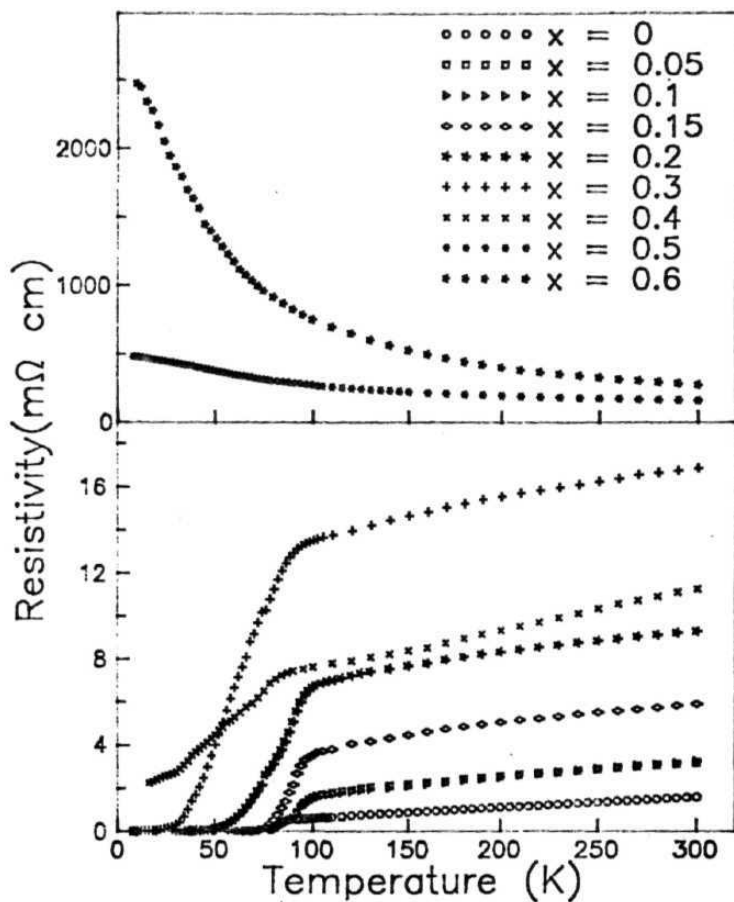
Fig.4.3 Plot of resistivity vs. temperature for $Bi_2Sr_2Ca_{1-x}Tb_xCu_2O_y$ samples
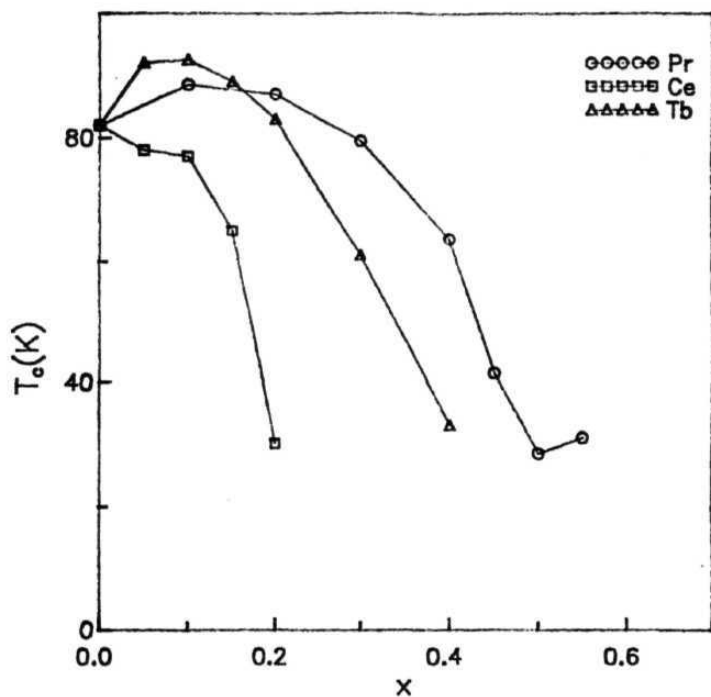
Fig.4.4 Plot of T_c vs. x for $Bi_2Sr_2Ca_{1-x}M_xCu_2O_y$ (M = Pr, Ce & Tb) samples

the oxygen content [2]. From STS studies, **Samanta *etal*** [3] found extra oxygen interca-
lated in the redox Bi-0 layers. The observed transition broadening may be due to the
intercalated oxygen **between** the Bi-0 layers. Chen *et al* [4] in the Pr-doped **Bi-2212**
system attributed this transition broadening to the existence of two phases with different
modulation periods. From the electron diffraction studies, they found two modulated
structures, one with a long period and other with short period. They have attributed
the short-period phase to a Pr-poor phase which possess high T_c, and the long period
phase to a Pr-rich phase having low T_c. The increase in transition width suggest the in-
tergrowth of these two phases in grains. At higher concentrations, the long period phase
governs the transport. This kind of model was used to explain the Pr-doping effects in
$YBa_2Cu_3O_{7-\delta}$ **[Y-123]** also [5-6].

Superconducting phase diagrams for several high T_c oxides [7-10] show that T_c in-
creases with increase in carrier concentration, passes through a maximum and then falls
steeply to zero when the carrier concentration reaches a critical value. So, the changes
in T_c values can be explained in terms of change in carrier concentration. The increase
in dopant content leads to a decrease in carrier **concentration**. Optimum carrier concen-
tration (for which maximum T_c is expected) is achieved as the dopant content increases,
leading to an increase in T_c**(onset)**.

Presland *et al* [10] have found that the phase diagram for several doped cuprate
systems is well described by the parabola

$$T_c/T_c(max) = 1 - 82.6(p - 0.16)^2 \qquad (4.2.1)$$

For Bi-2212 system T_c (max) = 92 K is taken to calculate the *p* value for the **super-**
conducting samples. The estimated *p* values are given in **Table-4.1.** The initial increase

in T_c with increase in dopant content indicates that undoped sample is slightly in the overdoped region.

The T_c depression rate is faster in the case of Ce-doped series compared to the other two series [Pig. 4.4] of samples. In other studies on rare-carth doped Bi-2212, the critical concentration x_{cr} at which T_c(zcro) goes to zero is reported to be generally between 0.4 and 0.6 [11-21]. In the present study, the critical concentration of Ce is about half that of other trivalent rare-earth dopant [22-24]. From this we can infer that Ce-exists pre-dominantly in +4 valence state. The faster decrease observed in the c-lattice parameter of Ce-doped Bi-2212 also supports this conclusion.

Jayaram *et.al.* [19] explained the observed gradual decrease in T_c as a function of normal state resistivity (in the range 3-$12m\Omega$ cm) in the Gd-doped Bi-2212 samples on the basis of a theoretical model derived for 2D conventional superconductors considering the disorder effects [25]. The T_c depression rate observed in the present series of samples with the normal state resistivity in the range 3-$12m\Omega$ cm does not permit the analysis on the lines adopted by Jayaram *et al* [19].

The rare-earth substitution at Y-site in Y-123 have been well studied. The $PrBa_2Cu_3O_7$ compound is the only isostructural member of the series of $RBa_2Cu_3O_7$ compounds, which is non-metallic and non-superconducting [26]. Several reasons have been proposed for the suppression of superconductivity by the Pr-substitution in $RBa_2Cu_3O_7$ [27] *i.e.,* hole filling effect, pair breaking effect via exchange scattering of mobile holes by Pr-magnetic moments and hole localization effect. The origin of T_c suppression in Y-123 by Pr-substitution still remains a subject of controversy.

The magnetic property measurements [28] suggested that Pr^{+4} ion in Pr-doped Y-123 system fills the holes in the conduction band. The recovery of superconductivity by partial substitution of Ca in $PrBa_2Cu_3O_7$ is interpreted as a verification of this view (29]. However, electron energy loss spectroscopy (EELS) study [30] indicates that the total hole concentration is uneffected by Pr. Optical measurements [30,31] such as x-ray photoemission spectroscopy suggest that Pr exists as a +3 ion and localizes the holes. The localization of holes is attributed to the hybridization of Pr-4/ states with the $Cu3d$-$O2p$ states in the CuO_2 planes [32,33]. From the studies like Hall effect and muon spin relaxation measurements [34], it is apparent that substitution of Pr at Y-site reduces the mobile hole concentration while the total hole concentration does not change.

It is well known for conventional superconductors that magnetic impurities have dramatic effects on T_c. Abrikosov and Gorkov (AG) developed a theory to explain the suppression of T_c due to magnetic impurity [35]. According to AG theory, the magnetic impurity interacts with the spins of the electrons in the Cooper pairs, making the spin states of the electrons change, which leads to the breaking of Cooper pairs and in turn suppression in T_c. The AG interactions deal with the exchange interaction between the magnetic impurity (of spin S) and a conduction electron (of spin s) given by H_{ex} = -JSs where J is the exchange integral, which characterizes the strength and the sign of the interaction. The theory predicts a decrease in T_c with x given by a universal relation

$$ln(T_c/T_{co}) = \Psi(1/2) - \Psi(1/2 + 0.14T_{co}x/x_{cr}T_c) \tag{4.2.2}$$

or

$$T_c/T_{co} = f(x/x_{cr}) \tag{4.2.3}$$

where x is the impurity concentration, T_c is the superconducting transition temperature of the sample with impurity concentration x. x_{cr} corresponds to the concentration

for $T_c = 0$ (complete suppression of superconductivity) and ty is digamma function.

For small values of x

$$T_c \approx T_{co} - \left[\frac{\pi^2}{4k_B}N(E_F)\mathbf{J}^2(g-1)^2 J(J+1)\right] x \qquad (4.2.4)$$

$N(E_F)$ is the density of states at the Fermi level. g and J are, Lande g factor and total angular momentum for the Hunds's rules ground state of impurity ion respectively. According to this formula, T_c depression should follow approximately the de Gennes factor $(G = (g\text{-}1)^2 J(J+1))$ and T_c is expected to decrease linearly with x at low carrier concentrations and at a critical concentrations x_{cr}, superconductivity completely vanishes. Substituting the slopes of the T_c vs x plot in the following equation one can calculate x_{cr}

$$x_{cr} = \frac{-\pi^2 e^{-\tau}}{(dT_c/dx)}\left[\frac{T_{co}}{8}\right] \qquad (4.2.5)$$

where r = -0.5772 is the Euler's constant.

It is seen that strong magnetic ions like Gd are not affecting the T_c, whereas Pr affects the T_c drastically. This result is not in accordance with the theory.

Zhao *et al* [36] suggested that the observed deviations from AG pair-breaking theory may be explained by taking into account the correlations between the spins of the impurity and their ordering. In the AG pair breaking theory, there are two basic assumptions. First, the magnetic impurities are distributed randomly. Secondly , the spins of the magnetic impurity do not show any correlation (such as magnetic order). These assumptions can be satisfied in conventional superconductors because x_{cr} is low. In the case of high T_c materials, x_{cr} is high; inter impurity interaction may arise. The spins of the magnetic impurity may have some correlation and this will weaken the effect of pair breaking. The inhomogeneous distribution of the dopant ion may weaken the effect of pair-breaking.

Considering the above factors, the deviation from the T_c vs x plot may be qualitatively explained.

Neumeier *et al* [37] from their studies on Pr doped Y-123 system, (Y partially replaced by Ca), suggested an empirical relation which incorporates the hole filling (or localization) of mobile holes in the CuO_2 planes and superconducting electron pair breaking via exchange scattering of mobile holes in the CuO_2 planes by Pr-magnetic moments [37,38]. Both these effects are assumed to involve hybridization of Pr 4/ with 0 *2p* states [39]. Hybridization could generate an appreciable exchange interaction between the Pr magnetic moments and the spins of the mobile holes in the CuO_2 planes. This results in a depression of T_c with paramagnetic impurity concentration that is linear in the low concentration regime [40,41].

Infante *et al* [42] discussed the T_c suppression in $LaCaBaCu_3O_{7-\delta}$ (the results obtained for this system are quantitatively similar to $Y_{1-x}Pr_xBa_2Cu_3O_{7-\delta}$ system) in view of a percolation model. According to this model, $Y_{1-x}Pr_xBa_2Cu_3O_{7-\delta}$ system contains two kinds of unit cells: Y- containing and Pr-containing. The unit cells with Y have itinerant electrons and those with Pr have localized electrons. The connectivity between these cells determines the conduction. The important conductivity is within the planes and the relevant geometry is square planar array. The site percolation threshold is then the relevant parameter in the connectivity problem. This value is 0.59 for square planar array [43]. That means for x<0.41, the unit cells containing Y are connected and the system resembles $YBa_2Cu_3O_{7-\delta}$; while for x>0.59 the unit cells containing Pr are connected so that the system resembles $PrBa_2Cu_3O_{7-\delta}$. In the region close to 0.41<x<0.59, there is no percolation of either of the unit cells and in effect a mixed phase behavior is

expected. The region in which Y unit cells are connected is the metallic **region. Super-**conductivity appears in this region only. The superconductivity transition is expected to be sharp in the region for x<0.4. The nature of the resistivity changes for the x>0.4 samples, which are at the border line of **MI** transition, is consistent with the nature of resistivity changes associated with the connectedness transition in other percolating systems of thin film superconductors [44]. The classical percolation threshold may not hold good for the superconductivity transition because of constraints on the size due to coherence length. This model is dependent only on the geometry and therefore explains the resistivity behavior of the both $Y_{1-x}Pr_xBa_2Cu_3O_{7-\delta}$ and $LaCaBa_2Cu_3O_{7-\delta}$ systems. The relevance of the percolation model in the **MI** transition in 3D perovskite oxides has been discussed by Ganguly [45]. In various $La_{1-x}Sr_xBO_3$ systems (B = Co, V and Mn), metallization appears at a value of x = 0.25 and 0.3 which is approximately equal to the site percolation threshold ($\sim$ 0.3) of cubic system.

In the present $Bi_2Sr_2Ca_{1-x}M_xCu_2O_y$ system, the **MI** transition is observed around x = 0.6 for M = Pr, around x = 0.2 for M = Ce and around x = 0.4 for M = **Tb.** This transition can not be explained in view of percolation model because this model depends only on the geometry of the system and **MI** transition is expected to occur at the same dopant concentration (x) in all the three systems.

T_c vs x plot for the present systems show that Ce suppresses the T_c faster than the other two rare-earth ions. The T_c depression rates of Pr and Tb doped **Bi-2212** systems are similar. The difference in the suppression rates at higher dopant concentrations (x), may be ascribed to the difference in ionic radii of the two rare-earth ions. The T_c suppression rate in the present system has no correlation with the magnetic nature of the dopant ion. According to the AG theory, the T_c suppression rate should vary linearly

with the concentration of the dopant ion at lower concentrations, which is not observed in the present system. The T_c depression rate should be more for strong magnetic ion. In our case Ce^{+4} ion which is non-magnetic shows a faster depression. The disorder introduced by the dopant ion may leads to Anderson localization [46], thereby depressing the T_c. Still the faster T_c depression in the case of Ce-doped series is difficult to explain.

The T_c suppression in the present system can be explained by hole filling mechanism. It is well established that the transition temperature in high T_c superconductors is highly sensitive to the hole concentration in CuO_2 planes [7,8]. The T_c suppression in the present system could be due to the extra electrons introduced by the substitution of trivalent rare-earth ion at Ca site which fills the Cu_{3d} - O_{2p} band. From the faster depression rate of T_c in the case of Ce doped Bi-2212 system, it can be inferred that Ce predominantly exist in +4 valence state. The faster decrease in the c-lattice parameter in the case of Ce doped Bi-2212 also supports this conclusion. Moreover, the closed shell of Ce^{+4} precludes the possibility of any pair breaking interaction. From the T_c depression rate and the decrease in c-lattice parameter, it can be concluded that Pr and Tb ions predominantly exist in the +3 valence state in the Bi-2212 system. The T_c suppression in the case of non-magnetic Y at the Ca-site follows the same trend as that of Pr and Tb. From the dc susceptibility studies [47] on Pr and Gd in Bi-2212, it has been pointed out that there is no interaction between rare-earth ion magnetic moments via Cu_{3d}-O_{2p} orbitals. This indicates that magnetization of the rare-earth ion has no additional effect on T_c suppression.

4.2.1 Theoretical models on T-linear resistivity of superconducting samples

The resistivity varies linearly with T in the normal state of the present superconducting samples.

The resistivity data reported in the literature show that, high T_c superconductors are generally characterized by linear temperature dependence of resistivity in the normal state over a wide temperature range [48-50]. The resistivity of La-system is linear in the temperature range, T_c to 1000 K. The linearity extends upto $\approx$ 600 K in Y-123 system. The residual resistivity is very small. There are a number of theoretical interpretations [51-55] proposed to explain the T-linear resistivity; ranging from electron-phonon inter-action picture to van Hove singularity picture. A brief description about some of these models is given in the following pages.

The linear temperature dependence of resistivity has been interpreted in view of stan-dard Bloch-Gruneisen [BG] transport theory based on the electron-phonon interaction [56,57]. Taking the scattering of electrons by the lattice vibrations into account, the tem-perature dependence of phonon-limited resistivity is given by the following BG formula

$$\rho(T) = \left(\frac{T}{\theta_D}\right)^5 \int_0^{T/\theta_D} \frac{x^5 dx}{(e^x - 1)(1 - e^{-x})} \tag{4.2.6}$$

Here, θ_D is an effective 'transport' Debye temperature. At high temperatures $(T \gg \theta_D)$, resistivity is approximately linear in T down to $T \approx \theta_D/4$, and crosses over to a higher power of T (usually T^5) at $T \ll \theta_D$. The observed T-linear resistivity at high temperatures observed in superconductors may be explained in view of phonon-limited resistivity and at low temperatures the sample goes to superconducting state and $p(T)$ is zero. In order to make the crossover to T^5 dependence invisible, T_c should be comparable to or higher than the cross over temperature of $\approx \theta_D/4$.

Based on the observed linearity, Gurvitch *et al* [50] derived an upper-bound estimate for electron-phonon coupling constant λ_{e-ph} (for **Y-123** λ_{e-ph}= 0.3) and concluded that high **T_c s** must be non-phonon in nature.

The BG formula can give a reasonable fit to the $\rho(T)$ curve in the case of **YBa$_2$Cu$_3$O$_7$** and **Bi$_2$Sr$_2$CaCu$_2$O$_y$,** which have their **T$_c$** in the 90 K range. However, for **Bi$_2$Sr$_2$CuO$_y$,** which has a much lower **T$_c$,** Martin *et al* [58] have demonstrated that force-fitting the **Bloch-Gruneisen** formula to the observed $\rho(T)$, linear in T down to $\approx$ 10 K would de-mand $\theta_D \approx$ 35 K, which is probably lower than a physically reasonable lower limit.

Although BG formula with cutoff at **T$_c$** seems to give a reasonable fit in a few in-dividual cases, the electron-phonon scattering alone does not seem to give a coherent account of $\rho(T)$ in all high **T$_c$** cuprates. If phonons were the only excitations coupled to electrons in any significant way, electron pairing at such high temperatures would probably not take place. The crossover of temperature dependence of resistivity from T to T^2 is reported in La-system [59] and **Tl-2201** [60,61] systems. The T^2 dependence of *p* can not be interpreted in terms of classical BG picture. To account for this cross over, the scattering mechanisms of **electronic** origin are discussed by a number of authors. In an ordinary Fermi liquid, the electron-electron scattering gives a T^2 dependence of the resistivity.

Moriya *et al* [62] calculated the temperature dependence of resistivity by assuming that the electrons are scattered by 2D antiferromagnetic (AF) spin fluctuations and explained the linear temperature dependence of resistivity. They also obtained a T^2 dependence at low temperatures in nearly AF regime, which is characteristic of Fermi

liquids. The relevant temperature scale for the crossover is set by the width of the spin fluctuation spectrum.

Ihle *et al* [63] calculated resistivity based on the two-band (Emery) model. They assumed that the oxygen holes are scattered by Cu spin fluctuations, and explained the cross over from a quadratic to linear T-dependence.

Anderson and Zhou [51] tried to explain the resistivity variation in view of RVB theory. The essence of this theory is that the strong electron-electron correlations lead to the separation of charge and spin degrees of freedom. The low energy excitations consists of charged Boson solitons (holons) and neutral Fermion solitons (spinons) with a pseudo fermi surface. From the particle statistics, the scattering rate of holons by spinons is inferred to be proportional to T. In the gauge field theory for a uniform RVB state Nagaosa and Lee [64] explained various physical quantities as a sum of the contribution from Bosons and Fermions. Due to the local constraint, motion of Bosons must be accompanied by a counterflow of Fermions. The resistivity is therefore given by $p \approx \rho_B \approx (m_B/x)T$, where m_B and x are the mass and the density of Bosons.

The marginal Fermi liquid theory by Varma *et al* [54] relates the T-linear relaxation rate of quasi-particles together with other experimentally observed anomalous normal state properties, to their specific form of polarization function.

Lee and Read [52] and Viroszek and Ruvalds [65] proposed that the temperature dependence of resistivity can be explained in view of 'nested Fermi liquid" model. According to this model, the flatness of the cylindrical Fermi surface and the amount of nesting determines the properties. According to their theory, the T^2 and T dependences of

can be attributed to electron-electron scattering and the linear temperature variation is mostly as a result of nesting.

For high temperature superconductors, it was suggested that a [52,66,67] two dimensional Fermi surface topology leads to a logarithmic divergence in density of states (DOS) (a van Hove sigularity). Here the characteristic temperature for the crossover from T^2 to T-behavior of resistivity is set by the van Hove energy scale.

Gasumyant *et al* [68] have given a narrow band model which can provide simultaneous quantitative description of temperature dependence of resistivity $\rho(T)$, thermoelectric power S(T) and Hall coefficient R(T). They assumed the existence of a narrow peak in the density of states and obtained expressions for $\rho(T)$, S(T) and R(T) in terms of three phenomenological parameters. The first parameter is the degree of band filling *F*, which is equal to the ratio of the number of electrons to the total number of states in the band. The second parameter is the total effective band width W_D and the third is the conduction band width W_σ which gives the main contribution to the electrical conduction process.

$$\rho = \frac{1}{<\sigma>} \frac{1 + e^{-2\mu*} + 2e^{-\mu*}cosh(C/T*)}{e^{-\mu*}sinh(C/T*)} \qquad (4.2.7)$$

where

$$\mu* = ln\frac{sinh(F/T*)}{sinh((1-F)/T*)}$$

$$T* = k_B T/W_D, C = W_\sigma/W_D, F = n/N$$

For $W < k_B T$, at high temperatures this expression reduces to

$$\rho = \frac{2k_B T}{k_\sigma} \left(1 + \frac{5}{12} W_\sigma *\right)^2 \tag{4.2.8}$$

where

$$k_\sigma = \int_0^W \sigma(E) dE \tag{4.2.9}$$

which can explain the linear temperature dependence of resistivity of high T_c materials in the normal state.

4.3 Conduction mechanism in insulating samples

4.3.1 Theory

From the studies of charge transport in the insulating phase, we can get the information about electronic correlation and the density of states [69]. Now it is well established that the charge transport in insulating samples related to high temperature superconductors is due to localized carriers [19,23,25]. The activated nature of the conductivity is attributed to hopping rather than excitation of carriers across an energy gap in a semiconductor. At low temperatures the conductivity of this sample rapidly decreases with decreasing temperature and the activation energy for hopping decreases with decreasing temperature. In many systems, the temperature dependence of resistivity is described by Mott's variable range hopping (VRH) [69]

$$\rho = \rho_o exp(T_o/T)^m$$

where $m = (n+1)/(n+D+1)$ where D is the dimensionality of the hopping process and n describes the energy dependence of the density of states $N(E_F)$ near the Fermi energy, which behaves like

$$N(E_F) \approx | E - E_F|^n \qquad (4.3.2)$$

For energy independent density of states n = 0, which is the case of Mott's variable range hopping. For Mott's case m is 1/3 for two dimensions (2D) and 1/4 for three dimensions (3D) respectively [69,70]. Schklovskii and Efros [71] assumed that for low carrier concentrations electrons interact via the unscreened coulomb potential, which leads to a gap in $N(E_F)$ that is pinned at E_F. According to them n = 1 and n = 2 for two and three dimensions respectively. This leads to the same exponent m = 1/2 for both two and three dimensions.

In eqn.(4.3.1) ρ_o and T_o are model dependent parameters. T_o depends on the density of states and β, which is the inverse of localization length (fall of length of the wave function of a localized state) near the Fermi level and density of states [72-74]. The relation is given by

$$T_o = \frac{16\alpha^3}{k_B N(E_F)} \qquad for \quad 3D \qquad \textbf{(4.3.3)}$$

$$T_o = \frac{27}{4\pi\alpha^2 k_B N(E_F)} \qquad for \quad 2D \qquad \textbf{(4.3.4)}$$

For **Shklovskii-Efros** case

$$T_o \approx \frac{2.8e^2\alpha}{4\pi\epsilon\epsilon_o k_B} \qquad \textbf{(4.3.5)}$$

where k_B and c are Boltzmann constant and static dielectric constant respectively. The **pre-exponential** factor in **eqn.(4.3.1)** depends on T. a and $N(E_F)$. Different groups have given **different** expressions for ρ_o [75-77]. According to Mott

$$\rho = \left(\frac{10}{\nu e^2}\right)\left(\frac{k_B T \beta}{N(E_F)}\right)^{\frac{1}{2}}$$ (4.3.6)

Ortuno-Pollak [78] have assumed that $N(E_F)$ depends on energy exponentially and obtained the expression given below

$$\rho_o = \frac{(k_B T)^{0.42}\beta^{0.74}}{[1.7e^2\nu N(E_F)^{0.58}]}$$ (4.3.7)

where ν is the phonon frequency, e is the electronic charge, k_B is Boltzmann's constant, $a"^1$ (a) is the localization length and $N(E_F)$ is the density of states at the Fermi level.

At any temperature, transition probability for the occurrence of a hop to a state at a distance R from the initial state separated by an energy W, is given by [79]

$$P \approx \exp[-2\alpha R - (W/k_B T)]$$ (4.3.8)

The term $\exp(-2\alpha R)$ denotes the probability of finding an electron at distance R from its initial site [80]. α is the inverse of localization length [a]. The hop distance (R) varies with temperature as

$$R = [(3a/2\pi)N(E_F)k_B T)]^{1/4}$$ (4.3.9)

The second term $\exp(-W/k_B T)$ arises due to the phonon assistance required by the electron in overcoming the energy barrier W, where W is the hopping energy given by [76]

$$W = 3/4\pi R^3 N(E_F)$$ (4.3.10)

The probability *p* decreases with decrease in temperature because of the second term in eqn.(4.3.8) as a result electron **prefers** to hop to sites with lower W value. R and W values are such that at any temperature, the most dominant hops contribute to the conductivity and are related by eqn.(4.3.10).

At high temperatures, the electrons acquire sufficient energy to hop to the neighboring sites at small hopping distance, R with large activation energy, W. The temperature dependence of resistivity is given by the eqn.(4.3.1) with m = 1.

4.3.2   Discussion

The values of resistivity of the present systems under study at room temperature and 10 K are listed in **Table-4.2.** The room temperature resistivity is **between 10^{-1}** and **$10^{-2}\Omega$** cm, and at low temperatures its value is between 10^{-1} and 3ft cm.

At low temperatures the resistivity variation with temperature could be **fitted** to eqn.(4.3.1). Almost all the insulating phases of high T_c materials are reported to exhibit VRH [21,23,81-102]. The temperature range over which VRH is operative is different for different materials. Some groups reported that it is operative over a wide temperature range, room temperature to around 20 K, while the others observed it only at low temperatures. Surprisingly. **Ponnambalam** *et al* [96] observed VRH over a large temperature range (100-900 K).

Fig.4.5 and 4.6 show the **$\ln\rho$** vs **T^{-m}** plots for various semiconducting samples for **m** = 1/3 and 1/4 (other values of exponents like m = 1/2 etc were also tried). Both

Table-4.2

The resistivity value at room temperature 300 K (ρ_{300}) and low temperature at 10 K (ρ_{10})

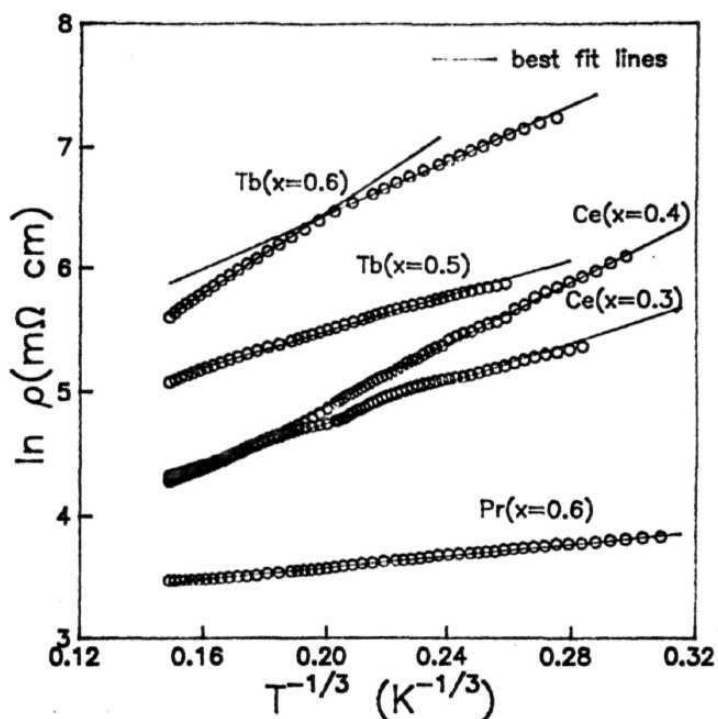| sample	(ρ_{300}) (mΩ cm)	(ρ_{10}) (*mil* cm)
Pr-doped		
x = 0.6	32.3	50.5
Ce-doped		
x = 0.3	72.2	314.0
x = 0.4	75.2	1132.0
Tb-doped		
x = 0.5	160.6	479.7
x = 0.6	271.1	2470.8

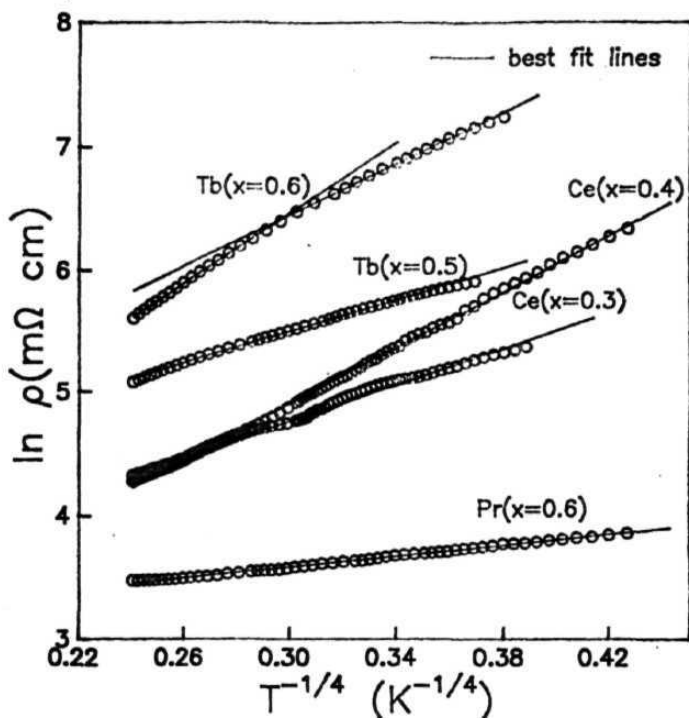Fig.4.5 Plot of $\ln\rho$ vs. $T^{-1/3}$ for various semiconducting samples

Fig.4.6 **Plot of lnρ vs. $T^{-1/4}$ for various semiconducting samples**

the plots appear linear over a wide range of temperature. The exponent can be calculated independently from the slope of log-log plot (expected values of slopes are -2/3 for 2D and -3/4 for 3D) of $d(\ln\rho)/d(1/T)$ vs. $1/T$ plot. Due to the **scattering** of derivative points, it is difficult to make a distinction between the two slopes, unless the temperature range extends over at least one **order** of magnitude. In the Gd doped **Bi-2212** samples, Jayaram *et.al.* [19] reported that their resistivity data in the semiconducting samples fits well to eqn.(4.3.1) for $m = 1/3$ (2D VRH) over a wide normal state resistivity range ($0.012 < p < 0.1\Omega$ cm). For O.K $p < 1\Omega$ cm, they found equally good fittings for $m = 1/3$ and m = 1/4 in the high temperature range. The T_o values calculated from the slopes of $\ln\rho$ vs T^{-m} and the derived parameters are not affected much by the choice of m. The equation with m = 1/4 is, therefore, used for the following discussion. It is also not possible to distinguish the difference between the $T^{-1/4}$ and T^{-1} dependence of $\ln\rho$ near the room temperature region. Fig.4.7 shows the $\ln p$ vs T^{-1} plots for various samples. T_o and ρ_o values calculated from these plots are given in **Table-4.3**.

The slope of $\ln p$ vs $T^{-1/4}$ plot increases with increase in x. This implies that the material becomes more and more disordered with increasing dopant content. Increase in disorder permits the electron to hop to the site located close by the initial state. The disorder tends to localize a state resulting in the formation of a small polaron [103]. If the carrier is confined to a single site it is called small polaron.

Assuming the value of $N(E_F)$ [$\approx 10^{23}$] as reported in the literature for Bi-system [104], the localization length *(a)* value is calculated for various samples of the present systems using the eqn.(4.3.3) [Table-4.4]. With increase in x, T_o value increases and the localization length decreases. The value of a is too high for the sample near the metal-insulator transition. As the **MI** transition approaches from the insulator side, the
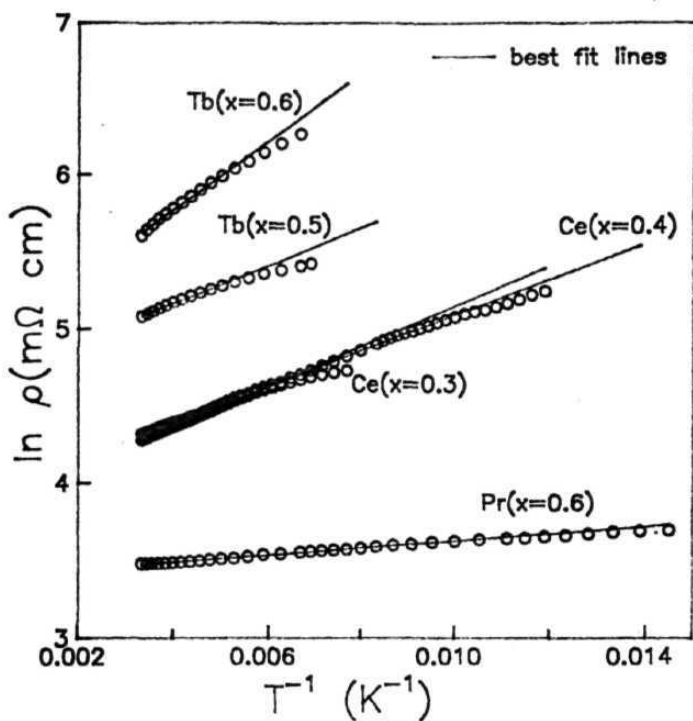
Fig.4.7 Plot of $\ln\rho$ vs. T^{-1} for various semiconducting samples

Table-4.3

The parameters obtained from $1/T$-lnρ fit for high temperature data

x	T_o (K)	ρ_o (*mil* cm)	Range of Fit
Pr-doped			
x = 0.6	23.0	29.8	95-300K
Ce-doped			
x = 0.3	130.4	46.9	170-300K
x = 0.4	116.1	51.1	100-300K
Tb-doped			
x = 0.5	121.9	107.8	200-300K
x = 0.6	223.1	131.6	190-300K

Table-4.4

The parameters obtained **from $T^{-1/4}$-ln/fit**

Sample	T_o (K)	P_o (mΩ cm)	a (Å)	v	Range of fit
Pr-doped					
x = 0.6	23	18.8	52.6	5.6×10^{11}	28-300K
Ce-doped					
x = 0.3	2946	12.8	10.4	1.8×10^{12}	38-270K
x = 0.4	16943	4.4	5.8	7.1×10^{12}	38-270K
Tb-doped					
x = 0.5	1760	35.0	12.3	6.2×10^{11}	64-270K
x = 0.6	15693	67.2	6.0	4.6x10"	54-130K
	76259	23.1	3.5	1.8×10^{12}	140-300K

T_o value decreases and goes to zero, *i.e.,.* localization length diverges, which indicates that carriers are delocalized. The phonon frequencies are estimated using eqn.(4.3.7) and the values are in the range 10^{11} - 10^{12} Hz which is within the expected limits (Table-4.4) [69,76].

The values of the hopping distance R and the hopping energy W calculated using eqn.(4.3.9) and (4.3.10) for different temperatures between 10 and 300 K are shown in Table-4.5-4.9. Hop distance R decreases with increase in x. The hopping energy W increases systematically with increasing x, because more energy is needed to cross the barrier with increase in disorder.

For a given dopant content, T_o and a are constants at different temperatures. R decreases and W increases with increase in temperature. Thermal energy decreases at low temperatures and the charge transport is governed by the carriers hopping between states with lower energy and larger distance. Variation of R and W as a function of temperature for various semiconducting samples are given in Fig.4.8.

The increasing slope of $\ln\rho$ vs $T^{-1/4}$ curve with x implies increase in T_o. The disorder in the material increases with the increase in x value, which implies that T_o is a measure of disorder in the material., The T_o value in the case of Ce and Tb doped samples is high compared to Pr doped samples for the same dopant level. This may be due to the lower degree of disorder introduced in the Pr-doped Bi-2212 system when compared to Ce and Tb doped Bi-2212 systems. The Tb-doped sample with x = 0.6 shows a double slope behavior in the $\ln\rho$ vs $T^{-1/4}$ plot, which may be due to the multiphonon assisted hopping [103,105] which operates when W> $k_B T$.

Table-4.5

Estimated values of R and W at various temperatures for
$Bi_2Sr_2Ca_{0.4}Pr_{0.6}Cu_2O_y$ sample

$a=52.6\text{Å}$		
T(K)	R(Å)	W (meV)
10	26.85	0.22
20	22.58	0.37
50	17.96	0.73
100	15.10	1.23
150	13.64	1.67
200	12.70	2.07
250	12.01	2.45
300	11.47	2.81

Table-4.6

Estimated values of R and W at various temperatures for
$Bi_2Sr_2Ca_{0.7}Ce_{0.3}Cu_2O_y$ sample

	$a=10.1\bar{A}$	
T(K)	**R($\overset{\circ}{A}$)**	**W (meV)**
10	17.90	0.74
20	15.05	1.24
50	11.97	2.47
100	10.07	4.16
150	9.10	5.64
200	8.47	7.00
250	8.01	8.27
300	7.65	9.49

Table-4.7

Estimated values of R and W at various temperatures for $Bi_2Sr_2Ca_{0.6}Ce_{0.4}Cu_2O_y$ sample

a=5.SA		
T(K)	R(Å)	W (meV)
10	15.48	1.15
20	13.01	1.93
50	10.35	3.83
100	8.70	6.44
150	7.86	8.73
200	7.32	10.84
250	6.92	12.81
300	6.61	14.69

Table-4.8

Estimated values of R and W at various temperatures for
$Bi_2Sr_2Ca_{0.5}Tb_{0.5}Cu_2O_y$ sample

T(K)		W (meV)
10	18.69	0.65
20	15.71	1.09
50	12.50	2.18
100	10.51	3.66
150	9.50	4.96
200	8.84	6.15
250	8.36	7.27
300	7.99	8.34

Table-4.9

Estimated **values of R and W at various temperatures for** $Bi_2Sr_2Ca_{0.4}Tb_{0.6}Cu_2O_y$ **sample**

T(K)	$R(\overset{\circ}{A})$	W (meV)	$R(\overset{\circ}{A})$	W (meV)
10	15.57	1.12	13.65	1.67
20	13.10	1.89	11.48	2.81
50	10.41	3.76	9.13	5.58
100	8.76	6.32	7.68	9.39
150	7.91	8.57	6.94	12.72
200	7.36	10.63	6.46	15.78
250	6.96	12.57	6.11	18.66
300	6.65	14.41	5.83	21.39
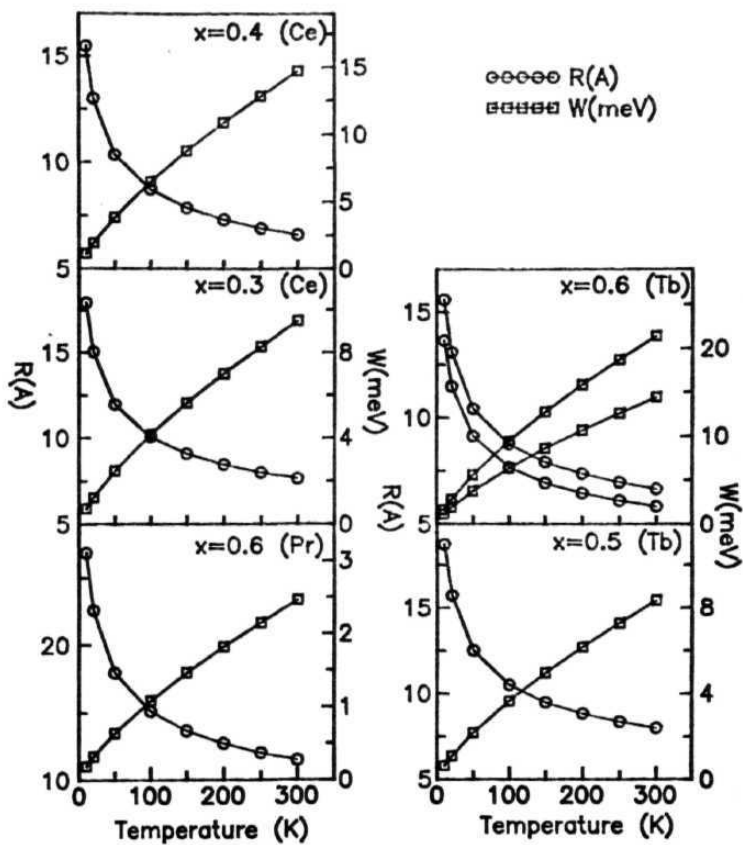
Fig.4.8 Variation of hopping distance **(R) and** hopping energy (W) as a function cf temperature

Quitmann *et al* [102] have analyzed the resistivity data of the insulating samples of $Bi_2Sr_2Ca_xY_{1-x}Cu_2O_y$ using generalized hopping approach based on connectivity criterion. For a given Ca concentration, they have plotted $\ln\rho$ vs. T^{-m} with values of m between 0.15 to 0.6. They have taken the value of m which gives a straight line over a large temperature range and calculated the exponent as a function Ca concentration. They found different values of m for samples with different Ca concentrations i.e., value of m = 0.5 for $Bi_2Sr_2YCu_2O_y$ sample and m = 0.2 for $Bi_2Sr_2Ca_{0.4}Y_{0.6}Cu_2O_y$ sample which is closer to Ml transition. They argue that depending on the **carrier** concentration of the sample, very different values of m and therefore dimensionality can be obtained. The observed variation in m with Ca concentration explains the disagreement in the literature about the exponent in the hopping conduction for the $Bi_2Sr_2Ca_xR_{1-x}Cu_2O_y$ system and with it the disagreement about the dimensionality. They found that insulating samples with Y content not too far from the critical concentration x = 0.43±0.02 show metallic conduction at high temperatures and hopping conduction at low temperatures. These two **regions** are **separated** by a shallow minimum (ρ_{min}). This kind of behavior has been reported in other systems also [9]. This shows the coexistence of **delo**calized states and localized states separated by a disorder induced mobility edge. From ultravoilet-photoemission spectroscopy studies, they observed a shift in the Fermi level to lower energies and the development of new states at Fermi level. From these experimental observations they concluded that the **MI** transition is probably of Anderson type [46]. They used a narrow band model to explain **qualitatively** the **MI** transition and crossover from insulating to metallic resistivity and the linear resistivity in the normal state for the metallic samples.

In the present set of **samples,** the insulating compositions available are not very much

away from the **MI** transition. So, it is not possible to determine the change in exponent value as a function of Ca concentration. Any crossover from hopping conduction to metallic conduction in the insulating samples and a shallow minimum in resistivity could not be observed in the temperature range studied. In the present samples, ρ_{min} may occur at higher temperatures.

A comparison of the results obtained on the three series of samples shows that

(1) In all the three series of samples, the room temperature resistivity increases and T_c decreases with increase in the dopant concentration. The **MI** transition is observed between 10-20 mΩ cm in all the three series of samples.

(2) **MI** transition is observed around x = 0.6 in Pr-doped system, around x = 0.2 in Ce-doped system and around x = 0.4 in Tb-doped system. The T_c depression is faster in Ce-doped **Bi-2212** system compared to the other rare-earth substitutions. From this it is inferred that Ce exists in +4 valence state. The faster decrease in the *c-lattice* parameter also confirms this conclusion.

(3) The T_c of present systems is sensitive to the hole concentration in CuO_2 planes. Rare-earth ion with +3 or +4 valence states substituted in the place of Ca ion (valence state +2) fills the holes and thereby reduces the T_c.

(4) The resistivity variation in semiconducting samples can be explained in terms of VRH. It is not possible to determine the exponent unambiguously. Using $N(E_F)$ ($\approx 10^{23}$) value, the localization length is estimated. For the sample which is closer to the **MI** transition, the estimated value of localization length is **large**, because as **MI** transition is **approached**, the T_o value approaches zero and localization length diverges. For higher dopant concentrations the localization length is small. The hopping distance (R) and hopping energy (\Y) were estimated at different temperatures and they obey Anderson localization conditions.

4.4 References

1. C. Kendziora, L. Forro, D. Mandrus, J. Hartge, P. Stephens and L. Mihaly *Phys. Rev.* **B45,** 13025 (1992).

2. J.M Tarascon, P. Barboux, G.W. Hull, R. Ramesh, L. H. Greene, M. Giroud, M. S. Hedge and W. R. McKinnon, *Phys. Rev.* **39,** 4316 (1989).

3. S. B. Samanta, P. K. Dutta, V. P. S. Awana, E. Gmelin and A. V. Narlikar, *Physica* **C178,** 171 (1991).

4. Xiaolong Chen, Jingkui Liang, Jinrong Min, Jianqui Li and Guanghui Rao, *Phys. Rev.* **B50,** 3431 (1994).

5. P. Ganguly, R. A. Mohan Ram, K. Srcedhar and C. N. R. Rao, *Solid State Commun.* 62, 807 (1987).

6. D. Bourgault, C. Martin. C Michel, M. Hervieu, J. Provost and B. Raveau, *J. Solid State Chem.* **78,** 326 (1989).

7. J. B. Torrance, Y. Tokura. A. I. Hazzal, A. Bezinge, T. C. Huang and S. S. P. Parkin, *Phys. Rev. Lett.* **61,** 1127 (1988); J. L. Tallon, *Physica* **C176,** 547 (1991)

8. C. N. R. Rao, J. Gopalakrishna, A. K. Santra and V.Manivannan, *Physica* **C174,** 11 (1991).

9. P. Mandal, A. Poddar, B. Ghosh and P. Chowdhury, *Phys. Rev.* **B43, 13102** (1991) and references therein.

10. M. R. Presland. J. L. Tallon, R. G. Buckley, R. S. Liu and N. E. Floer, *Physica* **C176,** 95 (1991).

11. A. Manthiram and J. B. Goodenough, *Appl. Phys. Lett.* **53,** 420 (1988).

12. K. Koyama et al *Jpn. J. Appl. Phys.* 28, 1354 (1988).

13. R. Yoshizaki et al *Physica* **C152,** 408 (1988).

14. V. P. S. Awana, S. K. Agarwal, R. Ray, S. Gupta and A. V. Narlikar, *Physica* **C191,** 43 (1992).

15. Y. Gao, N. Spencer, H. Chen and R. E. Salamon, *Phys. Rev.* **B45,** 13 (1992).

16. R. Yoshizaki et al *Supercond. Sci. Technol.* 4, S421 (1991).

17. K. Zhang. G. Seidler. B. H. Ma and C. U. Segre, *Physica* **C179,** 405 (1991).

18. S. Olivier et al, *Physica* C **157.** 531 (1989).

19. B. Jayaram. P.C. Lanchester and M. T. Weller, *Phys. Rev.* **B43,** 5444 (1991).

20. R. K. Nkum and \Y. R. Dattars. *Phys. Rev.* **B46.** 5686 (1992).

21. D. Rama Sita and R. Singh, *Int. J. of Mod. Phys.* B 8, 2283 (1994).

22. V. P. S. Awana, S. K. Agarwal and A. V. Narlikar and M. P. Das *Phys. Rev.* **B48,** 2 (1993).

23. D. Rama Sita and R. Singh, *Solid State Commun.* 94, 969 (1995).

24. A. Sawa, T. Han, T. Iwamatsu, H. Uwe and T. Sakudo, *Physica B* **165 & 166,** 1553 (1990).

25. S. Maekawa and H. Fukuyama, *J. Phys.Soc. of Jpn.* **51,** 1380 (1981).

26. J. K. Liang, X. T. Xu, S. S. Xie, G. H. Rao, X. Y. Shao and Z. G. Duan, *Z Phys.* B **69** (Cond. Mat.), 137 (1987).

27. Koki Takita and Takeshi Ohshima, *Physica* C **185-189,** 757 (1991) and references therein

28. Y. Dalichaouch, M. S. Torikachvilli, E. A. Early, B. W. Lee, C. L. Seaman, K. Yang, H. Zhou and M. B. Maple, *Solid State Commun.,***65,** 1001 (1988); B. Okai, M. Kosuge, H. Nozaki, K. Takahashi and M. Ohta, *Jpn. J. Appl. Phys.* 27, L41 (1988).

29. D. P. Norton, D. H. Lowndes, J. D. Budai, B. C. Chakoumakos and H. R. Kerchner, *Phys. Rev. Lett.* **66,** 1537 (1991).

30. J. Fink. N. Nuker, H. Romberg, M. Alexander, M. B. Maple, J. J. Neumeier and J. W. Allen. *Phys. Rev* **B42**,4823 (1990).

31. U. Neukirch, C. T. Simmons, P. S. Sladeczek. C. Lanbschat, O. Strebel, G. Kaindl and D. D. Sarma, *Europhys. Lett.* 5, 567 (1988).

32. X. X. Tang, A. Manthiram and J. B. Goodenough, *Physica* **C161,** 574 (1989).

33. Pan Wei. Hu Wen Ying and Zheng Qing Qi. *Physica* **C209,** 400 (1993).

34. A. Matsuda, K. Kineshita, T. Ishii, H. Shibata, T. Watanabe and T. Yamada, *Phys. Rev.* **B38,** 2910 (1988); C. L. Seaman. J. J. Neumeier, M. B. Maple, L. P. Lee, G. M. Luke, B. G. Sternlieb, Y. J. Uemura, J. H. Brewer, R. Kadono, R. F. Kiefl, S. R. Krietzman and T. M. Rigeman, *Phys. Rev.* **B42,** 6801 (1990).

35. A. A. Abrikosov and L. P. Gor'kov, *Zh. Eksp. Teor. Fiz.* **39,** 1781 (1960); ibid *Sov. Phys. JETP* 12, 1243 (1961).

36. Y. G. Zho. S. L. Jia, Y. Q. Zhou, Y. Yang and Z. X. Zhao, *Physica* **C209,** 472 (1993).

37. J. J. Neumeier, T. Bjormholm, M. B. Maple and I. K. Shuller, *Phys. Rev.Lett.* **63,** 2516 (1989).

38. J. J. Neumeier and M. B. Maple. Physica *C191.* 158 (1992).

39. J. J. Neumeier, M. B. Maple and M. S. Torikachvili, *Physica (Amsterdam)* **C156,** 574 (1988).

40. M. B. Maple, *Appl. Phys.* 9, 179 (1976) and references therein

41. E. Muller-Hartmann and J. Zittartz, *Z. Phys.* **234, 58** (1970) and references therein.

42. C. Infante, M. K. El Mously, R. Dayal, M. Hussain, S. A. Siddiqi and P. Ganguly *Physica* **C167,** 640 (1990) and references therein.

43. V. K. S. Shante and S. Kirkpatrick, *Adv. Phys.* **20,** 325 (1971).

44. B. G. Orr, H. M. Jaeger and A. M. Goldman, *Phys. Rev. Lett.* **B32,** 7586 (1985) and references therein.

45. P. Ganguly in *Advances in Solid State Chemistry,* ed C. N. R. Rao (Indian Academy of Science), New Delhi, 135 (1986).

46. P. W. Anderson, *Phys. Rev* **109,** 1492 (1958).

47. Y. Gao, P. Pernambuco-Wise, J. E. Crow, J. O. Reilly, N. Spencer, H. Chen and R. E. Sulomon, *Phys. Rev.* **B45,** 7436 (1992).

48. Y. Iye, in *Physical properties of High Temperature SuperconductorsIII,* edited by D. M. Ginsberg (World Scientific, Singapore, 1992) and references therein.

49. C. C. Tsuei. *Physica* **A168,** 238 (1990) and references therein.

50. M. Gurvitch and A. T. Fiory, *Phys. Rev. Lett.* **59,** 1337 (1987).

51. P. W. Anderson and Z. Zou, *Phys. Rev. Lett* 60, 132 (1988).

52. P. A. Lee and N. Read, *Phys. Rev. Lett.* 58, 2691 (1987).

53. D. Y. Xing. W. Y. Lai, W. P. Su and C. S. Ting. *Solid State Commun.* **65,** 1319 (1988).

54. C. Varma, P. B. Littlewood, S. Schmitt-Rink, E. Abrahams and A. E. Ruckenstein, *Phys. Rev. Lett.* **63,** 1996 (1989).

55. J. C. Philips. *Phys. Rev.* **B40,** 7348 (1989).

56. P. B. Allen. \Y. E. Picket and H. Krakauer, *Phys. Rev.* B **37,** 7482 (1988)

57. S. Martin. M. Guruvitch, C. E. Rice, A. F. Hebard. P. L. Gammel, R. M. Fleming and A. T. Fiory, *Phys. Rev.* B **39,** 9611 (1989).

58. S. Martin. A. T. Fiory. R. M. Fleming, L. F. Schneemeyer and J. V. Waszcak, *Phys-Rev.* **B41.** S46 (1990).

59. H. Takagi. T. Ido. S. Ishibashi. M. Uota, S. Uchida and Y. Tokura, *Phys. Rev.* **B40,** 2254 (19S9).

60. Y. Kubo, Y. **Shimakawa,** T. Manako, T. Sato, S. **Iijima,** T. Ichihashi and H. Igarashi, *Physica C* **162-164,**991 (1989).

61. Y. Kubo, Y. Shimakawa, T. Manako and H. Igarashi, *Phys. Rev.* **B43,** 7875 (1991).

62. T. Moriya, Y. Takahashi and K. **Ueda,** *J. Phys. Soc. Japan 59,* 2905 (1990).

63. D. **Ihle,** M. Kasner and N. M. Plakida, *Z. Phys.* **B82,** 193 (1991); Erratum *Z. Phys.* **B84,** 165 (1991).

64. N. Nagaosa and P. A. Lee, *Phys. Rev. Lett.* **64,** 2450 (1990).

65. A. Viroszek and J. Ruvalds, *Phys. Rev.* **B42,** 4064 (1990).

66. K. Levin, J. H. Kim, J. P. Lu and Q. Si, *Physica* **C175,** 449 (1991).

67. D. M. Ncwns, P. C. Pattnaik and C. C. Tsuei, *Phys. Rev.* **B43,** 3075 (1991).

68. V. E. Gasumyants, V. I. Kaidanov and E. V. **Vladimirskaya,** *Physica* **C248,** 255 (1995)

69. N.F. Mott and E.A.Davis, *Electronic Processes in Non-crystalline materials* 2nd Ed. (Clarendon, Oxford 1979) and **references** therein.

70. N. F. Mott, *J. Non. Cryst. Solids* 1, 1 (1969).

71. B. I. Shklovskii and A. L. Efros in *Electronic properties of Doped Semi-Conductors, eds. M. Cardona, P. Fulde and H. J. Queisser Springer Series in Solid State Sciences* (Springer, Berlin, **1984).**

72. V. **Ambegaokar,** B. I. Halperin and J. S. Langer, *Phys. Rev.* **B4,** 2612 (1971).

73. N. F. Mott, *Philos. Mag* 19, 635 (1969).

74. W. Brenig, G. H. Dohler and H. Heyszenau, *Philos. Mag.* **27,** 1093 (1967).

75. M. Pollak, in *Noncrystalline Semiconductors,* edited by M. Pollak, p 121 (CRC, Boca Raton, FL, 1987).

76. P. **Nagel,** in *Amorphous Semiconductors,* edited by M. H. Brodsky (Springer, Berlin, 1985).

77. W. Brenig, G. H. Dohler and P. Woelfe, *Z. Phys.* **258,** 381 (1973).

78. M. Ortuno and M. Pollak, *Philos. Mag.* **B47,** L93 (1983).

79. R. Zallen, *Physics of Amorphous solids* (wiley, New York, 1983).

80. H. M. Jaeger. D. B. Haviland. A. M. Goldman and B. G. Orr, *Phys. Rev.* **B34,** 4920 (1986).

81. M. A. Kastner, R. J. Birgenau, C. Y. Chen, Y. M. Chiang, D. R. Gabbe, H. P. Jenssen, T. Junk, C. J. Peters, P. J. Picone, T. Thio, T. R. Thurston and H. L. Tuller, *Phys. Rev.* **B37, 111** (1988).

82. K. Sreedhar and P. Ganguly, *Phys. Rev.* **B41,** 371 (1990).

83. A. Poddar, P. Mandal, A. N. Das, B. Ghosh and P. Choudhary, *Phys. Rev.* **B44,** 2757 (1991).

84. B. Fisher, G. Korean, J. Gennosa, I. Patlaggan and E. L. Gartstein, *Physica* **C176,** 75 (1991).

85. H. Taguchi, M. Nagao and M. Shimida, *J. Solid State Chem.* **92,** 277 (1991).

86. F. G. Aliev, V. Kovacik, S. R. Li, V. V. Moshchalkov, N. N. Oleinikov, N. A. Samarin, J. Scbek and L. Sherbek, *J. Magn. Magn. Mater.* **90-91,** 641 (1990).

87. Y. Xu and W. Guan, *Physica* C206, 59 (1993).

88. Wu Jiang, P. L. Peng, J. L. Hamilton and R. L. Greene, *Phys. Rev.* **B49,** 690 (1994).

89. Y. Xu and W. Guan, *Physica* **C212,** 119 (1993).

90. T. Sugita, M. Yabuuchi, K. Murase, H. Okabayashi, K. Gamo and S. Namba, *Solid State Commun.* **67,** 95 (1988).

91. B. Ellman, H. M. Jaeger, D. P. Katz, T. F. Rosenbaum, A. S. Cooper and G. P. Espinosa, *Phys. Rev* **B39,** 9012 (1989).

92. M. Z. Cieplak, S. Guha, H. Kojuma, P. Lindenfeld, G. Xiao, J. Q. Xiao and C. L. Chien, *Phys. Rev* **B46,** 5536 (1992).

93. M. A. Kastner, R. J. Birgenau, C. Y. Chen, Y. M. Chiang, D. R. Gabbe, H. P. Jenssen, T. Junk, C. J. Peters, P. J. Picone, T. Thio, T. R. Thurston and H. L. Tuller, *Phys. Rev.* **B46,** 5536 (1992).

94. B. Jayaram, P. C. Lancester and M. T. Weller, *Physica* **C159,** P2 (1989).

95. T. Manako and Y. Kubo, *Phys. Rev.* **B50,** 6402 (1994).

96. V. Ponnambalam and U. V. Varadaraju, *Phys. Rev.* **B52.** 16213 (1995).

97. B. Fisher, J. Genossar, L. Patlagan, G. M. Reisner and A. Knizhnik, *J. Appl. Phys.* 80, 898 (1996).

98. P. Mandal, A. Poddar, B. Ghosh and P. Chowdhury, *Phys. lit* **B43.** 13102 (1991).

99. P. Sumana Prabhu. M. S. Ramachandra Rao and U. V. Varadaraju and G. V. Subba Rao, *Phys. Rev.* **B50,** 6929 (1994).

100. P. **Sumana Prabhu** and U. V. Varadaraju, *Phys. Rev.* **B53,** 14637 (1996).

101. R. K. **Nkum** and W. R. **Dattars,** *Phys. Rev.* **B46,** 5686 (1992).

102. C. **Quitmann,** D. Andrich, C. **Jarchow,** M. Fleuster, B. Beschoten, G. Guntherodt, V. V. Moshchalkov, G. Mante and R. Manzke, *Phys. Rev.* **B46, 11813** (1992) and references there in.

103. D. **Emin,** *Phys. Rev. Lett* 32, 303 (1974); in *Electronic and structural properties of Amorphous semiconductors,* edited by P. G. Le Comber and J. Mart, (Academic, London) 261 (1973).

104. R. A. Fisher, S. Kim, S. E. Lacy, N. E. Philips, D. E. Morris, A. G. Markelz, J. Y. T. Wei and D. S. Ginley, *Phys. Rev* **B38,** 11942 (1988); N. Okazaki, T. **Hasegawa,** K. Kishio, K. **Kitazawa,** A. Kishi, Y. **Ikeda,** M. Takano, K. Oda, H. Kitaguchi, J. Takada and Y. Miura, *Phys. Rev.* **B41,** 4296 (1990).

105. M. L. Knotek and M. Pollak, *Phys. Rev.* B9, 664 (1974).

Chapter 5

THERMOELECTRIC POWER STUDIES

This chapter deals with the systematic study of thermoelectric power (TEP) **on** $Bi_2Sr_2Ca_{1-x}M_xCu_2O_y$ (M = Pr, Ce **&** Tb) samples. The experimental data are analyzed in view of various theoretical models existing in the literature. TEP measurements on the well characterized samples were carried out using dc differential technique as described in chapter II, as a function of temperature in the temperature range 40-300 K. The results and their analysis are presented in the following pages.

5.1 Background

5.1.1 Thermoelectric power of metals and semiconductors

The TEP (S) for a free electron gas in a metal in the classical picture can be written as [1,2]

$$S = \int_0^T \frac{C_e(T)}{neT} dT \tag{5.1.1}$$

where C_e (T) is the electronic specific heat per unit volume, n is the number of electrons per unit volume, e is charge of the electron and T the temperature.

For a free electrons in a metal, C_e is given by

$$C_e = \pi^2 k_B^2 nT/(2E_o) \tag{5.1.2}$$

TEP is given by the equation

$$S = \frac{\pi^2 k_B^2 T}{2 e E_o} \mu V K^{-1}$$

(5.1.3)

where C_e is the electronic specific heat per unit volume, n is the number of electrons per unit volume and k_B is Boltzmann constant. At absolute zero temperature, the lowest possible states will be occupied upto a certain maximum energy E_o.

According to this expression, TEP should be proportional to absolute temperature and dependent on the sign of charge. It should be negative and small in magnitude. In this expression the electron scattering processes are not taken into account.

Mott gave a more general expression needed for the interpretation of the TEP [3] as

$$S\sigma = \frac{k_B}{e} \int \sigma_E \frac{E - E_F}{kT} \frac{\partial f}{\partial E} dE$$

(5.1.4)

and σ is

$$\sigma = \int \sigma_E \frac{\partial f}{\partial E} dE$$

(5.1.5)

where f is Fermi function and σ_E is energy dependent conductivity.

For metals the current is determined by the electrons with energies in the neighborhood of E_F. So S can be written as

$$S = \frac{\pi^2}{3} \frac{k_B^2 T}{e} \left(\frac{d(\ln\sigma)}{dE} \right)\Bigg|_{E_F}$$

where the differential is the change in the electrical conductivity σ as the Fermi energy E_F changes evaluated at the actual Fermi surface of the metal E_F, which in turn is sensitive to the Fermi surface area and the mean free path.

The essential difference between metals and semiconductors is that in semiconductors the electrons are usually **non-degenerate** and they have Maxwellian distribution. Then the specific heat per electron is given by $3k_B/2$. This is much greater than the **specific** heat of electrons in a metal. Then the eqn.(5.1.1) becomes

$$S = \int_0^T \frac{3k_B}{2eT} dT = -\frac{k_B}{e} \frac{3}{2} lnT + constant \tag{5.1.7}$$

According to Heikes [4], if $k_B T$ is greater than the band width then S is given by

$$S = -\frac{k_B}{e} ln\left(\frac{c}{1-c}\right) \tag{5.1.8}$$

where c is the ratio of number of electrons to the number of sites.

In the case of semiconductors which have a mobility gap at the Fermi surface, TEP (S) is given by

$$S = \frac{k_B}{e}\left[\frac{E_c - E_F}{k_B T} + A\right] \tag{5.1.9}$$

E_c-E_F is the energy required to excite a carrier to the mobility edge and A is a constant.

In the case of variable range hopping (VRH), the characteristic energy for a hop is given by [3,5,6]

$$W \sim T^{d/(d+1)} \tag{5.1.10}$$

where d is the dimensionality of the hopping, the temperature dependence of conductivity is given by

$$\sigma \sim exp\{-W/T) \sim exp(-T_o/T)^{1/d+1} \tag{5.1.11}$$

and S is given by

$$S = \frac{1}{2}\frac{k_B}{e}\frac{W^2}{T}\left(\frac{dlnN}{dE}\right)_{E=E_F} \tag{5.1.12}$$

So S is proportional to W^2/T. The temperature dependence of S can be written as

$$S \sim T^{(d-1)/(d+1)} \tag{5.1.13}$$

So S varies as $T^{1/2}$ for 3D VRH and $T^{1/3}$ for 2D VRH.

For hopping between nearest neighbors $S \to$ oo as $1/T \to 0$. These equations are valid for spinless particles below Neel temperature in amorphous anitferromagnets. Above the Neel temperature there should be an additional term $(k_B/e)ln2$ in TEP, which is frequently observed in amorphous semiconductors in the hopping regime.

In the above treatment, contribution to TEP due to diffusion of carriers under the influence of temperature gradient has been considered. It has been assumed that the phonon distribution is in equilibrium whenever any interaction with the electron system is being considered. Its only contribution is to scatter the electrons by electron-phonon interaction, which gives rise to a mean free path for the diffusing electrons. If there is an electric current flowing, momentum will be transferred from the electrons to phonons and this momentum will not be able to be dissipated into the whole phonon system (because the relaxation time of the phonons, with the interaction with other phonons, impurities or boundaries is longer than the relaxation time for electron-phonon interaction) before further electron interaction occurs to increase the momentum still more. Hence these phonons will not be able to come to equilibrium with the rest of the system. Phonon-phonon and phonon-impurity interactions become very small as the temperature is reduced. Some momentum will be transferred from phonons to electrons and

extra carriers will be piled up at the cold end in addition to those coming from diffusion alone with a consequent change in current flow. This is called phonon-drag effect. Its effect is widely observed in TEP of metals and semiconductors as peaks and faster enhancement or decrement in TEP than that for pure diffusion alone. For detailed calculation of phonon-drag contribution one has to take all the scattering mechanisms into consideration.

5.1.2   Thermoelectric power of high T_c superconductors

Several groups have reported the TEP measurements on various cuprate superconducting systems, namely La - [7-10], Y- [7,10-22,74] Bi- [7,13-37] Tl- [7,23,26,38-41] and Hg- [42] based systems. From these mcasurements, some common features in the temperature and carrier dependence of TEP have emerged. For the overdoped system (high concentration), TEP is negative and small and it varies almost linearly with temperature. For the underdoped system (low carrier concentration), TEP is positive and large and approaches a temperature independent value at high temperatures. For the medium carrier concentrations, TEP first increases with temperature and then shows a broad maxima followed by a decrease.

It is now more or less established that different sign and magnitude of TEP and the T_c values are closely related to the carrier concentration. Presland *et al* [43] have given quite general relation between T_c and carrier concentration p for several doped cuprate systems. According to Presland, T_c appears to be maximized at $p = 0.16$. falls to zero on the underdoped and overdoped sides at $p = 0.05$ and p = 0.27, respectively and is

$$\frac{T_c}{T_c^{max}} = 1 - 82.6(p - 0.16)^2 \qquad (5.1.14)$$

Obertelli *et al* [26] examined the temperature dependent TEP of several high T_c systems Y-123, Bi-2212, Tl-1212, Bi-2223 and Tl-2223 and concluded that a universal correspondence between room temperature TEP vs carrier concentration (p) exists. In the overdoped region the variation of TEP with p is found to be linear and in the under-doped region it is logarithmic. Tallon *et al* [44] obtained a direct relationship between T_c and hole concentration p for $Y_{1-x}Ca_xBa_2Cu_3O_{7-\delta}$ by investigating the properties of fully oxygen deficient $(S \approx 1.0)$ compound for which $p = x/2$. They used these p values to check the previously reported correlation with the room temperature TEP [26] and found that their data follows the Obertelli's universal relation [26]. They parameterized the correlation by the relation

$$S_{290} = 372exp(-32.4p) \qquad 0.00 < p < 0.05,$$
$$S_{290} = 992exp(-38.1p) \qquad 0.05 < p < 0.155,$$
$$S_{290} = -139p + 242 \qquad p > 0.155 \qquad (5.1.15)$$

There is a discontinuity in S(290,p) in the neighborhood of the superconductor-insulator transition at $p = 0.05$.

According to the conventional Fermi liquid theory, the TEP is expected to be approximately linear in temperature, showing a phonon-drag peak below $\theta_D/2$ and goes to zero as T tends to zero. The TEP of high temperature superconductors in the normal state is temperature independent or weakly dependent on temperature, but the zero temperature extrapolated value is not zero. So, it is believed that the temperature dependence of S can not be explained in the conventional picture.

Several conventional and unconventional approaches have been adopted to explain

the TEP of high T_c superconductors. A brief summary of these models is given below.

In high T_c superconductors, the occurrence of peak in TEP is commonly observed in both polycrystalline samples and within *ab* plane of single crystals. Cohn *et al* [45] adopted a phonon-drag model to explain this peak as arising from freeze-out of carrier phonon umklapp process involving holes in the CuO_2 layers and optical-mode phonons. Uher and Kaiser *et al* [8,11] suggested that the peak in the TEP of high temperature superconductors is caused by phonon-drag. However, some groups are not in favor of this phonon-drag peak [12,40,46,47].

Kaiser [48,49] tried to explain the major features of TEP with the metallic diffusion model which is proved to be successful for normal metal systems with the only difference being the anomalously large size of the electron-phonon enhancement effect. Kaiser [48] has performed calculation of the enhancement of TEP due to electron-phonon interaction in the high T_c superconductors using the Eliashberg function calculated by Weber [50] and also inferred the existence of two types of carriers from the observed positive Hall coefficient and negative TEP. Vijayashree *et al* [12] emphasized the evidence that phonon- drag is not responsible for the peak from the TEP data of $YBa_2Cu_{3-x}Zn_xO_{7-\delta}$ and the enhancement of TEP is more steep with temperature over linear diffusion TEP than what would be expected for electron-phonon interaction.

Zhang *et al* [51] suggested that there are two kinds of carriers; localized carriers giving the constant part of TEP, and mobile carriers contributing to the diffusion part of the TEP which is proportional to the temperature

$$S = S_1 + S_2 = A + BT \qquad (5.1.16)$$

This is based on the assumption that the contribution of the phonon-drag is small above T_c.

Another model is based on the assumption that high T_c superconductors have strongly correlated electrons. According to Chaiken and Beni [52]

$$S_1 = -(k_B/e)ln(2(1-p)/p) \qquad (5.1.17)$$

for the constant part of the TEP [S_1 in eqn.(5.1.16)], which represents the contribution from the relatively localized carriers. p is the hole concentration per Cu ion.

Some groups, from photoemission spectroscopy studies reported the evidence of existence of two bands in $Bi_2Sr_2CaCu_2O_y$ [53,54]. Though it is possible to explain the sign change of S in a single-band model, many authors have adopted two band models to explain the experimental results. These models generally adopt the picture that the holes are in CuO_2 layers and electrons in Cu-0 chains in $YBa_2Cu_3O_y$ system or in Bi-0 or Tl-O layers in Bi- and Tl-based systems, respectively. Such two band models are consistent with the band structure calculations.

Allen *et al* [55] from the band structure calculations for $Tl_2Ba_2CuO_6$ (Tl-2201) suggested that the transport is dominated by a wide Cu-0 band with a possible contribution from the smaller Tl-O band. The transport properties of $YBa_2Cu_3O_y$ were also examined and it was concluded that YBCO does have a charge carrier in the Cu-0 chains analogous to the Tl-0 layer.

Wang *et al* [56] have proposed a two-carrier model in analogy to the two band model, concerning the O $2p$ holes and Cu $3d_{x^2-y^2}$ electrons and explained qualitatively the change

from +ve to -ve value of S. According to them, in parent insulators Cu $3d_{x^2-y^2}$ electrons are strongly localized and TEP is determined by O 2p holes. With increase in doping, Cu $3d_{x^2-y^2}$ electrons may become delocalized, so that they may contribute to conduction. In the overdoped region, Cu $3d_{x^2-y^2}$ electrons may play an important role in the transport mechanism and result in the -ve TEP.

Kubo *et al* [39] proposed a two-dimensional tight binding model of Cu-0 plane assuming next nearest-neighbor interactions. The single band showed both electron like and hole-like character depending on the geometry of the band. The model showed that in the areas of half filling, there can be a negative TEP and a positive Hall coefficient. In the nearest neighbor tight binding models, Seeback coefficient changes its sign at half filling. In his calculations, as the next-nearest neighbor interaction is turned on, this sign change occurs on either side of half filling (depending on the limiting case) by as much as 0.2 holes, which is very close to the experimentally observed value for various high T_c superconductors [26].

Fisher *et al* [57-60] used narrow band model which assumes the existence of a very narrow band in the band to explain the normal state transport properties structure near E_F. Tsidilovski and Tsidilovski [61] also used a phenomenological narrow band model which assumes the existence of narrow peak in the density of states near Fermi level.

Newns *et al* [62] explained the temperature and doping dependence of TEP of high T_c superconductors in view of a saddle point (SP) in logarithmic density of states singularity (van Hove singularity (VHS)). The universal relationship between the TEP and T_c can be explained in view of this model. As the Fermi level, controlled by doping, is swept through the SP, the density of states (DOS) at the Fermi level goes through a

maximum and so does T_c (T_c maximum) and the TEP zero corresponds to the Fermi level lying at the SP. As mentioned earlier, certain other anomalous properties of high T_c superconductors, such as marginal Fermi liquid behavior [63], specific heat jump [64] and isotope shift [65-67] have also been explained in terms of VHS.

Tallon *et al* [17] from the Zn substitution studies in **Y-123** reported that a strong enhancement in the S(T) is related with a smooth opening of energy gap in the normal state spectrum. The energy gap called normal **state** gap (NS), pseudogap or spin gap is observed from **NMR** [68,69] and heat capacity [70] measurements. In sufficiently underdoped samples this gap opens at a temperature T_g well above T_c. They showed that this gap is responsible for the p-dependent variation of TEP [26]. They showed that Zn substitution suppresses both the NS and the superconducting order parameter and, at an intermediate concentration, the former survives while the latter does not. This picture is consistent with the van Hove singularity picture [62] and phonon-drag picture [71] of TEP.

Recently, Tallon *et al* [22] reported TEP measurements on different sets of Y-123 compounds in which the interplanar coupling between the superconducting CuO_2 planes in $RBa_2Cu_3O_{7-\delta}$ is controlled by changing the size of the rare-earth (R) and by changing the oxygen deficiency in the chains while keeping the hole concentration on the planes fixed at optimum doping by means of Ca substitution at R site. From the insensitivity of T_c to interlayer coupling and the absence of peak in the density of states determined by Y-NMR, they concluded that the doping dependence of TEP and the density of states are inconsistent with the VHS model.

Trodhal [71] has recently explained the temperature and doping dependence of TEP within the conventional Fermi liquid picture itself. According to him. the anomalous

behavior is a manifestation of the strong scattering of phonons by electrons, which is already inferred from thermal conductivity data [72] that the acoustic phonons remain scattered predominantly by electrons up to room temperature. Trodhal has included a large phonon-drag contribution to the negative diffusion TEP for an electron gas. The cumulative TEP decreases **linearly** with temperature. The net TEP is set to zero below the superconducting transition temperature of 90 K, which is the value it would have in the absence of superconductivity.

From the brief summary it can be concluded that the TEP of high T_c superconductors still lacks a satisfactory explanation.

5.2   Results

The temperature variation of TEP (S) for $Bi_2Sr_2Ca_{1-x}M_xCu_2O_y$ (M = Pr, Ce **&** Tb) are shown in **Fig.5.1-5.3**. There are some common characteristic features in the S vs. T plots of the three series of samples. For all the three series of samples, the room temperature TEP (S300) is positive and its magnitude increases with increase in x. For the **super**-conducting samples S is small and S vs. T plots show a broad maxima in the normal state. In the temperature range above the maxima, S decreases almost linearly as the temperature increases. The S maxima shifts towards high temperatures as x increases. In the temperature range below the maxima. S decreases rapidly and goes to zero at the T_c. Superconducting samples in all the three series show the room temperature TEP value $< 11\mu V/K.$

Fig.5.4 shows room temperature TEP (S300) and room temperature resistivity (ρ_{300}) as a function of x for all the three series of samples. Their variations with x are simi-lar. Sharp change in TEP and resistivity are occurring at the same concentration except
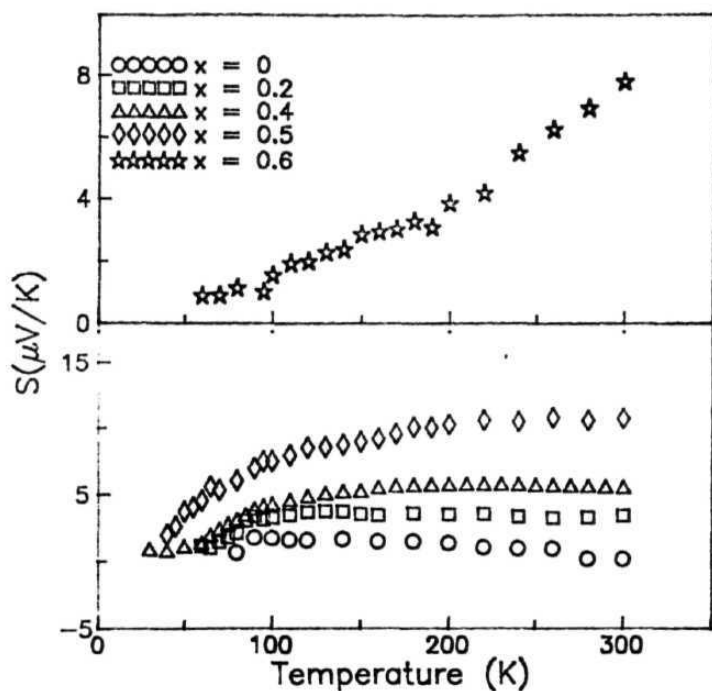
Fig.5.1 Temperature dependence of S for $Bi_2Sr_2Ca_{1-x}Pr_xCu_2O_y$ samples
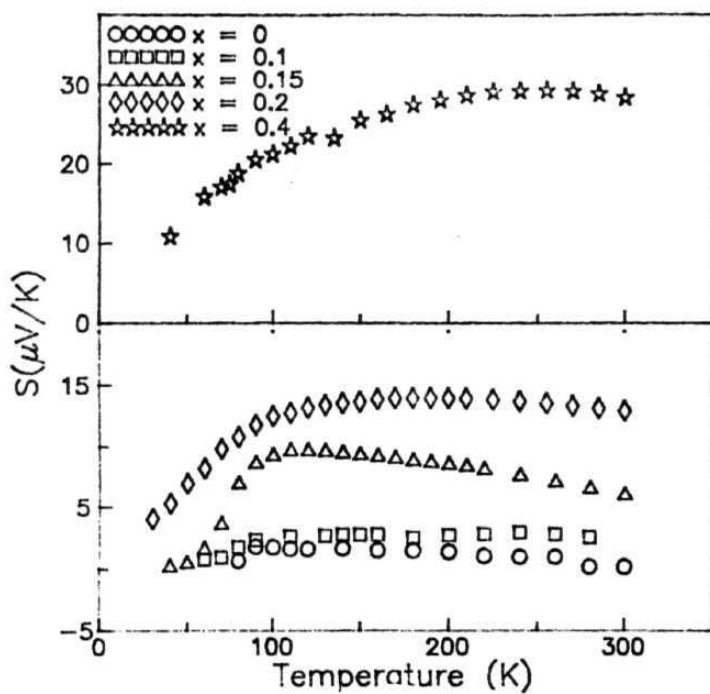
Fig.5.2 Temperature dependence of S for $Bi_2Sr_2Ca_{1-x}Ce_xCu_2O_y$ samples
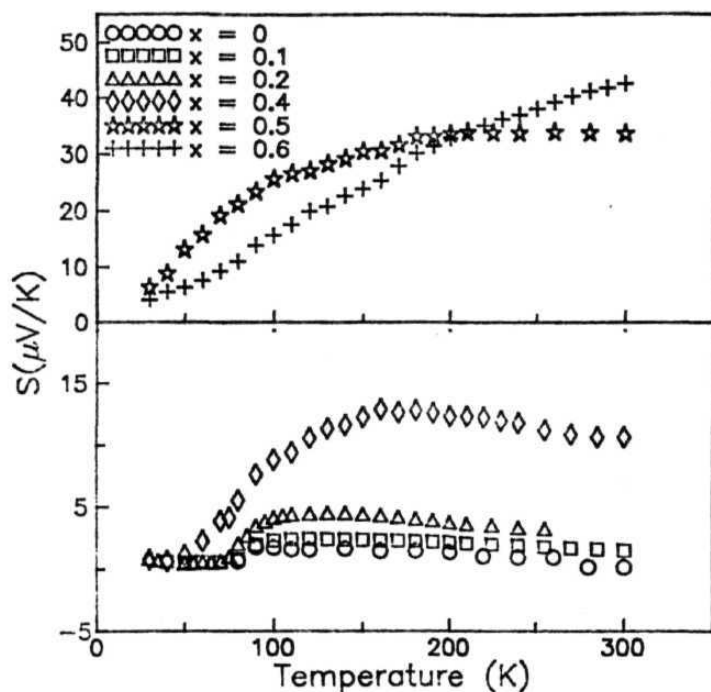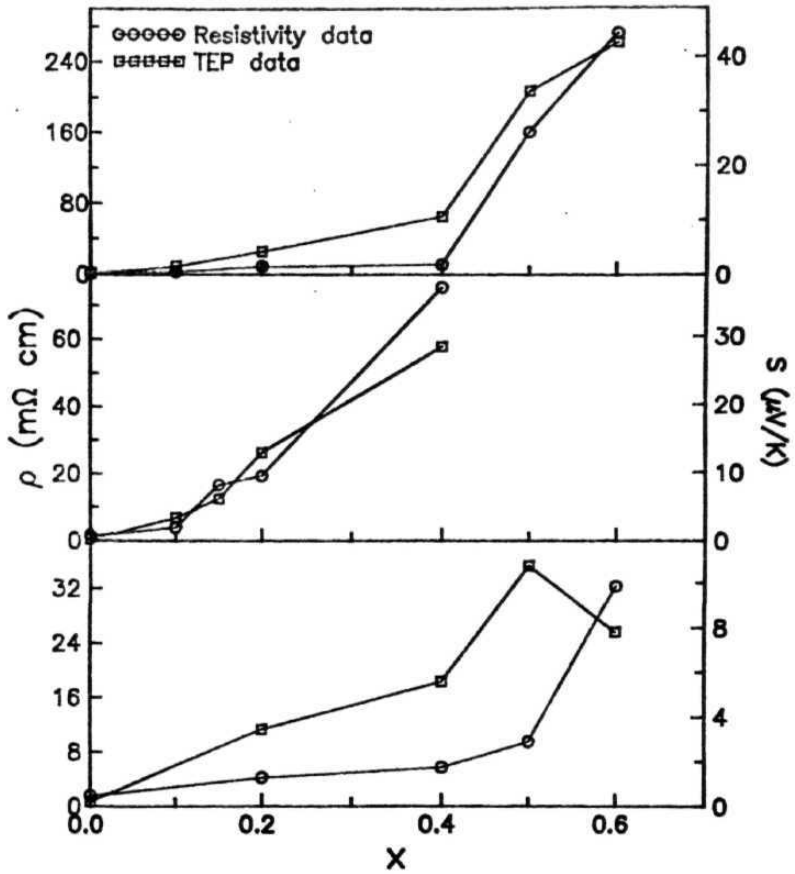
Fig.5.3 Temperature dependence of S for $Bi_2Sr_2Ca_{1-x}Tb_xCu_2O_y$ samples

Fig.5.4 The variation of room temperature resistivity (ρ_{300}) and thermoelectric power (S_{300}) with x for $Bi_2Sr_2Ca_{1-x}M_xCu_2O_9$ (M = Pr, Ce & Tb) samples

in the case of Pr-doped sample. From the TEP measurements the Metal-Insulator (MI) transition is found to occur at the same doping level as found from the resistivity studies. This indicates that the same carriers are responsible for resistivity and TEP properties.

The TEP value of the undoped sample is small (S_{300}=0.19 /iV/K) and positive throughout the measured temperature range. There are several reports on TEP measurements on Bi-2212 system. Mandal *et al* [34], Munakanta *et al* [33] and Rao *et al* [23] reported negative TEP value for the Bi-2212 sample in the temperature range of T_c to 300 K. Wang *et al* [36] reported negative S300 value and positive S in the temperature range T_c to 196 K. Mandrus *et al* [32] reported a positive TEP value for the Bi-2212 single crystal with T_c = 80 K.

The S_{300} value of $Bi_2Sr_2CaCu_2O_y$ (Bi-2212) reported by Obertelli *et al* [26] for polycrystalline sample (with T_c = 92 K, the maximum for Bi-2212 phase and the corresponding optimum carrier concentration according to eqn. (5.1.14) is p = 0.16) is $\approx 2\mu V/K$. A comparison of the TEP value of our polycrystalline sample of $Bi_2Sr_2CaCu_2O_y$ [with T_c $=$ 82 K] shows that our sample is slightly in the overdoped region with p = 0.20. The overdoping is reduced when the small amount of dopants (Pr, Ce and Tb) are substituted at Ca site as indicated by the initial increase in T_c and TEP value of the doped samples.

Fig.5.5 shows S300 vs. hole concentration p (calculated from Presland's equation as mentioned in chapter IV)) and Obertelli's universal curve for the superconducting samples (0.07<p<0.20). The figure shows that the experimental points follow the universal curve at higher carrier concentrations (p > 0.12) and at lower carrier concentrations the present experimental data is below the universal curve.
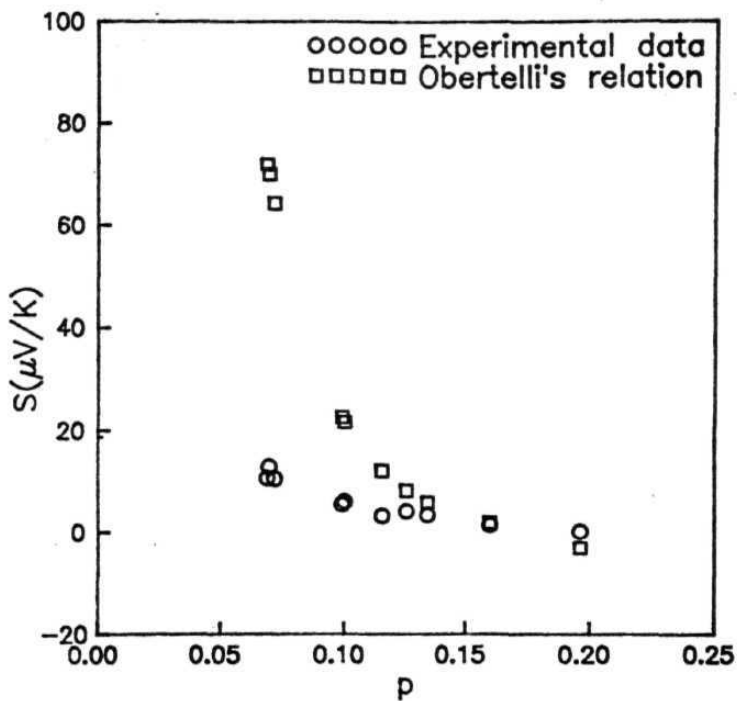
Fig.5.5 Plot of room temperature thermoelectric **power** (S_{300}) **vs. carrier** concentration (p).

TEP of the semiconducting samples is high $\approx$ 30-40 μ V/K except in the case **of** Pr-doped **Bi-2212** sample with x = 0.6, which has TEP $\approx$ 8 μV/K. The plot of S versus T for the semiconducting sample in the Pr-doped series with x = 0.6 shows a slow increase in S with T in the temperature range 40-200 K and **a** sharp increase in the temperature range **200-300** K. This type of temperature dependence of S is similar to what has **been** reported in La-system [9] and in amorphous semiconductors in the hopping regime [3,5]. In the case of other semiconducting samples *i.e.,* in Ce-doped (x = **0.4** and 0.5) and Tb-doped (x = 0.5) Bi-2212 series, S is almost constant around room temperature and as we go to the low temperatures a smooth decrease in S is observed. For the Tb-doped (x = 0.6) Bi-2212 sample, S decreases continuously with the decrease in temperature.

5.3   Analysis of the experimental data of the superconducting samples

The temperature and carrier concentration dependence of S in the present systems **are** similar to that reported in other high T_c systems and having the common characteristics mentioned earlier. A detailed analysis of the experimental data in view of various two-band models and a phenomenological narrow band model proposed for high T_c superconductors is undertaken. The band structures and formulas proposed in these models are different. Thus, it is essential to ascertain which model is more suitable for describing the TEP behavior of high T_c superconductors. A brief description of each model and its applicability to the experimental data is discussed in the following pages.

5.3.1   Two band model with linear T term

The temperature dependence of S of high T_c systems resemble that observed in mixed valent heavy Fermion systems [73]. In heavy Fermion system $CeNi_x$ the TEP variations were analyzed using an expression (assuming Lorenzian resonance near the Fermi level)

$$S = \frac{AT}{B^2 + T^2} \qquad (5.3.1)$$

where

$$A = 2\frac{(E_o - E_F)}{e} \qquad \textbf{(5.3.2)}$$

$$B^2 = 3\frac{(E_o - E_F)^2 + \gamma^2}{\pi^2 k_B^2} \qquad (5.3.3)$$

where E_o and γ are the center and the width of the resonance respectively. This theory is based on the assumption that, superimposed on a broad band there is a localized band in the density of states near the Fermi level. This resonance peak gives the characteristic temperature dependence of S. To explain the temperature variation of S of Bi-2212 single crystal Forro *et al* [24] added a linear term to eqn.(5.3.1) and obtained the best fit using the equation

$$S = \frac{AT}{B^2 + T^2} + \alpha T \qquad (5.3.4)$$

where αT is the normal band contribution. It is essentially different from the two band models which fits the temperature dependence of S with the usual formula, with electrons and holes having different mobilities.

Present data also fits well to the eqn.(5.3.4) (Fig.5.6-5.8). Mandal *et al* [34] and Keshri *et al* [40] also got good fittings for $Bi_2Sr_2Ca_{1-x}Y_xCu_2O_y$ and $Tl_2Ba_2Ca_{1-x}Y_xCu_2O_y$ systems respectively. The fitting parameter A. B and α and the estimated values of E_o - E_F and 7 are given in Table-5.1.

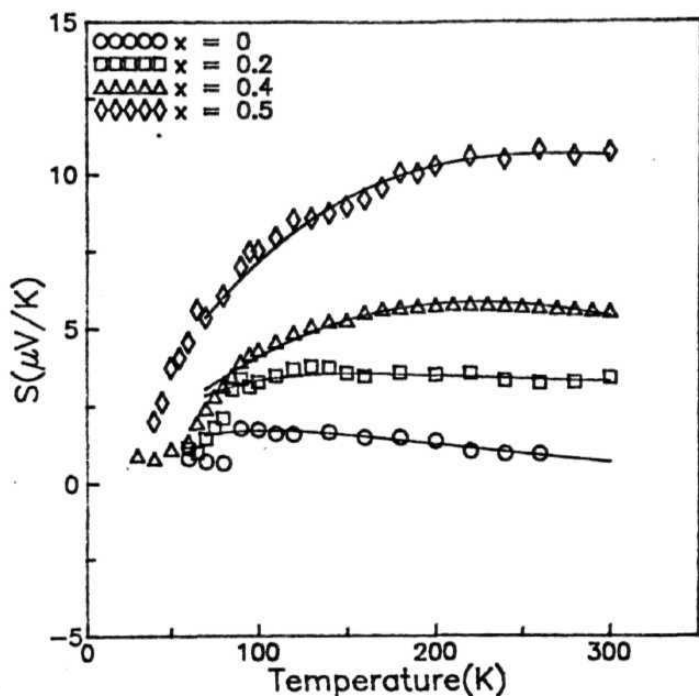Fig.5.6 **Best fit curves** (solid lines) for $Bi_2Sr_2Ca_{1-x}Pr_xCu_2O_y$ samples corresponding to Eqn.(5.3.4)
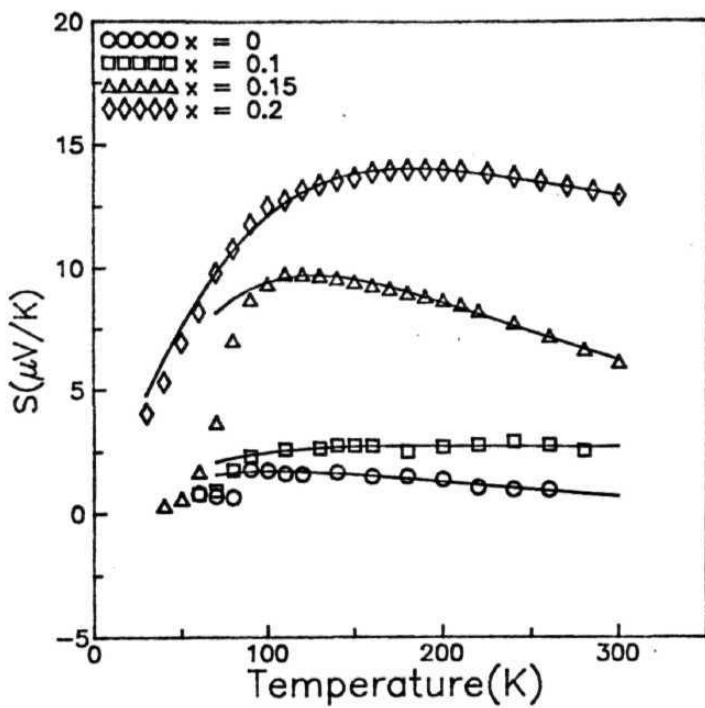
Fig.5.7 Best fit curves (solid lines) for $Bi_2Sr_2Ca_{1-x}Ce_xCu_2O_y$ samples corresponding to Eqn.(5.3.4)
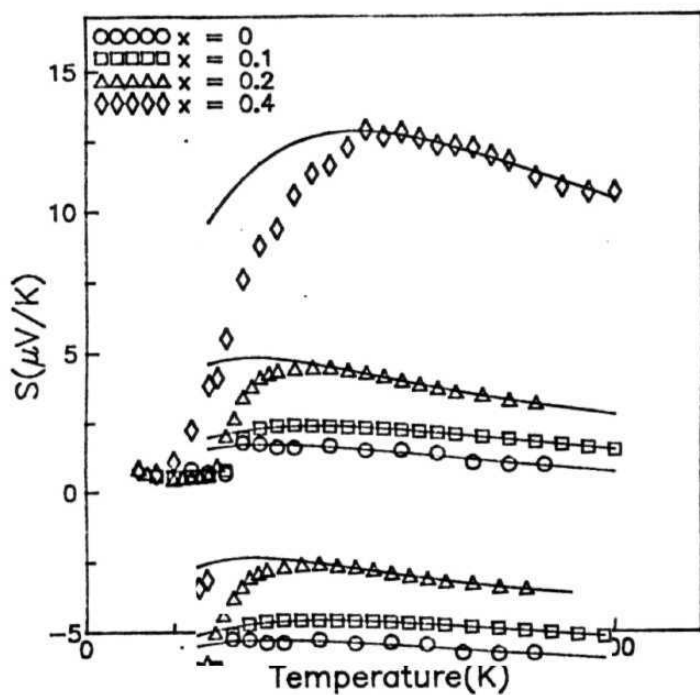
Fig.5.8 Best fit curves (solid lines) far $Bi_2Sr_2Ca_{1-x}Tb_xCu_2O_y$ wimples corresponding to Eqn.(5.3.4)

Table-5.1

Best fit parameters A, B, α of eqn.(5.3.4) and the estimated values E_o - E_F & 7 for $Bi_2Sr_2Ca_{1-x}M_xCu_2o_y$ (M = Pr, Ce & Tb) samples

x	A (foV)	B (K)	α (μ V/K²)	E_o - E_F (K)	7 (K)
Pr-doped					
0	444.2	115.2	-0.0195	2.58	208.9
0.2	752.7	124.8	0.0040	4.38	226.4
0.4	2195.0	202.8	0.0018	12.76	367.9
0.5	3706.8	218.9	0.0090	21.55	396.9
Ce-doped					
0.1	548.6	126.6	0.0039	3.19	229.7
0.15	2758.0	133.5	-0.0048	16.05	241.7
0.2	3761.6	153.3	0.0103	21.87	277.2
Tb-doped					
0.1	735.5	126.6	0.0039	3.19	229.7
0.2	917.1	133.5	-0.0048	16.05	241.7
0.4	4044.9	248.7	-0.0010	33.49	450.0

For all the three series of samples in the present study, no systematic variation of α with x is observed. $E_o\text{-}E_F$ and 7 values increase with increase in dopant concentration (x). It is expected that with the increasing carrier (hole) density the Fermi level should go down relative to the top of the band. But $(E_o\text{-}E_F)$ increases with x. This is in contradiction to the expected result. Moreover, there is no evidence of the existence of the assumed band structure in high T_c systems.

5.3.2 Nagaosa-Lce model

Using gauge-field theory for a uniform RVB [75] state, Nagaosa-Lee [76] proposed that, for superconducting cuprates TEP can be expressed as

$$S = S_F + S_B \tag{5.3.5}$$

where S_F and S_B estimated using Fermi and Maxwellian states are

$$S_B = \frac{k_B}{e}\left[1 - ln\frac{2\pi p}{m k_B T}\right] \tag{5.3.6}$$

and

$$S_F = -\left[\frac{k_B}{e}\right]\frac{k_B T}{E_F} \tag{5.3.7}$$

Here p denotes the concentration of holes on CuO_2 sheet per [Cu-O] and m is the mass of the Bosonic carrier. In order to fit the experimental data, m & E_F were regarded as fitting parameters. However, those fitted curves were not in reasonable agreement with experimental data. Ikegawa et al [77] slightly modified this model by introducing an additional parameter F and fitted for the $(EuCe)_4(BaEu)_4Cu_6O_y$ and $Nd_{1.4}Ce_{0.2}Sr_{0.4}Cu_{1-x}Zn_xO_y$ systems using the equation for S given by

$$S(T) = \frac{k_B}{e} \left[1 - Fln \left(\frac{2\pi pG}{T} \right) - \frac{T}{H} \right] \tag{5.3.8}$$

where F, G and H are the fitting parameters. From this model, the value of $G(\approx m^{-1})$ and $H(\approx E_F)$ are expected to be of the order of exchange energy J $(\approx 1000 \text{ K})$.

Using the *p* value calculated from Presland's relation [43] (chapter IV), the experimental data is fitted to eqn.(5.3.8) (Fig. 5.9-5.11). The fitting parameters obtained for the superconducting samples are given in Table-5.2. For all the three series of samples the value of F increases and the value of G and H decreases with increasing x. As expected from the theory, H is of the order of J. But G values are large. Wang *et al* [36], Mandal *et al* [34] and Keshri *et al* [40] also obtained high values of G for higher carrier concentration samples of the $Bi_2Sr_2Ca_{1-x}Ce_xCu_2O_y$, $Bi_2Sr_2Ca_{1-x}Y_xCu_2O_y$ and $Tl_2Ba_2Ca_{1-x}Y_xCu_2O_y$ systems, respectively. Though, good fittings were obtained for this model, the parameter G obtained from the fittings is unreasonably large, which cannot have any physical basis. The large H value and small F value indicates that Boson contribution turns out to be negligible, which is unreasonable.

5.3.3 Two band model of Xin *et al*

Xin *et al* [41] have used the two band model to analyze the temperature dependence of TEP of $Tl_2Ba_2Ca_2Cu_3O_{10-\delta}$. For the case of a system which contains both electrons and holes, S can be written as [2]

$$S = (S^+\sigma^+ + S^-\sigma^-)/\sigma \tag{5.3.9}$$

where $\sigma = \sigma^+ + \sigma^-$ is the sum of the electrical conductivities by holes (σ^+) and by electrons (σ^-) and S^+ and $S\sim$ are the TEP values due to holes and electrons respectively. In the case of high T_c superconductors, it is assumed that one band which is formed by
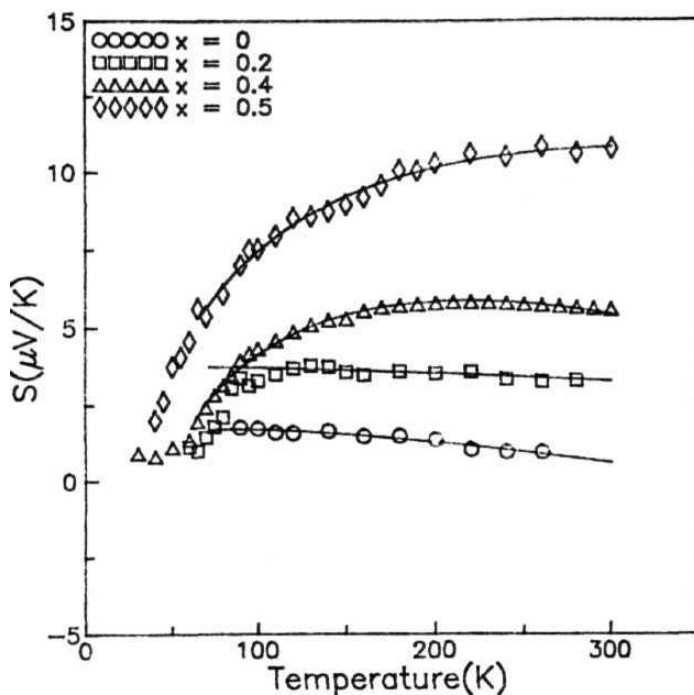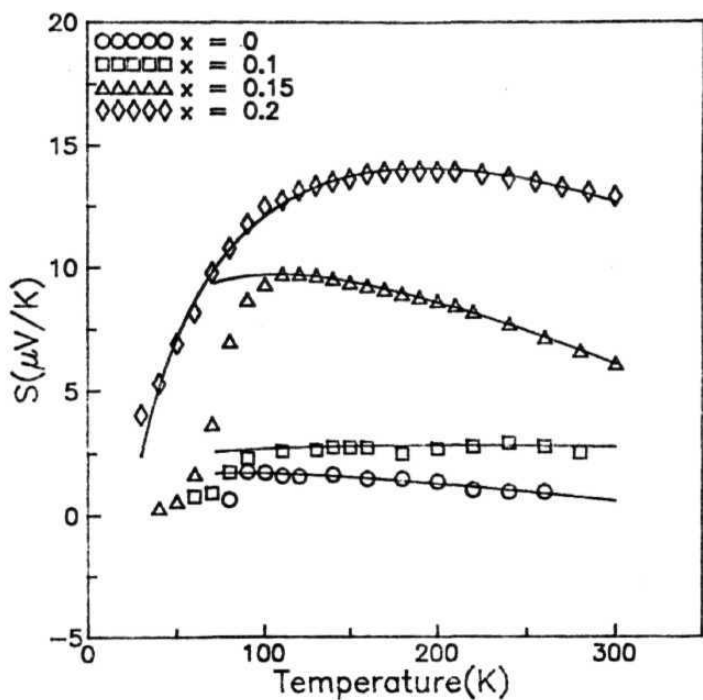
Fig.5.9 Best fit **curves (solid lines)** for $Bi_2Sr_2Ca_{1-x}Pr_xCu_2O_y$ samples corresponding to **Eqn.(5.3.8)**

Fig.5.10 Best fit curves (solid lines) for $Bi_2Sr_2Ca_{1-x}Ce_xCu_2O_y$ samples corresponding to Eqn.(5.3.8)
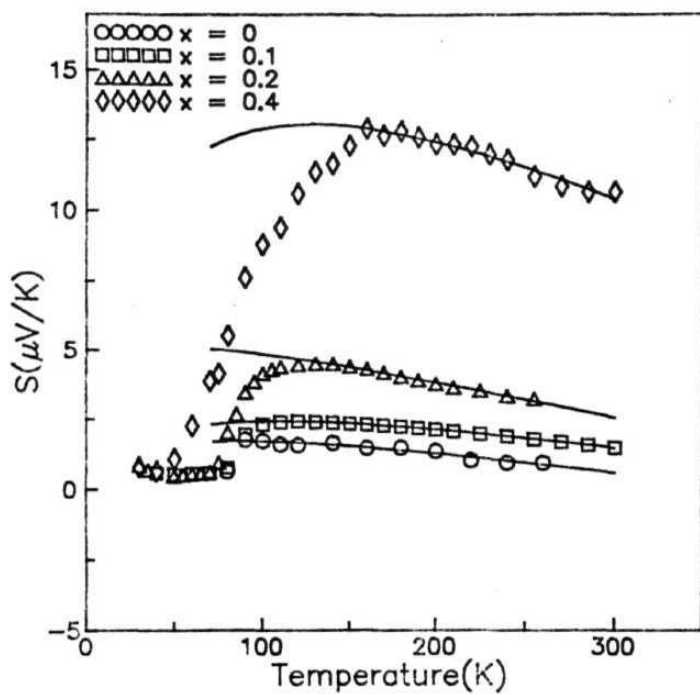
Fig.5.11 **Best fit curves** (solid **lines) for** $Bi_2Sr_2Ca_{1-x}Tb_xCu_2O_y$ samples **corresponding to** Eqn.(5.3.8)

Table-5.2

Best fit parameters F, G and H of eqn.(5.3.8) for $Bi_2Sr_2Ca_{1-x}M_xCu_2O_y$ (M = Pr, Ce & Tb) samples

X	P	F	G(K	H(K)
Pr-doped				
0	0.20	0.0146	8.50×10^{30}	6792.6
0.2	0.13	0.0281	4.20×10^{16}	5615.8
0.4	0.10	0.0821	$\mathbf{1.12} \times 10^7$	2679.0
0.5	0.07	0.1274	2.00×10^5	1904.8
Ce-doped				
0.1	0.12	0.0305	4.00×10^{15}	6005.0
0.15	0.10	0.0657	4.99×10^7	1764.4
0.2	0.07	0.1323	8.88×10^4	1424.1
Tb-doped				
0.1	0.16	0.0259	1.01×10^{18}	5216.1
0.2	0.13	0.0259	2.50×10^9	2416.7
0.4	0.07	0.1575	1.52×10^4	970.9

Cu-0 planes contribute to holes and another formed by Bi-0 layers contribute to electrons. CT$^+$ is proportional to $1/T$ because Cu-0 layers are metallic and σ^- is proportional to $\exp(E_c/kT)$. The following equation is used by Xin *et al* [41] for Tl-based and by Awana *et al* [27, 30] for Bi-based high T_c superconductors

$$5 = AT + (B\lambda + CT)\exp(-\lambda/T) \tag{5.3.10}$$

A, B, C and A are constants for a particular sample. The fits of the above equation to the TEP data are shown in **Fig.5.12-5.14.** Parameters estimated from the fittings are given in **Table-5.3.** The estimated values of the energy gap ($E_g = E_c/k_B$ where $E_c = \lambda/k_B$) of the semiconducting band of Bi-0 layers are listed in Table-5.3. The E_g value increases with increase in x. These E_g values are consistent with the room temperature energy gap values in a wide range 0-0.3 eV obtained from scanning-tunneling spectroscopy studies on Bi-2212 system [78-80]. This gap depends on the extent of intercalation of excess oxygen in the Bi-0 layers. In the absence of excess oxygen the gap approaches zero. We have attributed As pointed out earlier the transition broadening with dopant content observed in the resistivity vs. T plots is due to the excess oxygen intercalated in the Bi-0 layers. The increasing E_g values can, therefore, be correlated to the T_c depression as the dopant content is increased. We did not observe any systematic variation in A parameter value, which represents contribution from mobile holes does not vary systematically with the dopant content.

Though this model works well for Bi [27,30] and Tl [41] systems and reasonable energy gaps are obtained, but still it is unsatisfactory because many experiments have demonstrated that the Bi-0 and Tl-O layers or Cu-0 chains are insulating. It is unlikely that universalities observed in various physical parameters can be attributed to different bands, because universality rovers a wide variety of physical systems.
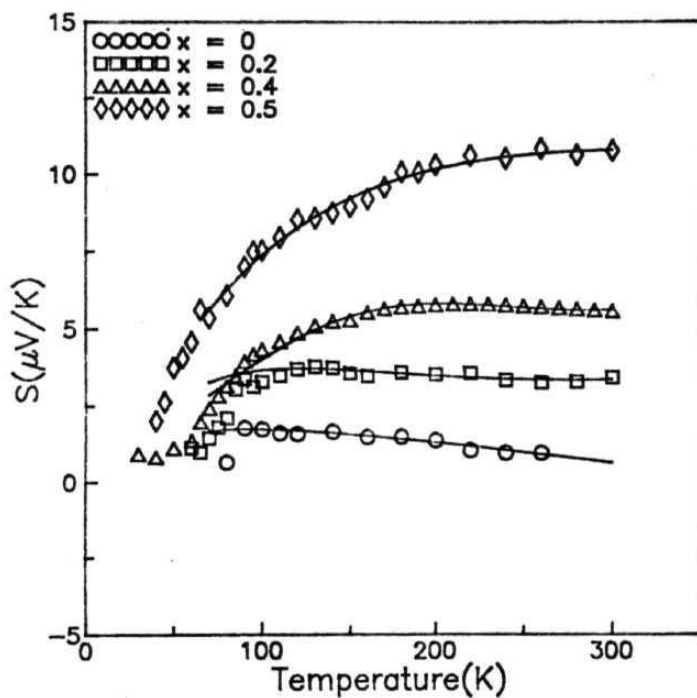
Fig.5.12 **Best fit curves (solid lines) for** $Bi_2Sr_2Ca_{1-x}Pr_xCu_2O_y$ samples corresponding **to** Eqn.(5.3.10)
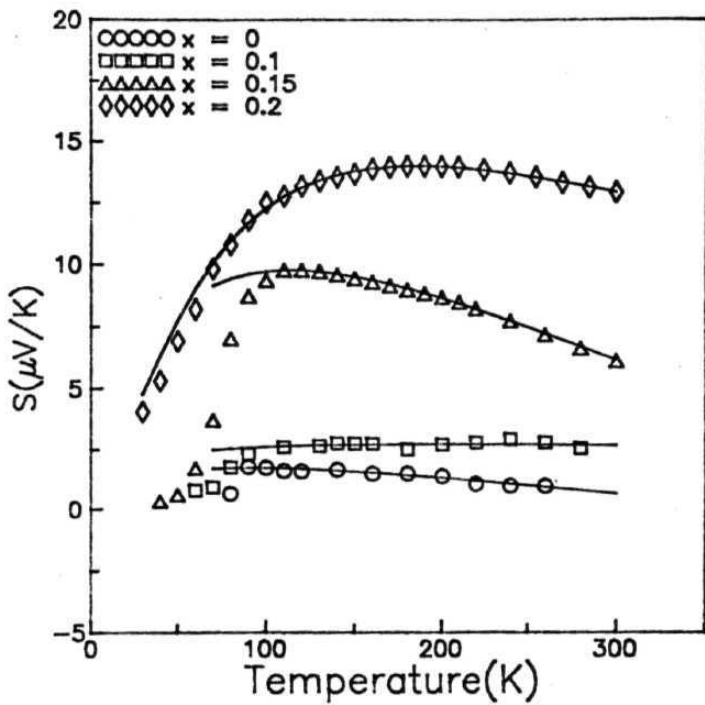
Fig.5.13 Best fit curves (solid lines) for $Bi_2Sr_2Ca_{1-x}Ce_xCu_2O_y$ samples corresponding to Eqn.(5.3.10)
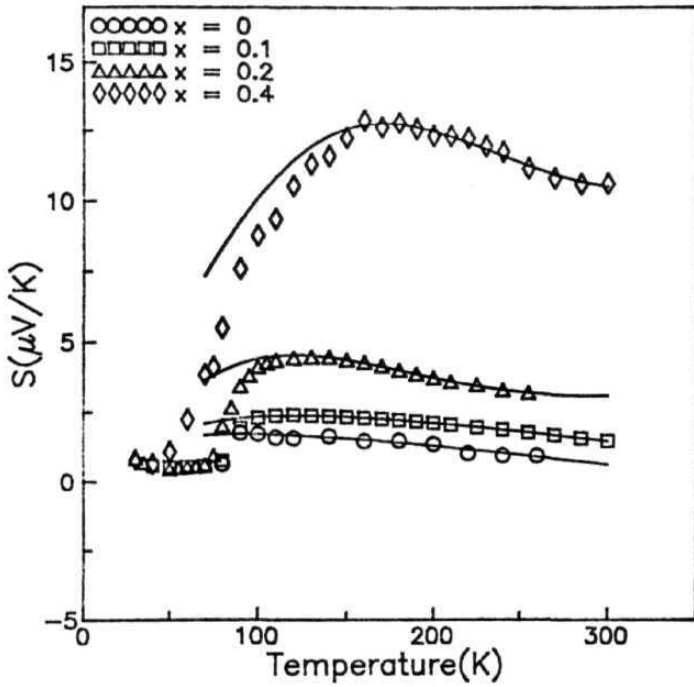
Fig.5.14 Best fit curves (solid lines) for $Bi_2Sr_2Ca_{1-x}Tb_xCu_2O_y$ samples corresponding to Eqn.(5.3.10)

Table-5.3

Best fit parameters A, B, C and A of eqn.(5.3.10) and corresponding E_g values for $Bi_2Sr_2Ca_{1-x}M_xCu_2O_y$ (M = Pr, Ce Tb) samples

x	A (μV/K)	B (μV/K)	C (μV/K)	A (K)	(eV)
Pr-doped					
0	0.0474	0.0002	-0.0555	61	0.0105
0.2	0.0558	-0.0722	-0.0417	244	0.0420
0.4	0.0463	-0.0547	-0.0422	450	0.0774
0.5	0.0774	-0.1124	-0.0257	484	0.0552
Ce-doped					
0.1	0.0965	-0.00003	-0.0978	33	0.0057
0.15	0.2241	-0.0009	-0.2576	71	0.0122
0.2	0.1598	**-0.1125**	-0.1756	252	0.0433
Tb-doped					
0.1	**0.0385**	.-0.0244	-0.0463	180	0.0310
0.2	0.0551	-0.1375	0.0151	**386**	0.0664
0.4	0.1056	-0.3954	0.2582	625	0.1075

5.3.4   **Phenomenological narrow band model**

From the positron-annihilation [81,82], photoemission [83,84] and the transmission spectroscopy [85] studies, the existence of narrow band in the HTSC systems is inferred. Gasumyant *et al* [16] used the approach of **Kazmin** *et al* [86] and proposed a band spectrum model which supposes the existence of a narrow peak in the electron density of states (DOS) close to the Fermi level to explain the behavior of all the transport coefficients; resistivity *p(T),* TEP S(T) and the Hall coefficient $R_H(T)$ in the normal state of **Y-123** system as a function of oxygen content and different cation substitutions. They have **estimated** quantitatively some band spectrum parameters which characterize the band width and the band filling degree.

According to Gasumyant *et al* [16]], if the Fermi level E_F is located in the (DOS) peak, the narrowness of this peak determines the transport properties whatever may be the nature and origin of the peak. This peak can either be a single narrow band or a sharp DOS peak on wide band. If the DOS inside the peak is significantly greater than the outside, the normal state electron transport will also be determined by the structure and the properties of this peak. The van Hove singularity near Fermi level can be the most probable reason for this peak [62]. As mentioned earlier, many properties of HTSC such as marginal Fermi liquid behavior [63], specific heat jump [64]. isotope shift [65-67] and transport coefficients could be explained satisfactorily in van Hove singularity picture. The transport coefficient analysis by Gasumyant *et al* [16] also supports this picture. Whatever may be the origin of the peak, the term "narrow **band**" is used for this narrow peak in density of states whose width (W) is comparable to $k_B T$.

This model includes three phenomenological parameters. One F, is the degree of band filling with electrons, which is the ratio of number of electrons to the total number of

states in the band. The sign and value of TEP depends on this parameter. In the high temperature limit ($k_BT > W$, where W is the bandwidth, k_B is Boltzmann constant)

$$S = \frac{k_B}{e} \ln \frac{F}{1-F} \tag{5.3.11}$$

$S = 0$ at $F = 1/2$, $S>0$ at $F>1/2$ and $S<0$ for $F<1/2$.

They have used the rectangular approximation for $N(E)$ and $\sigma(E)$ because of the narrowness of the band. The second parameter is the total effective bandwidth W_D and the third is W_σ, effective width of an energy interval of the electrons which gives main contribution to the electrical conduction process.

According to the present model S is given by

$$S = \frac{-k_B}{e} \left\{ \frac{W_\sigma*}{sinhW_\sigma*} \left[e^{-\mu*} + coshW_\sigma* - \frac{1}{W_\sigma*} \right. \right.$$
$$\left. \left. \times (cosh\mu* + coshW_\sigma^*) ln \frac{e^{\mu*} + e^{W_\sigma*}}{e^{\mu*} + e^{-W_\sigma*}} \right] - \mu* \right\} \tag{5.3.12}$$

$$\mu^* = \mu/k_BT = \ln \frac{sinh(FW_D^*)}{sinh[(1-F)W_D^*]} \tag{5.3.13}$$

where μ is the chemical potential, $W_D^* = W_D/2k_BT$ and $W* = W_\sigma/2k_BT$.

Gasumyant et al [16] fitted their TEP data on Y-123 system to the above equation and calculated the band structure parameters. To analyze the TEP data of their $Bi_2Sr_2Ca_{1-x}Nd_xCu_2O_y$ system [35], they have used the same model with an additional assumption that the band is asymmetric. To take band asymmetry into account, the asymmetry parameter b is introduced between the $N(E)$ and $\sigma(E)$ rectangles centers. The above expression is still valid, if μ is replaced by μ-bW_D. The same approach is used

to explain the temperature dependence of TEP for the present systems under study. The best fits of the present to the eqn.(5.3.12) are shown in **Fig.5.15-5.17.** The estimated band spectrum parameters are listed in **Table-5.4.** The variation of these parameters with x is similar to those observed in **Y-123** and Nd-doped **Bi-2212** system. With increase in x, F value increases. This variation is non-linear. The increase in x leads to an increase in number of electrons (which should be linear) but also decreases the total number of states in the band. So, F is expected to be non-linear.

The total effective band width increases with increase in x. The increase observed in W_σ is small compared to that in W_D. The ratio of W_σ/W_D decreases as x changes from 0 to 0.5. The value of W_D obtained for the present samples are close to the values obtained in $Bi_2Sr_2Ca_{1-x}Nd_xCu_2O_y$ system. With increase in x, disorder in the system increases which leads to Anderson localization, *i.e.*, broadening of the band (W_D value increase) and the relative reduction in energy interval shared by the delocalized states (W_σ/W_D decrease) occurs. On the other hand, the increase in effective band width causes a decrease in $N(E_F)$ value which in turn causes the decrease in T_c.

5.4   Analysis of the data of the Semiconducting samples

The TEP variation with temperature for semiconducting samples, which have mobility gap at the Fermi level, is given by the eqn.(5.1.8). According to this equation, S should decrease with increase in temperature. Contrary to this, in the present samples S increases with increase in temperature. From the resistivity data, it is observed that the conduction in these samples at low temperatures is governed by variable range hopping (VRH). The expression for TEP in the VRH regime is given by the eqn.(5.1.12). **Fig.5.18** and 5.19 show the S vs T^{-m} plots for various semiconducting samples for m = 1/3 and 1/2. Both the plots appear linear over a wide range of temperature. For the present
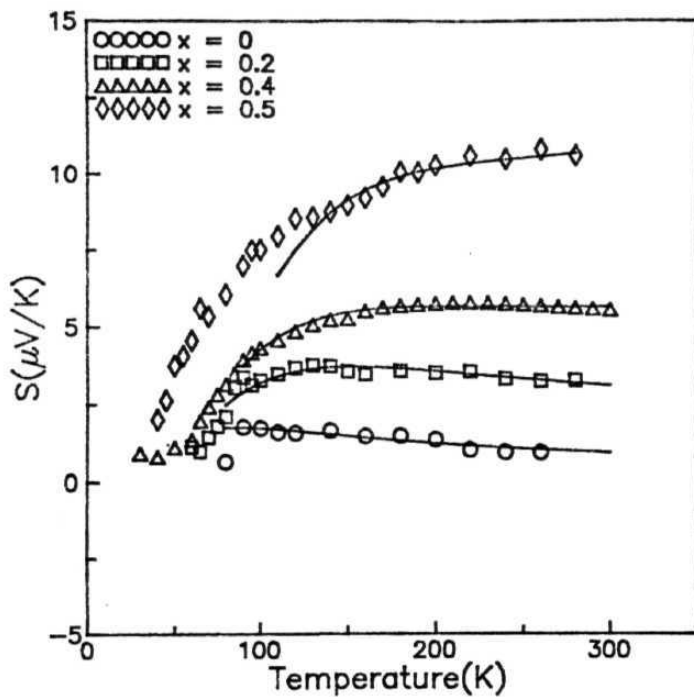
Fig.5.15 Best fit curves (solid lines) for $Bi_2Sr_2Ca_{1-x}Pr_xCu_2O_y$ **samples corresponding to Eqn.(5.3.12)**
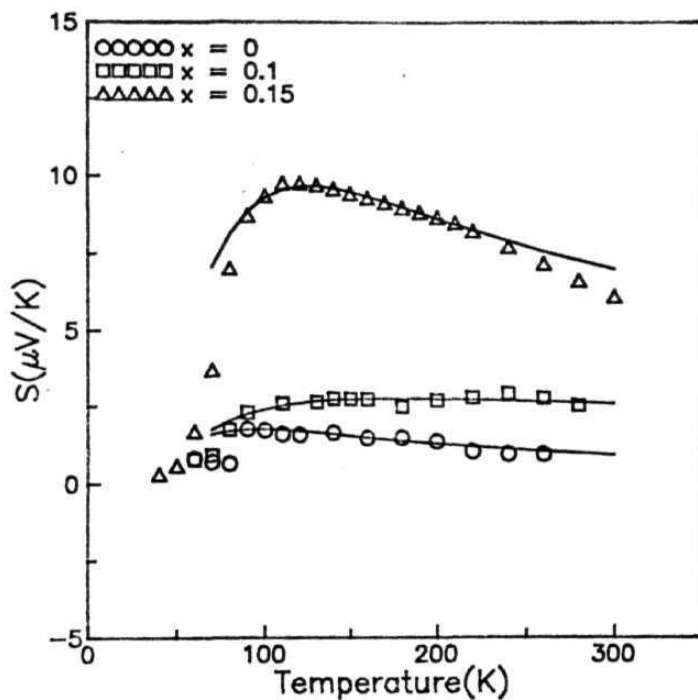
Fig.5.16 Best fit curves (solid lines) for $Bi_2Sr_2Ca_{1-x}Ce_xCu_2O_y$ samples corresponding to Eqn.(5.3.12)
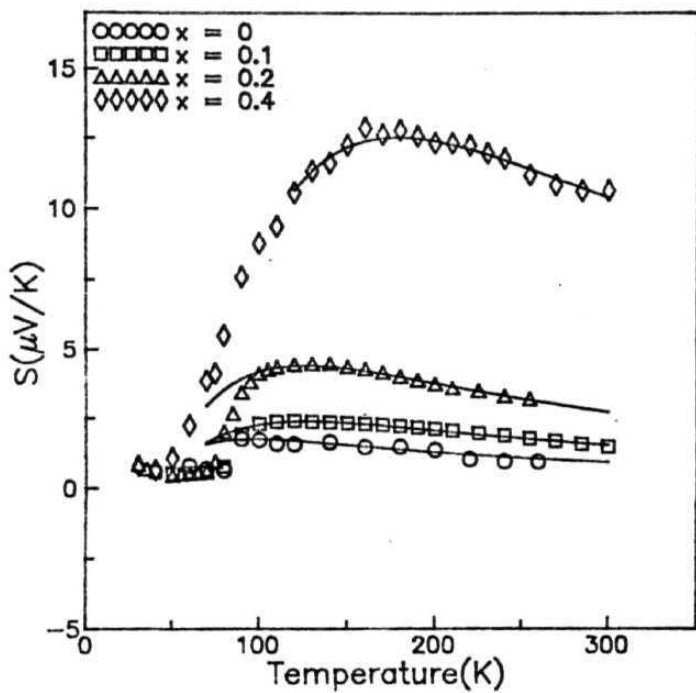
Fig.5.17 Best fit curves (solid lines) for $Bi_2Sr_2Ca_{1-x}Tb_xCu_2O_y$ samples corresponding to Eqn.(5.3.12)

Table-5.4

Best fit parameters W_D, W_σ and F of eqn. (5.3.12) and the corresponding W_σ/W_D values for $Bi_2Sr_2Ca_{1-x}M_xCu_2O_y$ (M sa Pr, Ce & Tb) system

x	W_D (meV)	W_σ (meV)	F	W_σ/W_D
Pr-doped				
0	74	28	0.501	**0.39**
0.2	131	**49**	0.509	**0.37**
0.4	164	56	0.532	0.34
0.5	215	fifi	0.608	0.31
Ce-doped				
0.1	220	54	0.504	0.25
0.15	322	**43**	0.509	0.13
Tb-doped				
0.1	176	**40**	0.503	0.23
0.2	216	**37**	0.506	0.17
0.4	459	60	0.509	0.13

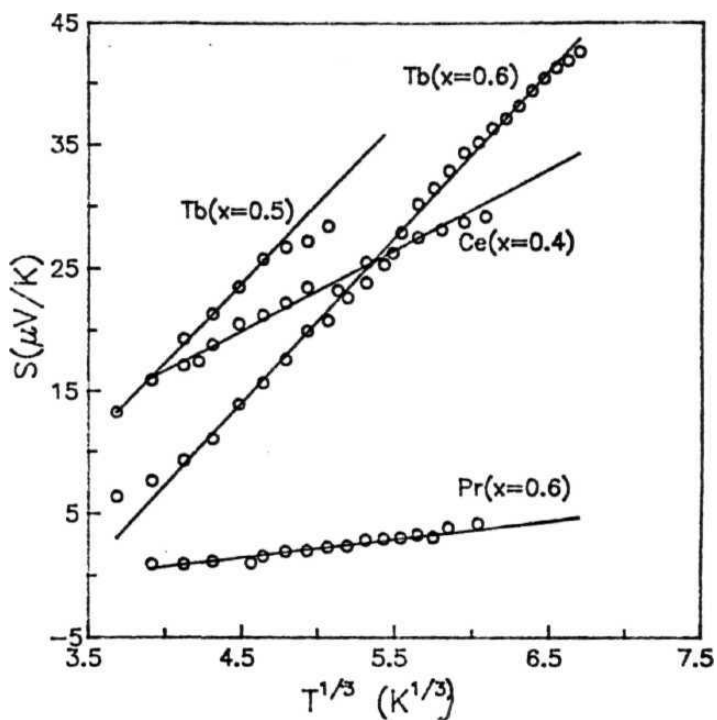**Fig.5.18** Plot of S vs. $T^{1/3}$ for various semiconducting samples
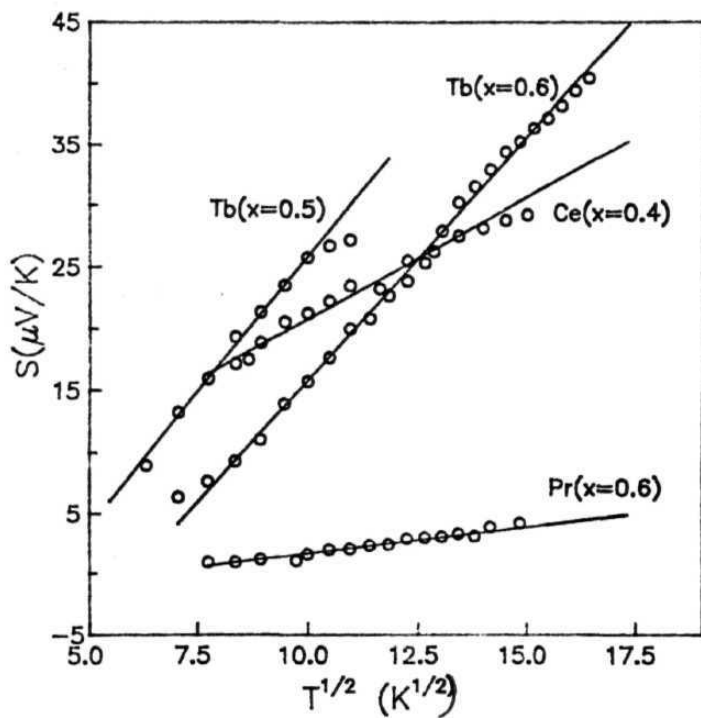
Fig.5.19 **Plot of S vs. $T^{1/2}$ for** various semiconducting samples

series of samples it is hard to distinguish the difference between $T^{1/3}$ or $T^{1/2}$ dependence of S *(i.e.,* whether the hopping is in 3D or in 2D). From the resistivity data also, it is not possible to distinguish whether the hopping is in **3D** or in **2D.**

5.5　References

1. H. M. Rosenberg, *Low temperature Solid State Physics* (Clarendon, Oxford, 1965) and references therein.

2. D. K. C. MacDonald, ***Thermoelectricity:*** *an introduction to the principles* (Wiley, New York, 1962) and the references therein.

3. N. F. Mott and E. A. Davis, *Electronic Processes in Nonccrystalline **Materials,*** 2nd ed. (Clarendon, Oxford, 1979) and references therein.

4. R. R. Heikes and Ure, *Thermoelectricity,* P. 81 (Interscience, New York, 1961)

5. P. N. Butcher, *Electronic Phenomena in **Non-Crystalline** Semiconductors,* 89 (1976).

6. M. J. Burns and P. M. Chaiken, *Phys. Rev.* **B27,** 5924 (1983).

7. A. B. Kaiser and C. Uher in *Studies of High temperature Superconductors,* Vol.7 ed. A. V. Narlikar (Nova Science, New York, 1990).

8. C. Uher, A. B. Kaiser, E. Gmelin and L. Walz, *Phy. Rev.* **B36,** 5676 (1987) and references therein

9. F. Devaux. A. Manthiram and J. B. Goodenough, *Phys. Rev.* B41, 8723 (1990); S. W. Cheong, M. F. Hundley, J. D. Thompson and Z. Fisk, *Phys. Rev* **B69,** 6567 (1989).

10. T. Ohtani, K. Kobatake and T. Takehara, *Physica* C179, 376 (1991) and references therein.

11. C. Uher and A. B. Kaiser, *Phys. Rev.* **B36,** 5680 (1987).

12. V. Radhakrishnan, C. K. Subramaniam, V. Sankaranarayanan, G. V. Subba Rao and R. Srinivasan, *Phys. Rev.* 40, 6850 (1989).

13. C. K. Subramaniam, A. B. Kaiser, H. J. Trodhal, A. Mawdsley and R. G. Buckley, *Physica* C203, **98** (1992).

14. J. L. Cohn. E. F. Skelton, S. A. Wolf and J. Z. Liu, *Phys. Rev.* **B45,** 13140 (1992).

15. P. Gerdanian and C. Picard, *Physica* **C246,** 145 (1995).

16. V. E. Gasumyants, V. I. Kaidanov and E. V. Vladimirskaya, *Physica* **C248,** 255 (1995).

17. J. L. Tallon. J. R. Cooper, P. S. I. P. N. de Silva, G. V. M. Williams and J. W. Loram, *Phys. Rev. Lett.* **75,** 4114 (1995).

18. J. W. Cohrane. A. Hartmann, G. J. Russell, *Physica* C265. 135 (1996).

19. B. Fisher. J. Genossar, L. Patlagan and G. M. Reisner. *Phys. Rev.* **B48,** 16056 (1993).

20. B. Fisher, J. Genossar, L. Patlagan, G. M. Rcisner, and A. Knizhnik, *J. Appl. Phys.* 80, 898 (1996).

21. C. Bernhard and J. L. Tallon, *Phys. Rev.* B54, 10201 (1996).

22. J. L. Tallon, G. V. M. Williams, C. Bernhard, D. M. Pooke, M. P. Staines, J. D. Johnson and R. H. Meinhold, *Phys. Rev.* B53, R11972 (1996).

23. C. N. R. Rao, T. V. Ramakrishnan and N. Kumar, *Physica* C165, 183 (1990).

24. L. Forro, J. Lukatela and B. Keszei, *Solid State Commun.* 73, 501 (1990).

25. M. F. Crommie, Amy Y Liu, Marvin L. Cohen and A. Zettl, *Phys. Rev.* B41, 2526 (1990).

26. S. D. Obertelli, J. R. Cooper and J. L. Tallon, *Phys. Rev.* B46, 14928 (1992).

27. V. P. S. Awana, V. N. Moorthy and A. V. Narlikar, *Phys. Rev.* B49, 6385 (1994).

28. C. K. Subramaniam, H. J. Trodhal, D. Pooke and K. Kishio, *Physica* C249, 139 (1995).

29. C. J. Liu, Wu Ting, X. J. Wu, N. Koshizuka and H. Yamauchi, *Phys. Rev.* B52, 10499 (1995).

30. V. P. S. Awana, R. Lal and A. V. Narlikar, *J. Phys: Condens. Matter* 7, L171 (1995).

31. X. F. Chen, G. X. Tessema and M. J. Skove, *Phys. Rev.* B48, 13141 (1993).

32. D. Mandrus, L. Forro, C. Kendziora and L. Mihaly, *Phys. Rev.* B44, 2418 (1991).

33. F. Munakata, K. Mastsuura, K. Kubo. T. Kawana and H. Yamauchi, *Phys. Rev.* B45, 10605 (1992).

34. J. B. Mandal, S. Keshri, P. Mandal, A. Poddar, A. N. Ghosh and B. Ghosh, *Phys. Rev.* B46, 11849 (1992).

35. V. E. Gasumyants, N. V. Ageev, E. V. Vladimirskaya, V. I. Smirnov, A. V. Kazanskiy and V. I. Kaydanov *Phys. Rev.* B53, 905 (1996) and references therein.

36. Ruiping Wang, Hisashi Sekine and Hua Jin, *Supercond. Sci. Technol.* 9, 529 (1996).

37. B. Chanda, S. K. Ghatak and T. K. Dey, *Physica* C232, 136 (1994).

38. N. Mitra, J. Trefny, B. Yarat, G. Pine. Z. Z. Sheng and A. M. Hermann, *Phys. Rev.* B38, 704 (1988).

39. W. Kiehl, H. M. Duan and A. M. Hermann, *Physica* C253, 271 (1995) and references therein.

40. S. Keshri, J. B. Mandal, P. Mandal, A. Poddar, A. N. Das and B. Ghosh, *Phys. Rev.* **B47,** 9048 (1993) and references therein.

41. Y. Xin, K. W. Wang, C. X. Fan, Z. Z. Sheng and F. T. Chan, *Phys. Rev* **B48,** 557 (1993).

42. C. K. Subramaniam, M. Paranthaman and A. B. Kaiser, *Phys. Rev.* **B51,** 1330 (1995) and references therein.

43. M. R. Presland, J. L. Tallon, R. G. Buckley, R. S. Liu and N. E. Floer *Physica* **C176,** 95 (1991).

44. J. L. Tallon, C. Bernhard, H. Shaked, R. L. Hitterman and J. D. Jorgensen, *Phys. Rev.* **B51,** 12911 (1995).

45. J. L. Cohn, S. A. Wolf, V. Selvamanickam and K. Salama, *Phys. Rev. Lett.* **66,** 1098 (1991).

46. R. Srinivasan, V. Sankarnarayanan, N. P. Raju, S. Natarajan, U. V. Varadaraju and G. V. Subba Rao, *Pramana - J. Phys.* 29, L225 (1987).

47. M. N. Hlopkin, J. Toth, A. A. Sikov and E. Zsoldos, *Solid State Commun.* **68, 1011** (1988).

48. A. B. Kaiser, *Phys. Rev.* **B35,** 4677 (1987); A. B. Kaiser, *Phys. Rev.* **B37,** 5924 (1988).

49. A. B. Kaiser and G. Mountjoy *Phys. Rev* **B43,** 6266 (1991).

50. W. Weber, *Phys. Rev. Lett* 58, 1371 (1987);58, 2154 (1987).

51. H. Zhang, H. Ma. S. Yan, S. Liang, L. Wand and S. Yan, *Physica* **B165&166, 1209** (1990).

52. P. M. Chaikin and G. Beni, *Phys. Rev.* **B13,** 647 (1976).

53. C. G. Olsen, R. Liu. D. W. Lynch, R. S. List, A. J. Arko, B. W. Veal, Y. Chang, P. Z. Jiang and A. Paulikas, *Phys. Rev.* **B42,** 381 (1990).

54. B.O. Wells, Z. X. Shen. D. S. Dessau, W. E. Spicer, C. G. Olsen, D. B. Mitzi, A. Kapitulnik, R. S. List and A. Arko, *Phys. Rev.Lett.* 65, 3056 (1994).

55. P. B. Allen, Warren E. Pickett and H. Krakauer, *Phys. Rev.* **B37,** 7482 (1988).

56. N. L. Wang, Y. Chong. C. Y. Wang and D. J. Huang. Z. Q. Mao, L. Z. Cao and Z. J. Chen, *Phys. Rev.* **B47.** 3347 (1993).

57. B. Fisher, J. Genossar. I. 0. Lelong, A. Kessel and J. Ashkenazi, *J. Superconduct.* 1, 53 (1988)

58. J. Genossar, B. Fisher. I. 0. Lelong, J. Ashkenazi and L. Patlagan, *Physica* **C157.** 320 (1989).

59. S. Bar-Ad, B. Fisher, J. Ashkenazi and J. Genossar, *Physica* C156, 741 (1988).

60. B. Fisher, J. Genossar, L. Patlagan and G. M. Reisner, *Phys. Rev.* **B48,** 16056 (1993).

61. I. M. Tsidilkovski and V. I. Tsidilkovski, *Solid State Commun.,*66, 51 (1988).

62. D. M. Newns, C. C. Tsuei, R. P. Huebener, P. J. M. van Bentum, P. C. Pattnaik and C. C. Chi, *Phys. Rev. Lett* 73, 1695 (1994).

63. P. C. Pattnaik, C. L. Kane, D. M. Newns and C. C. Tsuei, *Phys. Rev.* **B45,** 5714 (1992).

64. C. C. Tsuei, C. C. Chi, D. M. Newns, P. C. Pattnaik and M. Daumling *Phys. Rev. Lett.* 69, 2134 (1992).

65. C. C. Tsuei, D. M. Newns, C. C. Chi and P. C. Pattnaik, *Phys. Rev. Lett.* 65, 2724 (1990).

66. D. M. Newns, C. C. Tsuei, P. C. Pattnaik and C. L. Kane, *Comments Condens. Matter Phys.* **15,** 273 (1992).

67. D. M. Newns et al, *Physica* **186-188B,** 801 (1993).

68. H. Alloul, T. Ohno and P. Mendels, *Phys. Rev. Lett.* 63, 1700 (1989).

69. K. Kakurai, S. Shamoto, T. Kiyokura, M. Sato, J. M. Transquada and G. Shirane, *Phys. Rev.* **B48,** 3485 (1993).

70. J. W. Loram, K. A. Mirza, J. R. Cooper and W. Y. Liang, *Phys. Rev. Lett.* **71,** 1740 (1993); *J. Supercond.* 7, 243 (1994).

71. H. J. Trodhal, *Phys. Rev.* **B51,** 6175 (1995).

72. C. Uher, in *Physical Properties of High Temperature Superconductors,* edited by D. M. Ginsberg (World Scientific, Singapore, 1992) Vol. III.

73. V. Gottwick, K. Glass. F. Horn, F. Steglich and N. Grewe, *J. Magn. Magn. Mat.* **47-48,** 536 (1985).

74. L. Forro, M. Raki, J. Y. Henry and C. Ayache, *Solid State Commun.* 69, 1097 (1989).

75. P. W. Anderson, *Science*¡ **235,** 1196 (1987).

76. N. Nagaosa and P. A. Lee. *Phys. Rev. Lett* 64, 2450 (1990).

77. S. Ikegawa, T. Wada. T. Yamashita, A. Ichinose, K. Matsuura, K. Kubo, H. Ya-mauchi and S. Tanaka. *Phys. Rev* **B43,**11503 (1991).

78. V. P. S. Awana, S. B. Samanta P. K. Dutta, E. Gmelin and A. V. Narlikar. *J. Phys: Condens. Matter 3.* 8893 (1991).

79. S. B. Samanta, P. K. Dutta, V. P. S. Awana and A. V. Narlikar, *Europhys. Lett.* 16, 391 (1991).

80. S. B. Samanta, P. K. Dutta, V. P. S. Awana, E. Gmelin and A. V. Narlikar, *Physica* C178, 171 (1991).

81. N. Yu. Arutyunov, in: *Positronium Chemistry,* ed. Y. C. Jean (World Scientific, Singapore, 1990) p.518

82. V. F. Masterov, V. A. Kharchenko and N. Yu. Arutyunov, *sverkhprovodimost (KIAE)*5, 1211 (1992) *[Sov. Supercond.* 5 (1992)].

83. T. Takahashi, *Nucl. Instr. Meth.* A303, 515 (1991).

84. T. Takahashi, H. Matsuyama, H. Katayama-Yoshida, K. Seki, K. Kamiya and H. Inokuchi, *Physica* C170, 416 (1990).

85. M. Sato, R. Horiba and K. Nagasaka, *Phys. Rev. Lett.* 70, 1175 (1993).

86. S. A. Kazmin, V. I. Kaidanov and G. Leising, *Fix. Tverd. Tela* (Leningrad) 30, 2955 (1988) *[Sov. Solid State Phys.* 30, *1703 (1988)]*

Chapter 6

SUMMARY AND CONCLUSIONS

Samples of nominal compositions $Bi_2Sr_2Ca_{1-x}M_xCu_2O_y$ (M = Pr, Ce and Tb) were pre-
pared by the standard solid state reaction method and characterized by X-ray diffraction
(XRD) and AC susceptibility techniques. X-ray diffraction patterns reveal predominantly
single phase formation in the range 0<x<0.6 for Pr, 0<x<0.4 for Ce and 0<x<0.6 for
Tb doped samples. For higher dopant content, the secondary phases appear and the
dopant segregation takes place. The lattice parameters were estimated by LSQ fitting
of the reflections in the XRD spectra of the samples. With the increase in dopant con-
tent, the a-lattice parameter shows a marginal increase. These changes in the a-lattice
parameter value are comparable to the changes reported in other rare-earth substituted
Bi-2212 systems and Tl-based systems. The expansion along the a-axis is attributed to
the reduction in effective Cu-valence, which is responsible for the increase in Cu-0 bond
length and thus the increase in the a-lattice parameter.

The c-lattice parameter decreases with the increase in x. Among the three series
studied, the c-lattice parameter falls sharply for Ce-doped samples in comparison to the
other two series. From the comparison of ionic radii of Sr+2 (1.13), Ca^{+2} (0.99), Ce^{+3}
(1.11), Ce^{+4} (1.01), Pr^{+3} (1.09), Pr^{+4}(0.92), Tb^{+3}(1.0) and Tb^{+4} (0.90), it is likely that
the larger trivalent rare-earth ion may substitute for Sr site in preference to Ca site and

thus lead to the decrease in c-lattice parameter. However, there can be another explanation for the decrease in c-lattice parameter. The rare-earth ion at Ca site introduces excess oxygen between Bi-0 double layers. This excess oxygen reduces the net positive charge and thus the repulsion between Bi-0 double layers. The observed decrease in c-lattice parameter can be ascribed to the excess oxygen between the Bi-0 double layers. This effect is likely to be more pronounced, if Ce exists as Ce^{+4} ion and thus the faster decrease in c-lattice parameter in the case of Ce-doped Bi-2212 system compared to other rare-earth doped Bi-2212 system can be explained. This is consistent with the faster depression in T_c with x in the case of Ce-doped Bi-2212 system.

AC susceptibility measurements were carried out on the three series of samples at a field of 0.3 Oe and frequency of 33 Hz. The sample was cooled in zero field. A double drop in χ'-T plot is observed. The drop in χ' observed at high temperature is due to the randomly distributed and weakly coupled grains (intragranular $T_c = T_{c(gran)}$) and the other drop in χ', at low temperature, is intergranular drop which is due to the bulk superconducting nature of the compound $(T_{c(bulk)})$. The double drop in \'-T plot can be seen in multiphase compounds also, but from our XRD studies it is clear that there are no impurity phases present in the samples. With increasing x, the decrease in the diamagnetic onset temperature is observed for all the three series of samples. Width of the χ''-T peak determines the coupling between the grains. Broadening of \"-T peak is seen with increase in x, which is due to the reduction in volume fraction of superconducting phase.

Systematic resistivity studies were carried out on the three series of samples. All the superconducting samples in the three series are characterized by linear temperature

dependence of resistivity in the normal state with positive temperature derivative of resistivity $(d\rho/dT)$. The increase in the normal state resistivity (ρ_{300}) and the residual resistivity (ρ_o) with the increase in dopant content is observed, which is due to the impurity scattering brought by the dopant ion into the lattice. Metal-Insulator transition is observed around the resistivity value $(2 \times 10^{-2}\Omega$ cm) in all the three series . The transition temperature (T_c) decreases with the increase in dopant content (x). The transition broadening may indicate the presence of secondary phases, but XRD patterns do not indicate the presence of any secondary phases. The dopant ion introduced into the lattice decreases the hole concentration and raises the oxygen content intercalated in the Bi-0 layers. So, the observed transition broadening may be due to the intercalated oxygen between the Bi-0 layers.

The Metal-Insulator (MI) transition is observed at around x=0.6 for Pr, x = 0.2 for Ce and x=0.4 for Tb doped Bi-2212 system. From the faster depression rate of T_c and the lattice parameter with x in the case of Ce-doped system, it can be concluded that Ce exists predominantly in the +4 valence state.

The T_c depression with the increase in dopant content can not be explained in view of a theoretical model derived for 2D conventional superconductors considering the disorder effects. Neumier et al attributed the T_c depression in Pr doped Y-123 system to hole filling/localization in the CuO_2 planes by the Pr-ion and pair breaking via exchange scattering of mobile holes in the CuO_2 planes by Pr-magnetic moment. Both these effects must be related to hybridization of Pr-ion with the CuO_2 planes. Now it is well established that the T_c of high T_c oxides is sensitive to the hole concentration in CuO_2 planes. Dopant ion (Pr, Ce or Tb) with +3 or +4 valence states substituted in the place of Ca ion (valence state +2) in Bi-2212 system fills the holes and thereby reduces the T_c.

If dopant ion exists in +4 valence state the suppression of T_c will be faster. The disorder introduced by the dopant ion leads to Anderson localization which depresses the T_c. In the case of Pr and Tb there is a possibility of the existence of pair breaking mechanism also. However, in the case of Ce-doped Bi-2212 system the Ce^{+4} state precludes the possibility of any pair breaking interaction. It is difficult to explain the results in view of a single model.

The temperature dependence of resistivity in the semiconducting samples can be explained in terms of variable range hopping (VR.H) $p = \rho_o exp(T_o/T)^m$[11]. Both m=1/3 and 1/4 give good fits to the experimental data. It is not possible to determine the exponent (m) unambiguously. Localization length (a) is estimated by taking the value of density of states $(N(E_f) \approx 10^{23})$ from the literature. The value of localization length obtained is too high for the samples near the MI transition (53 A for Pr series with x = 0.6 sample). The reason for this may be that as we approach the MI transition from the insulator side, the T_o value decreases and approaches zero, consequently the localization length diverges indicating the delocalization of carriers. For the other samples with high resistivity, the values of localization lengths (4-15 A). are reasonable. For higher dopant concentrations two slopes in the \np vs T^{-m} plot are observed. which may be due to the multiphonon assisted hopping conduction. The phonon frequencies are estimated using the calculated values of localization of length a. These are in the range of 10^{11} - 10^{12} Hz, which is within the expected limits.

The values of hopping distance (R) and hopping energy (\Y) were calculated by using a and $N(E_F)$ values at different temperatures between 10 and 300 K. R decreases with the increase in x, because the increase in disorder permits the carriers to jump to the states located close to the initial state. The hopping energy \Y increases with increasing

x, because more energy is needed to cross the barrier with the increase in disorder. For a given dopant content, T_o and a are constants, R increases and W decreases with the decrease in temperature. Thermal energy decreases at low temperatures and the charge transport is governed by carriers hopping between the states with lower energy and larger hopping distance (R).

The MI transition and the linear variation of resistivity with temperature in the normal state of the superconducting samples have been discussed in view of a narrow band picture, which considers the existence of the localized states (induced by disorder) in the band tails and the delocalized states at the band center in the conduction band.

The TEP (S) measurements as a function of temperature on $Bi_2Sr_2Ca_{1-x}M_xCu_2O_y$ (M = Pr, Ce & Tb) system were undertaken in vacuum in a closed cycle He-refrigerator using dc differential technique in the temperature range 40-300 K. The room temperature TEP (S_{300}) is positive and its magnitude increases with increase in x for all the three series of samples. For the superconducting samples, S is small and S vs T plots show a broad maxima in the normal state. In the temperature range above the maxima, S decreases almost linearly as the temperature increases. The S maxima shifts towards high temperatures as x increases. In the temperature range below the maxima, S decreases rapidly and goes to zero at the T_c. Superconducting samples show the room temperature TEP value $< 11\mu V/K$.

TEP of the semiconducting samples is high fcs 30-40 μ V/K except in the case of Pr-doped Bi-2212 sample with x = 0.6, which has TEP $\approx$ 8 //V/K. The plot of S versus T for the semiconducting sample in the Pr-doped series with x = 0.6 shows a slow increase in S with T in the temperature range 40-200 K and a sharp increase in the temperature

range 200-300 K. This type of **temperature dependence** of S is similar to what has been reported in La-system and in amorphous semiconductors in the hopping regime. In the case of other semiconducting samples *i.e.,* in Ce-doped (x = 0.4) and Tb-doped (x = 0.5) **Bi-2212** samples, S is almost constant around room temperature and as we go to the low temperatures a smooth decrease in S is observed. For the Tb-doped (x = 0.6) Bi-2212 sample, S decreases continuously with the decrease in temperature. The temperature dependence of TEP of the semiconducting samples has been ascribed to variable range hopping (VRH). However, it is not possible to distinguish whether the hopping is in 2D **or** 3D.

Various theoretical models presented in the literature, like van Hove singularity model and the phonon drag model, are discussed. The TEP experimental data are analyzed in view of various two-band models and a phenomenological narrow band model proposed for high T_c superconductors. **The** applicability of each of these models to the experimental **data** is discussed.

The temperature variation of S in high T_c oxide systems is similar to that of the mixed valent heavy Fermion systems The model used to explain the TEP variation with temperature of the heavy Fermion systems has, therefore, been used for high T_c oxides by Forro *et al* [16] with some modification. The model is based on the assumption that there is a narrow band superimposed on a broad band and a normal band. Though this model fits well to our experimental data, evidence for this kind of band structure is not available for high T_c superconductors.

Using RVB theory, Nagaosa and Lee proposed that the TEP of superconducting cuprates can be expressed as sum of Fermion and Boson part which are proportional to

T and ln(1/T) respectively. Good fits to our experimental data have been obtained using this model, but one of the fitting parameters which is proportional to m^{-1} (boson mass) is high compared to the theoretical value.

Experimental data has been fitted to the two band model of Xin *et at.* According to this model, TEP of Bi-2212 consists of two parts. The first part represents the role of p-type conduction (holes) in Cu-0 planes and the second part represents the role of n-type conduction (electrons) in the semiconducting Bi-0 layers. The energy gap (E_g) in the semiconducting like band structure of the Bi-0 layers is estimated. The E_g values are consistent with the values obtained from scanning tunneling microscopy studies on Bi-22l2 system. E_g values increase with the increase in x for the superconducting samples. E_g depends on the extent of intercalation of excess oxygen in the Bi-0 layers. In the absence of any excess oxygen, band gap is zero. Though this model works well for the present systems and reasonable energy gap values are obtained, there is a growing evidence that TEP is the property of CuO_2 planes and not that of the Bi-0 charge reservoirs in the Bi-based high T_c superconducting oxides.

Finally, a phenomenological narrow band model is used to explain the TEP experimental data. This model assumes existence of a narrow peak in the density of states. If the Fermi level E_F is located in this peak, the narrowness of this peak determines the transport properties, whatever may be the nature and origin of the peak. This model includes three phenomenological parameters. The first one F, is the degree of band filling with electrons, which is the ratio of number of electrons to the total number of states in the band. The sign and the value of S depends on F in the high temperature limit.(S=0 at F=l/2, S > 0 at F > 1/2 and S < 0 for F < 1/9). The second parameter is the total effective band width (W_D) and the third one is the conductivity effective band width W_σ

which gives the main contribution to the electrical conduction process.

The best fits of this model to the TEP experimental data were obtained to estimate the three phenomenological parameters. F is found to increase non-linearly with x as per the predictions of the model. The total effective band width increases with the increase in x. The increase in the value of W_σ is small compared to that of Wp. The ratio W_σ/W_D decreases as x increases. With the increase in x, the disorder in the system increases, which leads to Anderson localization, *i.e.*, broadening of the band indicated by the increase in W_D value and the relative reduction in energy interval shared by delocalized states takes place. Consequently the increase in effective band width causes a decrease in density of states $(N(E_F))$ value, which in turn causes the decrease in T_c. Although this model explains our data in a better way than the other models, but still more experimental as well as theoretical work is necessary to understand the mechanism of superconductivity in high T_c superconductors.

CURRICULUM-VITAE

Name   : D. Rama Sita
Address : Visweswarayapuram P. 0.
            Malikipuram Mandal
            E. G. Dt. (A. P.)
            PIN - 533 253

Educational Qualifications

- Ph.D. (Thesis submitted) (1997)
  Thesis title : Resistivity and thermoelectric power studies on
                 $Bi_2Sr_2Ca_{1-x}M_xCu_2O_y$ (M = Pr, Ce & Tb) systems
  University : University of Hyderabad, Hyderabad

- M. Phil. in Physics (1991)
  Dissertation : Synthesis, characterization and ESR studies of $YBa_2Cu_3O_7$
                 and $YBa_2Cu_4O_8$ high temperature superconductors
  University : University of Hyderabad, Hyderabad

- M.Sc in Physics (1990)
  Specialization : Solid State Physics
  University   : University of Hyderabad, Hyderabad (1990)

- B. Sc. (1988)
  Subjects   : Maths, Physics and Chemistry
  University : Andhra University

Research Experience

- Junior Research Fellow (JRF) in Department of Science and Technology (DST, India) project entitled "Studies of structural instabilities, glass, granular and texture effects in high T_c superconductors"- June 1990 to Sept. 1991. at University of Hyderabad.

- Council of Scientific and Industrial Research (CSIR, India) Fellow Oct. 1991 to Sept. 1996 at University of Hyderabad.

Academic Achievements

- Awarded gold medal for securing first position in M. **Phil.examination of** University of Hyderabad for the academic year 1990-91.

- Qualified Graduate Aptitude Test in Engineering (GATE) in 1990 conducted by Ministry of Human **Resorces** Development, **Govt. of** India.

- Qualified the **CSIR-UGC** National Entrance Test (NET) **for JRF** and **elibility** for University Lecturership in 1990.

- **Received** National Merit Scholarship during High School, Senior High School and Undergraduation period 1983-88.

Software Knowledge

Languages	:	C, Fortran, Basic.
Operating Systems	:	Unix, Vax, Dos, Windows.
Packages	:	**Mathematica,** Tex, and **GPIB** etc.

List of publications

Journals

1. Structural and Superconducting properties of $Bi_2Sr_2Ca_{1-x}Pr_xCu_2O_y$
   D.Rama Sita and R.Singh
   Int. J. of Mod. Physics. **B8**, 2283 (1994).

2. Structural and Superconducting properties of $Bi_2Sr_2Ca_{1-x}Ce_xCu_2O_y$
   D.Rama Sita and R.Singh
   Solid State Commun., 94. 969 (1995).

3. Thermoelectric power of the $Bi_2Sr_2Ca_{1-x}Tb_xCu_2O_y$ system
   R. Singh and D. Rama Sita (communicated)

4. Thermoelectric power of the $Bi_2Sr_2Ca_{1-x}Ce_xCu_2O_y$ system
   D. Rama Sita and R. **Singh.** (communicated)

5. Thermoelectric power of the $Bi_2Sr_2Ca_{1-x}Pr_xCu_2O_y$ system
   D. Rama Sita and R. **Singh.** (communicated)

Presented at symposiums and conferences

1. Effect of mechanical processing and isothermal annealing on the **ESR** of $YBa_2Cu_3O_7$ and $YBa_2Cu_4O_8$ high temperature superconductors
D.Rama Sita and R.Singh
Proceedings of the SSP symposium **34C,** 273 (1991).

2. Conduction mechanism in semiconducting $Y_{1-x}Pr_xBa_2Cu_3O_y$ compounds
D.Rama Sita and R.Singh
American Institute of Physics Conference Proceedings, **286,** 273 (1993).

3. Structural and Superconducting properties of $Bi_2Sr_2Ca_{1-x}Ce_xCu_2O_y$
D.Rama Sita and R.Singh
Proceedings of SSP symposium, 37C, 315 (1994).

4. Structural and Superconducting properties of $Bi_2Sr_2Ca_{1-x}Tb_xCu_2O_y$
D.Rama Sita and R.Singh
Proceedings of SSP Symposium, **38C,** 283 (1995).

5. Structural and Superconducting properties of $Bi_2Sr_{2-x}Ce_xCaCu_2O_y$
D.Rama Sita and R.Singh
Proceedings of SSP Symposium, **39C,** 271 (1996).

6. Thermoelectric power of $Bi_2Sr_2Ca_{1-x}M_x$ (M = Pr, Ce)Cu_2O_y
D.Rama Sita and R.Singh
Presented at Symposium on *current topics in physics of materials,* March 27-29, University of Hyderabad, Hyderabad, 1997.(p2-9).

Personal Profile

Date of Birth	:	20th August 1968.
Father's Name	:	D.Suryanarayana
Sex	:	Female
Nationality	:	Indian
Languages Known	:	English, Hindi and Telugu